2022

Therapeutic Approaches for Respiratory Distress Syndrome

Franck J. Kamga Gninzeko
Virginia Commonwealth University

Therapeutic Approaches for Respiratory Distress Syndrome

A Dissertation submitted in partial fulfillment of the requirements for the degree of Doctor of Philosophy in Biomedical Engineering at Virginia Commonwealth University.

By

Franck Jivago Kamga Gninzeko

B.S. Biomedical Engineering, Virginia Commonwealth University, 2017

Director: Rebecca L. Heise, Ph.D.,

Associate Professor, Undergraduate program Director, Virginia Commonwealth University

Virginia Commonwealth University

Richmond, Virginia

May, 2022

Acknowledgement

This work will not have been possible without the financial support of the NIH NIA, which provided me with an R award for materials purchase, services, and stipends. I also want to thank VCU graduate school for awarding me a dissertation assistantship award which provided me with the necessary stipend to finish my dissertation. A special thanks to the Koerner Family Foundation (KFF) for awarding me additional stipend to boost my morale at the height of the pandemic.

There is an African adage; it takes a village to raise a child. This proverb is a testament to my journey throughout my academic life. I want to thank the Catholic community of Richmond and my pastors with a special mention to Fr. Marsolle, who were always present every time I needed to refocus my mind so I could be successful in the lab. Thank you to VCU faculty members, students, and Heise's lab members past and present, with a special thanks to Drs. Young, Valentine, and Link for always being there for me, for their mentorship, and for pushing me to my full potential. Special thanks to my committee members for guiding me through this process. I also want to thank my family, particularly my younger siblings Lyly, Chanelle, and Arthur, for inspiring me in other aspects of my life that I am not proficient in. I want to thank my mom for the sleepless nights that she had to spend awake with me when I was younger to help me with my homework, and my dad for working hard so I did not have to, and so I could focus on my studies. I want to thank my grandparents, Grand-pere †, Grand-mere, Papa Edouard†, Mama Landou† for their wise words. Lastly, most importantly, I would like to thank the fearless leader, my advisor Dr. Heise for taking a chance on me, mentoring me since undergrad, and giving me the tools necessary to be successful.

Table of Contents

ACKNOWLEDGEMENT ..... **III**

LIST OF FIGURES: ..... **X**

LIST OF TABLES: ..... **XIII**

LIST OF ABBREVIATIONS: ..... **XIV**

ABSTRACT: ..... **XVI**

CHAPTER 1: INTRODUCTION **1**

NEONATAL RELATED LUNG INJURY: 2

SURFACTANT REPLACEMENT THERAPY: 2

ADULT RELATED LUNG INJURY: 4

CELLULAR SENESCENCE: 6

SENOLYTIC DRUGS: 6

MECHANISM OF SENESCENCE: 7

HYPOTHESES: 9

CONTRIBUTION TO THE FIELD 10

SPECIFIC AIMS 12

CHAPTER 2: SURFACTANT REPLACEMENT THERAPY **17**

ABSTRACT 19

INTRODUCTION: 20

MATERIALS AND METHODS: 22

Novel dry powder inhaler: *22*

EEG formulation: *25*

Powder formulation particle size characterization: *25*

Animal Use: *25*

IVIS Imaging: *26*

Depletion and Lung Mechanics: *26*

Treatments: *27*

Mechanical Ventilation: *30*

Bronchoalveolar lavage: *30*

BALF Cytology: *30*

Histology: *31*

Statistics: *31*

RESULTS: 32

Powder formulation particle size characterization: *32*

Particle deposition: *34*

Compliance: *36*

Elastance: *36*

Resistance: *37*

Inflammatory Assessment: *39*

DISCUSSION: 42

Limitations: *46*

Conclusion: *46*

CHAPTER 3: A REVIEW OF PULMONARY SENESCENCE: ACUTE VS. CHRONIC INJURY 48

INTRODUCTION: 49
LUNGS MECHANICS: COPD, IPF, AND ARDS 50
SENESCENCE: 52
History 52
Cause 53
HALLMARKS OF SENESCENCE: 53
DNA Damage: 53
Cyclin-Dependent Kinase Inhibitors: 54
Proliferation and Apoptosis: 56
Senescence Associated Secretory Phenotype: 56
Clearing Senescent cells: 57
CONCLUSION AND FUTURE DIRECTIONS: 58
CHAPTER 4: MECHANICAL VENTILATION INDUCED SENESCENCE IN AN ACUTE MODEL OF LUNG INJURY 59
INTRODUCTION: 61
METHODS: 62
Animal: 63
Sample Collection: 63
In vitro cell stretch: 63
qPCR: 64
Inflammatory Cytokine Analysis: 64
Immunofluorescent staining: 65
Tissue Protein extraction: 66

Western Blot: *66*

TUNEL staining: *67*

Statistical analysis: *67*

RESULTS: 67

Mechanical Ventilation and Age Cause Structural Damage and Increased Polymorphonuclear in BALF *67*

Lung Mechanics: *70*

TUNEL: *70*

Presence of Senescence-like phenotypes in Mechanical Ventilation induced Acute Lung Injury *73*

Age and mechanical Ventilation lead to an Increase in Cells expressing keratin 8 (KRT8+): *76*

Cell stretch-induced senescence markers in human SAEC *78*

Inhibition of P38 Decreased KRT8+ Cells: *82*

DISCUSSION: 85

Damage due to MV *85*

DNA damage and P21 in VILI *86*

The potential role for P38 ..... *88*

Limitations: *88*

Conclusion: *90*

CHAPTER 5: SENOLYTIC DRUGS AS THERAPY IN AN AGING MODEL OF ACUTE LUNG INJURY 92

INTRODUCTION: 94

METHODS: 95
In vitro cell stretch: *95*
Animal: *96*
Sample Collection: *97*
qPCR: *98*
Inflammatory Cytokine Analysis: *98*
Immunofluorescent staining: *99*
Tissue Protein extraction: *100*
Western Blot: *100*
Statistical analysis: *101*
RESULTS: 101
Dimethyl sulfoxide (DMSO) does not cause Increase P21: *101*
SAEC can keep senescence P21 phenotype after recovery: *103*
Stretch causes Senescence and DQ decrease Senescent Cells. *105*
Increase dosing of LPS increase P21 positive cells. *108*
DQ improved lung compliance: *110*
DISCUSSION: 111
Establishing an In Vitro Two-hit VILI Model with Recovery: *111*
Mechanical stretch, DNA Damage and Senescence: *112*
ER Stress, DNA Damage and Senescence: *112*
Removal of Senescent Cells Causes Harm: *113*
LIMITATION: 113
CONCLUSION: 114

CHAPTER 6: PROOF OF CONCEPT FOR IN VIVO SURVIVAL MODEL OF VILI....115

INTRODUCTION:....116

METHODS:....116

RESULTS:....117

Survival Injurious Mechanical ventilation and HCL lead to Neutrophil Influx:....119

DISCUSSION / CONCLUSION:....120

CHAPTER 7: CONCLUSIONS AND FUTURE DIRECTIONS....122

SURFACTANT REPLACEMENT THERAPY....123

VILI AND CELLULAR SENESCENCE:....124

Conclusion:....132

CODES AND MISCELLANEOUS....134

IMAGEJ: CODE USED FOR ZOOMING IN IMAGES AND STACKS....135

MATLAB CODE: PV-LOOP VENTILATION MECHANICS....136

MATLAB CODE: LUNG COMPLIANCE....144

MATLAB CODE: LUNG ELASTANCE GRAPH....145

MATLAB CODE: LUNG RESISTANCE GRAPH....146

CURRICULUM VITAE....147

REFERENCES:....157

List of Figures:

FIGURE 1. 1 CHARACTERISTICS OF VILI. ATELECTRAUMA: ALVEOLI COLLAPSED, VOLU/BAROTRAUMA: OVEREXTENSION OF ALVEOLI, AND BIOTRAUMA: ALVEOLI INFLAMMATION.....6

FIGURE 1. 2 MECHANISM OF VILI.....8

FIGURE 2. 1 CUSTOM DRY POWDER INHALER.....24

FIGURE 2. 2 CYTOSPIN METHOD.....31

FIGURE 2. 3 PARTICLE SIZE CHARACTERIZATION OF EEG SURVANTA.....33

FIGURE 2. 4 FLUORESCENT IMAGES OF EEG POWDER DEPOSITION (10 MG).....35

FIGURE 2. 5 COMPLIANCE, ELASTANCE, AND RESISTANCE MEASUREMENTS.....38

FIGURE 2. 6 WHITE BLOOD CELL COUNT.....40

FIGURE 2. 7 HEMATOXYLIN AND EOSIN STAINING.....41

FIGURE 3. 1 COMPARISON OF DIFFERENT EFFECTS BROUGHT BY COPD AND ARDS ON THE LUNGS.....51

FIGURE 3.2: EMPHYSEMA VS HEALTHY VS FIBROTIC TRANSPULMONARY P-V CURVES.....52

FIGURE 4. 1 LUNG MECHANICS, BCA AND WHITE BLOOD CELL COUNT.....69

FIGURE 4. 2 SINGLE COMPARTMENT COMPLIANCE.....70

FIGURE 4. 3 TUNEL STAINING.....72

FIGURE 4. 4 EVIDENCE OF SENESCENCE IN VILI.....75

FIGURE 4. 5 INCREASE KRT8 POSITIVE CELLS WITH AGE AND MECHANICAL VENTILATION.....78

FIGURE 4. 6 GENE EXPRESSION AND IMMUNOFLUORESCENT STAINING OF HUMAN SAEC CELLS AT STATIC AND STRETCH CONDITIONS 79
FIGURE 4. 7 GENE EXPRESSION AND IMMUNOFLUORESCENT STAINING OF HUMAN SAEC CELLS AT STATIC AND STRETCH CONDITIONS WITH DMSO AND P38 INHIBITOR 81
FIGURE 4. 8 STRETCH SAEC DOES NOT INCREASE KRT8. RAGE, AN AT1 MARKER. 83
FIGURE 4. 9 P38 INHIBITOR DECREASE KRT8+ CELLS. RAGE, AN AT1 MARKER. 84
FIGURE 4. 10 FIGURE SUMMARY OF VILI LEADING TO LUNG DAMAGE AND CELLULAR SENESCENCE. 90

FIGURE 5. 1 IN VITRO EXPERIMENTAL SETUP 96
FIGURE 5. 2 IN VIVO EXPERIMENTAL SETUP 97
FIGURE 5. 3 DMSO IS NON-TOXIC TO THE SAEC 103
FIGURE 5. 4 POSITIVE CONTROL EXPERIMENT REPRESENTATIVE IMAGES 105
FIGURE 5. 5 IN VITRO STRETCH WITH RECOVERY 107
FIGURE 5. 6 IN VITRO STRETCH IN RECOVERY WITH 10X LPS 110

FIGURE 6. 1 SURVIVAL STUDY: LUNG MECHANICS 119
FIGURE 6. 2 NEUTROPHIL COUNT 120

FIGURE 7. 1 BCA ON BALF 128
FIGURE 7. 2 DQ LUNG COMPLIANCE OF TWO-HIT VILI OLD MICE 129
FIGURE 7. 3 P21 AND IL6 IN VIVO GENE EXPRESSION OF YOUNG AND OLD TOTAL LUNG LYSATE 131

FIGURE 7. 4 SUMMARY OF THE POTENTIAL ROLE OF SENESCENCE IN VILI. 132

List of Tables:

TABLE 1. 1 : LIQUID AND EEG SURVANTA AEROSOL DOSES 29

List of Abbreviations:

ALI	Acute Lung Injury
ARDS	Acute Respiratory Distress Syndrome
AT1	Alveolar Type I
AT2	Alveolar Type II
ATM	Ataxia-Telangiectasia, Mutated
ATR	ATM And Rad3-Related
BALF	Bronchoalveolar Lavage
BCA	Bicinchoninic Acid Assay
CDK	Cyclin-Dependent Kinases
CDKs	Cyclin-Dependent Kinases
ChK1	Checkpoint Kinase 1
ChK2	Checkpoint Kinase 2
COPD	Chronic Obstructive Pulmonary Disease
DDR	Dna Damage Response
DMSO	Dimethylsulfoxide
DPPC	Dipalmitoylphosphatidylcholine
DQ	Dasatinib + Quercetin
ECM	Extracellular Matrix
EEG	Excipient Enhanced Growth
ELISA	Enzyme-Linked Immunosorbent Assay
ER	Endoplasmic Reticulum
H&E	Hematoxylin And Eosin
HP	High Pressure
IL	Interleukin
IPF	Idiopathic Pulmonary Fibrosis
IVIS	In Vivo Imaging System

KRT8	Keratin 8
LPS	Lipopolysaccharide
MAP	Mitogen-Activated Protein Kinases
MCP-1	Monocyte Chemoattractant Protein-1
MMAD	Mass Median Aerodynamic Diameter
MMPs	Matrix Metalloproteinases
MV	Mechanical Ventilation
NRDS	Neonatal Respiratory Distress Syndrome
NV	Non-Ventilated
PEEP	Positive End-Expiratory Pressure
PL	Phospholipids
PMN	Polymorphonuclear
PV-loops	Pressure- Volume Loops
SA-b-Gal	Senescence-Associated Beta Galactosidase Activity
SAEC	Small Airway Epithelial Cells
SASP	Senescence-Associated Secretory Phenotype
SD	Surfactant Depletion
SP	Surfactant Protein
STAT	Static
STR	Stretch
TGF-β	Transforming Growth Factor Beta
TNFα	Tumour Necrosis Factor Alpha
TUNEL	Terminal Deoxynucleotidyl Transferase Dutp Nick End Labeling
UPR	Unfolded Proteins Response
VILI	Ventilator-Induced Lung Injury

Abstract:

THERAPEUTIC APPROACHES FOR RESPIRATORY DISTRESS SYNDROME

By Franck J. Kamga Gninzeko

A Dissertation submitted in partial fulfillment of the requirements for the degree of Doctor of Philosophy in Biomedical Engineering at Virginia Commonwealth University.

Virginia Commonwealth University, 2022.

Major Director: Rebecca L. Heise, Ph.D.

Associate Professor, Undergraduate Program Director, Department of Biomedical Engineering

Respiratory distress syndrome (RDS) is characterized by shortness of breath and low oxygen levels. RDS affects the neonatal and adult populations. In the neonatal population, RDS can be classified as NRDS (Neonatal respiratory distress syndrome), while in adults, it is known as ARDS (acute respiratory distress syndrome). This dissertation examines a therapeutic approach to NRDS and a mechanistic approach to ARDS with *in vivo* and *in vitro* models of lung injury. NRDS is characterized by a deficiency or lack of surfactant. Surfactant is an essential compound composed of phospholipids and proteins to prevent the lungs from collapsing. There are several surfactant replacement therapies to remedy NRDS. However, these therapies are given in liquid instillation forms. Adding more liquid to an already compromised lung can exacerbate the injury. To solve these issues, we utilized Survanta (one of the drugs

clinically used as a surfactant replacement therapy) in powder form (most particles less than 1.5 um in size) with hygroscopic properties (excipient enhanced growth, EEG) so that the drug will increase in diameter with humidity. EEG Survanta improved lung mechanics compared with liquid instilled Survanta in surfactant depleted rats. Moreover, lower EEG Survanta doses had a better effect on lung mechanics than the higher doses. In all, we used hygroscopic properties of the EEG Survanta to coat the lungs with surfactant and improve lung mechanics successfully. In the dissertation we then explored the role of senescence in VILI (ventilator-induced lung injury). The shortness of breath and hypoxemia observed in ARDS leads to mechanical ventilation. However, mechanical ventilation can lead to VILI. The inflammatory environment created by VILI, and ARDS compounded with the overstretched of the alveoli due to mechanical ventilators can lead to senescence (stable cell cycle arrest). However, the relationship between senescence and VILI remains elusive. Using both in vivo and in vitro models of VILI, we found that mechanical ventilation and stretch lead to structural lung damage, DNA damage (via γH2AX), and increased P21, a marker of senescence. In C57BL/6 mice, we discovered that age and VILI cause increased KRT8+ cells (transiently differentiated AT2 cells susceptible to DNA damage). Furthermore, by inhibiting the P38 pathway, we also demonstrated that P38-MAPK is involved in stretch-induced senescence. Separately, we performed a pilot study with senolytic drugs Dasatinib/Quercetin (DQ) cocktail to remove senescent cells *in vitro* and *in vivo* selectively. Initial results show that removing senescent cells in vivo led to more damage in young mice characterized by increased proteins in the bronchoalveolar lavage fluid and less damage in old mice characterized by decreased inflammation,

suggesting that senescence may be protective in young mice and harmful in old mice in an acute model of lung injury. All in all, we used preclinical models to elucidate different aspects of RDS that will inform clinical therapies.

CHAPTER 1: INTRODUCTION

NEONATAL RELATED LUNG INJURY: 2

SURFACTANT REPLACEMENT THERAPY: 2

ADULT RELATED LUNG INJURY: 4

CELLULAR SENESCENCE: 6

SENOLYTIC DRUGS: 6

MECHANISM OF SENESCENCE: 7

HYPOTHESES: 9

CONTRIBUTION TO THE FIELD 10

SPECIFIC AIMS 12

Neonatal Related Lung Injury:

The lung is a complex organ whose main role is to facilitate gas exchange between the capillary blood and the humidified air of the alveoli. However, there are diseases that can impede that critical function. Those diseases range from chronic to acute and can reduce the lifespan substantially, especially the elderly population [1] [2] and the neonate population [3], [4]. In the latter population the disease is characterized as neonatal respiratory distress syndrome (NRDS). In fact, NRDS accounts for about 20% of all neonatal death [5] and 50-70% of death of premature infants [6]. Premature infants are more prone to this disease as surfactant production does not mature until the last weeks of gestation [7]. Surfactant mixture consisting of phospholipids (PL) and proteins whose purpose is to lower the surface tension, thereby increasing the compliance of the lungs during respiration [4]. The surfactant PL are mainly composed of dipalmitoylphosphatidylcholine (DPPC), which functions to reduce surface tension, and four surfactant associated proteins (SP-A, SP-B, SP-C, and SP-D) that regulate surfactant function [8]. Together, the PL and proteins ensure the stability of the alveoli and allow for alveolar expansion and diffusional transport across that layer [9]. To remedy NRDS, multiple therapies have been used including breathing support and surfactant replacement therapy to enable the alveoli to expand and prevent their collapse [3].

Surfactant Replacement Therapy:

There are a varieties of surfactant replacement drugs; they span from synthetics to animal derived, with neonate receiving animal derived having a better outcome [10]. Animal derived surfactant replacement drugs include Alveofact®, Curosurf® and Survanta® [11]. These treatments are delivered by instillation of the liquid in volumes

ranging from 2-8 ml in order to reach the distal alveoli; however, adding more fluid to an already distressed lung may complicate the injury by hindering gas exchange [12]. Delivering these drugs as an aerosol has been investigated as an alternate method of delivery that could deliver functional lipids and proteins to the distal alveoli to effectively replace the deficient surfactant [13]. However, efficiently delivering milligram quantities of aerosol to the lungs of infants has proven challenging using conventional inhalers and nebulizers. High efficiency aerosol drug delivery using excipient enhanced growth (EEG) methods have been recently described [14].

This technology has been employed to produce a dry powder aerosol formulation of EEG Survanta [15]. The EEG Survanta formulation is a micrometer sized combination particle consisting of Survanta, mannitol (which act as a hygroscopic excipient) and leucine (dry powder dispersion enhancer) engineering using spray drying technology. Powder aerosols are formed by dispersing the particles using a novel low dispersion air volume dry powder inhaler. The EEG particle size delivered in the lungs are approximatively 1.5 μm (figure 1.1: particle size graph) which deposit well in the upper airways using a dry powder inhaler. However, due to quick exhalation, particles of that size will be exhale. A key component of EEG delivery is the inclusion of the hygroscopic excipient, in this case mannitol, which absorbs water vapor in the warm and humid respiratory airways rapidly increasing the size of the aerosol [16] as it travels to the deep lung and fostering deposition within this region.[17], [18]. To cure NRDS we are planning on using EEG Survanta aerosol powder to deliver the necessary surfactant to the lungs of surfactant depleted animals.

Adult Related Lung Injury:

ALI is condition that is characterized by a compromised blood air barrier at the alveoli level formed by epithelial and endothelial cells as well as basement membrane. This leads to influx of blood in the alveoli space, recruitment of cytokines and inflammation. The most severe form of ALI is acute respiratory distress syndrome or ARDS, this condition is lethal amongst the elderly population [2]. Patients with ARDS require mechanical ventilation (MV) to mitigate the effects of this dangerous disease and attempts to use surfactant replacement therapies as in neonate have failed in the elderly population [13]. While MV is crucial to treating ARDS, it has some adverse effects, including ventilation induced lung injury (VILI). The blood-air barrier at the alveoli is very thin; therefore, the strain caused by MV due to the movement of air in and out of alveoli compromises the integrity of that barrier and allows liquid filled with protein to cross into the alveolar space causing VILI. The consequences of VILI are characterized as: biotrauma, volutrauma and atelectrauma. In biotrauma the mechanical stress caused by the MV creates a proinflammatory environment by causing the secretion of cytokines and chemokines therefore resulting in the recruitment of immune cells to the cite of the injury. Volutrauma is characterized by overdistention of normal alveoli due to a tidal volume forced by MV into the lungs. Finally, atelectrauma is due to cyclic opening and collapse of alveoli impeding the main function of the lung, i.e. gas exchange. It has been shown that VILI is exacerbated with age. Studies performed in our lab suggest the adverse effects of VILI due to aging, including our own [19]. In most of those studies it was shown that aging rodent models when put on MV, present more signs of inflammation due to elevated levels of inflammation makers, changes in lung mechanics and structural damage, injury and

edema relative to younger rodents [19], [20]. Again, during MV, due to the movement of air in and out of the lungs, and the increased pressure in the lungs, most cells experience stretch. Cell stretch models have been used to model VILI in vitro, and studies, including our own, have shown increased inflammation in stretched old alveolar cells lining the air blood barrier [21]. However, it is not clear how the combined effect of age and the hostile mechanical environment created by VILI can lead to senescence. In brief, investigating the effects of senescence in VILI in the elderly population and surfactant therapy replacement therapy in the neonate population could shed lights on different methods that could be used to curb these conditions.

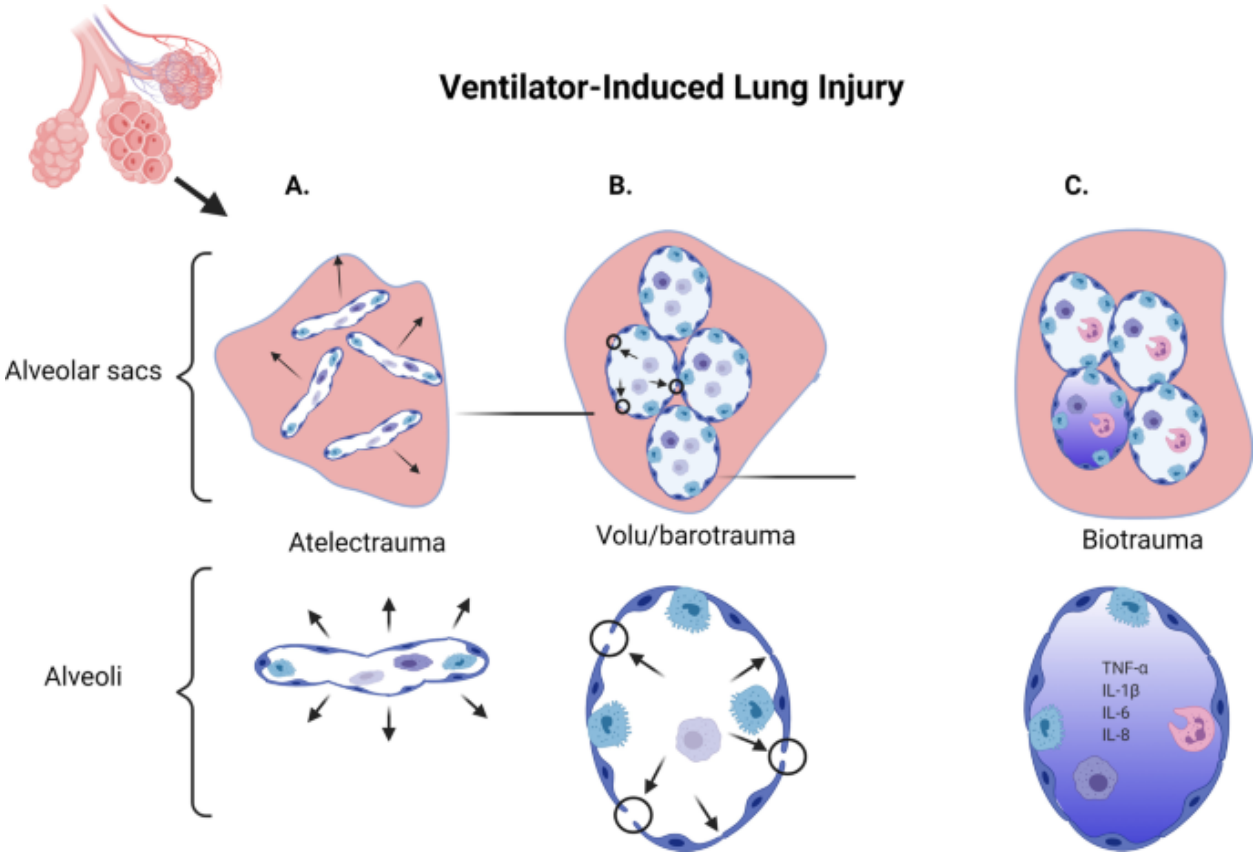

Figure 1. 1 Characteristics of VILI. Atelectrauma: alveoli collapsed, volu/barotrauma: overextension of alveoli, and Biotrauma: alveoli inflammation. [22]

Cellular senescence:

Senescence is a process by which cellular division comes to a complete stop. Cellular senescence prevents damaged cells from replicating hence allowing the body's immune system to clear them out. However, with age, the ratio of cells that are becoming senescent and non-senescent cells is very high [23]. This can be detrimental to the body as senescent cells produce secretomes called senescence associated secretory phenotypes (SASP). The SASP is composed of inflammatory cytokines such as MCP1 and TNFα, growth factors such as TGF-β, matrix metalloproteinase such as MMP10 and 12 [24]–[26]. These secretomes will cause the recruitment of other immune cells to the cite of the injury therefore exacerbating the inflammatory process and affecting surrounding cells. Senescent cells show a change in morphology and appear flattened and enlarged compared to other surrounding cells[27]. Moreover, senescence is characterized by upregulation of genes such as P16, P53 and P21, all of which are cyclin dependent kinase inhibitors [24], [28], [29]. These genes play an important role as they regulate the cell cycle at different stages. In addition, senescence is also characterized by increased senescence associated beta galactosidase (SA-b-Gal) activity in the cells [30]. Senescent cells may be targeted and removed with senolytic drugs.

Senolytic Drugs:

Senolytic drugs such as fisetin and the cocktail of dasatinib/quercetin have been used to selectively clear out senescent cells in animal models of lung diseases such as COPD and IPF [24] and other disease models [31]. In fact, the results of a clinical trial that used

the cocktail of dasatinib/quercetin show senolytic drugs alleviate physical dysfunction in people suffering from IPF [32]. The mechanisms by which senolytic drugs act differ. Fisetin, found in a variety of fruits and vegetables, is a dietary antioxidant that affects the metabolic pathway [33], [34]. Dasatinib is a receptor tyrosine kinase and Src family of kinases inhibitor [35] and quercetin inhibits PI3K [36]. These compounds may be useful in VILI as Src protein tyrosine kinase and PI3K have been shown to be upregulated with lung injury [37], [38]. Despite, the advantages that these senolytic drugs can provide, in terms of eliminating senescent cells and therefore prolonging the lifespan of an individual, they have not yet been utilized to treat experimental lung injury.

Mechanism of Senescence:

Our preliminary data indicate that during VILI there is a cascade of events that leads to cellular senescence causing inflammation via the production of cytokines. These cytokines can cause remodeling of the extracellular matrix (ECM) via the secretion of MMPs by those senescent cells. Our hypothesized pathway is shown in Figure 1.3. Some of this pathway is already known but to our knowledge it has not been fully explored in the context of VILI. During MV, the movement of air in and out of the lungs causes increased pressure which then causes the ECM to stretch and release latent TGF-β1 [39]. TGF-β1 then binds to TGF-β receptor on the surface of the cell leading to the phosphorylation of P38 MAPK. P38 MAPK will then activate P53, lastly, P53 will control the synthesis of P21 [40] causing senescence and SASP, worsening injury.

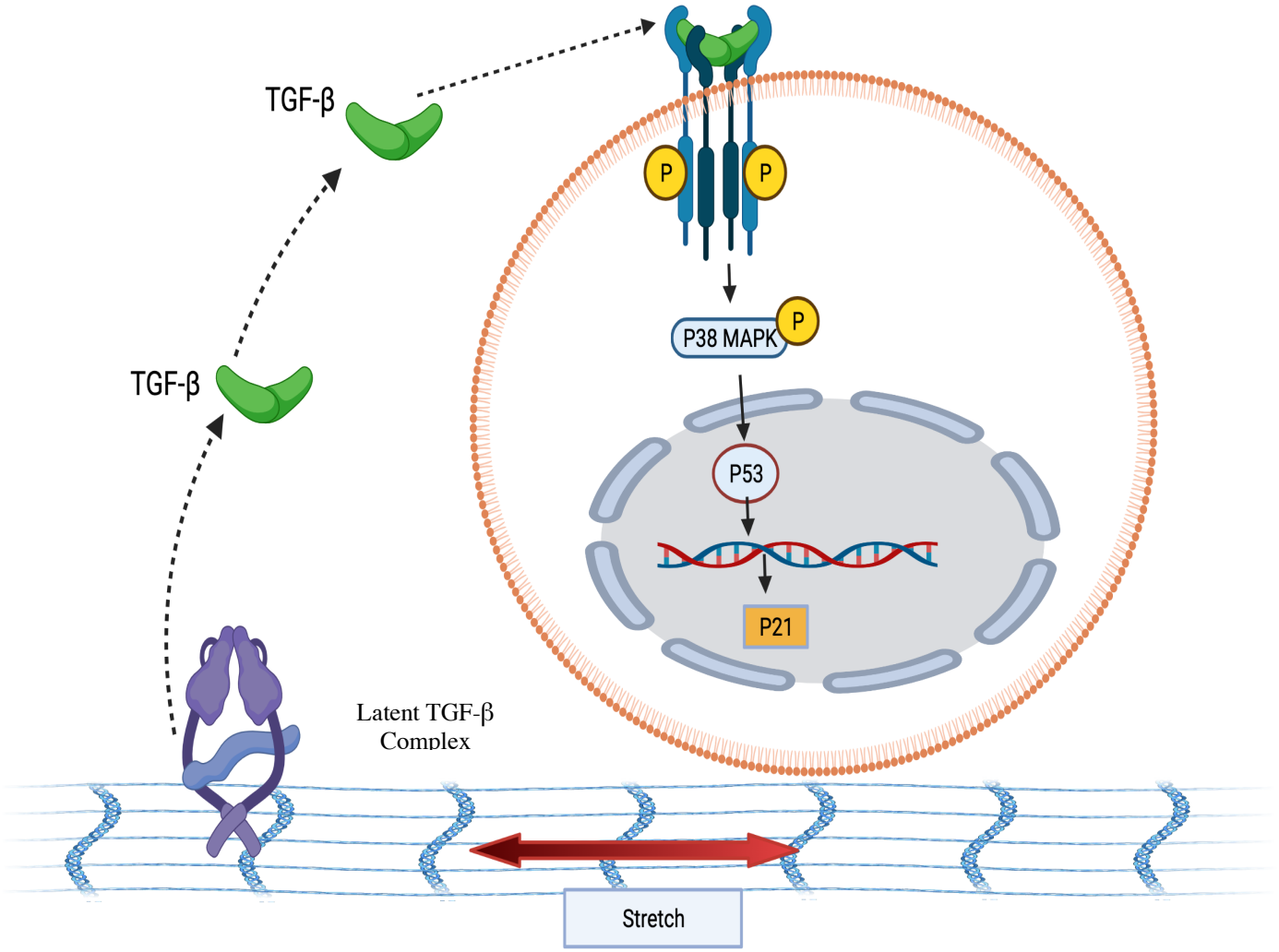

Figure 1. 2 Mechanism of VILI Stretch activation of TGFβ, and subsequent activation of P38 and P53 induced P21 in an in vitro aging model of VILI. (Biorender)

Hypotheses:

We hypothesize EEG Survanta powder will improve rat's lung mechanics compared to instilled liquid Survanta. We also hypothesize that during mechanical ventilation alveolar epithelial cells become senescent due to ventilator-induced cell stretch contributing to the loss of barrier integrity and SASP inflammatory response causing VILI. We aim to establish the relationship between senescence and age-related VILI. We further hypothesize that senolytic drugs may be a possible therapeutic target for senescence related VILI and can attenuate the stretch-induced SASP.

Contribution to the Field

Though there are drugs that exist on the market to remedy to NRDS, these drugs are not very efficient at replacing surfactant due to the drugs being delivered as liquid forms. In this study, we are using a novel formulation technique to make EEG Survanta powder, this will allow the powder to swell as it travels down the airways due to the increased humidity and to deposit functional lipids and proteins into those distal alveolar regions. Moreover, we have adapted and fine-tuned a surfactant depletion model to Sprague Dawley rats to deliver those various treatments and to improve lung mechanics. Indeed, successful achievement of the delivery of the EEG Survanta powder will be a proof of concept on alternative surfactant replacement therapy and will be one step toward reducing or eliminating the mortality rate of those neonate suffering from NRDS.

On the other hand, the way lung injury in general, and specifically VILI, causes cellular senescence is poorly understood. Specifically, as our preliminary data indicates, we are the first to show that mechanical stretch alone can cause cellular senescence in alveolar epithelium. In this proposed study, we will shed light on that pathway by utilizing in vitro and in vivo models of lung injury to investigate the TGF-β and P38 pathway in senescence induced by MV. Moreover, for the first time we will examine the use of senolytic drugs for the treatment of experimental VILI. We will determine the effects of those drugs on clearing out senescent cells and helping to rebuild the integrity of the blood air barrier. Using senolytic drugs to alleviate the negative effect of ventilator proposed in this study is novel Furthermore, introducing the age factor in lung injury is also novel. In fact, as

mentioned earlier, the aging population are more prone to the negative effects of VILI, the senolytic drugs treatment proposed may reduce the rate of ventilator-associated mortality.

Specific Aims

Respiratory distress syndrome (RDS) is a form of breathing disorder that is caused by multiple factors including surfactant deficiency. RDS affects both the neonate and the adult's populations; it is known as NRDS in neonates and ARDS for the adults. Due to the immaturity of their lungs hence the inability to produce surfactant or functional surfactant, premature infants are more prone to NRDS while in the adult population, there is about 13–59 ARDS cases/100,000 persons per year, with higher mortality among the elderly [2], [41]. Both NRDS and ARDS patients require mechanical ventilators to keep the keep the alveoli open. However, mechanical ventilation (MV) itself can lead to ventilator-induced lung injury (VILI). The biotrauma, volutrauma, and atelectrauma observed in VILI increase mechanical stress on alveolar epithelial cells causing inflammation. The molecular cascade causing epithelial inflammation is poorly understood, especially in the aging lung. In addition, the overdistension of the alveolar during MV can also lead to the loss of the barrier integrity, therefore, causing the leakiness of the membrane and allowing protein-rich fluid to inter the alveolar space and resulting in more stress to surrounding cells. Considering these inimical consequences, new therapies need to be investigated to remedy to NRDS and ARDS and to mitigate the effects of MV

Surfactant replacement therapy has been used to remedy to NRDS; however, most of those drugs are in liquid form, adding more liquid to an already distressed lung could exacerbate the injury. Delivering the necessary surfactant as a powder form could mitigate that effect. Conventional dry powder inhaled drugs are large in diameter (>2 μm)

hence cannot reach the distal alveoli and would not be efficient at replacing surfactant at that region. Excipient enhanced growth (EEG) surfactant aerosol delivery of diameters less than 2 μm could be key at treating NRDS as the drug particles will reach down the distal alveoli. In addition, EEG possess hygroscopic properties that allow the particles to swell as they travel down the airways due the increased humidity hence increasing the surface area of the aerosol deposition.

On the other hand, attempts to use surfactant therapy for ARDS as in NRDS have not been successful [13] resulting in the emphasis used of mechanical ventilator to maintain patients alive. Furthermore, the hostile environment created by VILI especially on aging lung can lead to increase senescence. Cellular senescence is a process by which the cell cycle is halted and is characterized by increased P16, P21 and P53 [42] cyclin dependent kinase inhibitors, senescence-associated beta galactosidase activity (SA-b-Gal) and senescence-associated secretory phenotype (SASP) markers (MCP1 and TNFα, MMP10 and 12, and TGFβ [24], [43]). We aim to establish the relationship between senescence and age-related VILI. In other senescent related diseases such as chronic obstructive pulmonary disease (COPD) and idiopathic pulmonary fibrosis (IPF), senolytic drugs including dasatinib/quercetin cocktail and fisetin have been used to target tyrosine kinase inhibitors or target PI3K/AKT/metabolic pathway within senescent cells [31], [44]; however, the effects of these drugs on VILI induced cellular senescence are still poorly understood. Moreover, PI3K and tyrosine kinase inhibitions have been shown to increase

during lung injury [37], [38], targeting these pathways with senolytic drugs will bring therapeutic solutions to age related or VILI induced cellular senescence.

Aim1: Test the hypothesis that EEG Survanta will improve lung mechanics in an NRDS model. We hypothesize that EEG Survanta powder will improve lung mechanics compared to instilled liquid Survanta. A rat surfactant depletion model of NRDS will be used. First, Sprague Dawley rats will be surfactant depleted via two PBS lavages at 10 ml/kg. Then the treatments at nominal doses of 3, 5, 10 and 20 mg EEG Survanta aerosol (0.61, 0.97, 1.73 and 3.46 mg PL) deliver via a custom aerosolizer and instilled liquid Survanta at 2 and 4 ml/kg (18.6 and 34 mg PL) deliver via a syringe will be administered followed by a 10-minute mechanical ventilation (MV) at 8 ml/kg 90 bpm and 3 PEEP. Lung mechanics will be taken before and after surfactant depletion and at the end of the 10-minute MV. We expect the group receiving EEG Survanta aerosol to have improved lung mechanics compared to the groups receiving instilled liquid Survanta.

Aim2: Investigate the mechanism of stretch induced cellular senescence in an aging model of VILI. We hypothesize that stretch-induced cellular senescence occurs via TGF- β pathway, and its inhibition will reduce stretch-induced senescence. A two-hit model of VILI with LPS will be used. First, primary alveolar type 1 (AT1) and type 2 (AT2) epithelium isolated from young (8-10 weeks) and old (20-22 months) mice will be exposed to LPS then stretched at 15% at 0.86 Hz for 0, 24, 48 and 72 hours. Senescence inducing drugs (paclitaxel, tunicamycin) and/or senolytic drugs (Dasatinib/Quercetin cocktail) will be added. We will examine the signaling pathway that

links stretch to senescence. To assess the role of TGF-β1 and P38 in stretch-induced senescence, young and old AT1 and AT2 cells will be exposed to TGF-β, SB-431542 (TGF-β receptor inhibitor), SB203580 (a P38 inhibitor), or sham control prior to stretch. Gene expression and protein levels of SASP (MCP1, TNFα, MMP10 and 12, and TGFβ) and senescence markers (P16, P21 and P53) will be quantified by qPCR, ELISA and western blot analyses of the proteins they encode. Our hypothesis predicts that senescence and SASP will be increased with stretch and paclitaxel and tunicamycin will enhance, while senolytic drugs will attenuate this effect. We also predict that inhibitors of TGF-β receptor and P38, in both age groups, will decrease levels of senescence markers and SASP.

Aim3: Assess the effect of senolytic drugs in a mouse model of VILI. We hypothesize that during mechanical ventilation alveolar epithelial cells become senescent due to ventilator-induced cell stretch contributing to the loss of barrier integrity and SASP inflammatory response causing VILI. Female and male C57BL6/J young (8-10 weeks) and old (20-22 months) will be ventilated at both injurious (high tidal volume) and protective (low tidal volume) settings with LPS. Senolytic drugs (dasatinib/quercetin) will be dosed during MV and recovery. The lung mechanics (compliance, resistance, elastance, and pressure volume curve) will be measured. Bronchoalveolar lavage will be performed to probe for SASP proteins and albumin levels to quantify barrier disruption and lung injury. Lungs will be analyzed for gene expression and protein production of SASP and senescence markers. We expect senescence and SASP to be upregulated with age and with injurious settings and senolytic drugs to downregulate SASP following recovery.

This innovative proposal will investigate therapeutic approaches towards treating RDS in both neonates and the elderly using relevant preclinical models.

Chapter 2: SURFACTANT REPLACEMENT THERAPY

Portions of this chapter has been published as Kamga Gninzeko et. Al. [45]

ABSTRACT 19

INTRODUCTION: 20

MATERIALS AND METHODS: 22

Novel dry powder inhaler: *22*

EEG formulation: *25*

Powder formulation particle size characterization: *25*

Animal Use: *25*

IVIS Imaging: *26*

Depletion and Lung Mechanics: *26*

Treatments: *27*

Mechanical Ventilation: *30*

Bronchoalveolar lavage: *30*

BALF Cytology: *30*

Histology: *31*

Statistics: *31*

RESULTS: 32

Powder formulation particle size characterization: *32*

Particle deposition: *34*

Compliance: *36*

Elastance: *36*

Resistance: *37*

Inflammatory Assessment: *39*

DISCUSSION: 42

Limitations: *46*

Conclusion: *46*

Abstract

Background: In neonatal respiratory distress syndrome breathing support and surfactant therapy are commonly used to enable the alveoli to expand. Surfactants are typically delivered through liquid instillation. However, liquid instillation does not specifically target the small airways. We have developed an excipient enhanced growth (EEG) powder aerosol formulation using Survanta®.

Methods: EEG Survanta powder aerosol was delivered using a novel dry powder inhaler via tracheal insufflation to surfactant depleted rats at nominal doses of 3, 5, 10 and 20 mg of powder containing 0.61, 0.97, 1.73, and 3.46 mg of phospholipids (PL) while liquid Survanta was delivered via syringe instillation at doses of 2 and 4 ml/kg containing 18.6 and 34 mg of PL. Ventilation mechanics were measured before and after depletion, and after treatment. *We hypothesized that EEG Survanta powder aerosol would improve lung mechanics compared to instilled liquid Survanta® in surfactant depleted rats*.

Results and Conclusions: EEG Survanta powder aerosol at a dose of 0.61 mg PL significantly improved lung compliance and elastance compared to the liquid Survanta at a dose of 18.6 mg, which represents improved primary efficacy of the aerosol at a 30-fold lower dose of PL. There was no significant difference in white blood cell count of the lavage from the EEG Survanta group compared to liquid Survanta. These results provide an *in vivo* proof-of-concept for EEG Survanta powder aerosol as a promising method of surfactant replacement therapy.

Key words: Surfactant Depletion, Ventilation mechanics, Compliance, Elastance, Resistance, Inflammation, EEG Survanta Powder Aerosol

Introduction:

The main function of lungs is to facilitate gas exchange between the capillary blood and the alveoli sacs. To accomplish this function, the lungs have a large surface area. Lining the alveoli at the air to liquid interface is a complex surfactant mixture consisting of phospholipids (PL) and proteins that lower the surface tension, thereby increasing the compliance of the lungs during respiration.[4] The surfactant PL are mainly composed of dipalmitoylphosphatidylcholine (DPPC), which functions to reduce surface tension and four surfactant associated proteins (SP-A, SP-B, SP-C, and SP-D) that regulate surfactant function.[8] Together, the PL and proteins ensure the stability of the alveoli and allow for alveolar expansion and diffusional transport across the alveolar interface.[9] Deficiency of surfactant due to the immaturity of the lungs in premature infants or disruption of surfactant composition due to surfactant protein gene mutations can lead to respiratory distress syndrome (RDS).[46], [47]

Premature infants are prone to RDS as surfactant production does not mature until the last weeks of gestation.[7] RDS accounts for about 20% of all neonatal deaths [5] and 50-70% of death in premature infants[6] (about 1.1 million premature infant die each year[48]). Numerous therapies used in the treatment of RDS include breathing support and surfactant replacement therapy that enable the alveoli to expand and prevent their collapse.[3] Surfactant replacements include Alveofact®, Curosurf®, and Survanta®.[49] Treatments are delivered by instillation of the liquid[50] in volumes

ranging from 2-8 ml per kilogram of body weight in order to reach the distal airways. However, adding more fluid to an already distressed lung may complicate the injury by hindering gas exchange and causing inflammation.[12] Administering these drugs as an aerosol is an alternative method that could deliver functional lipids and proteins to the distal airways to effectively replace the deficient surfactant.[13] However, efficiently delivering sufficient aerosolized medication to the lungs of infants using conventional inhalers and nebulizer has proven challenging .[9]

High-efficiency aerosol drug delivery using excipient enhanced growth (EEG) methods have been recently described.[14] This technology was employed to produce a dry powder aerosol formulation of EEG Survanta®.[15] The EEG Survanta® formulation consists of micrometer-sized combination particles containing Survanta®, mannitol (which acts as a hygroscopic excipient) and leucine (dry powder dispersion enhancer) prepared by spray drying. Powder aerosols are formed by dispersing the particles using a new low-dispersion-air-volume dry powder inhaler.

In the EEG aerosol delivery method, a relatively small aerosol with a mass median aerodynamic diameter (MMAD) approximately ≤ 1.5 μm is initially created through a combination of high-efficiency aerosolization and a highly dispersible spray-dried formulation.[51], [52] The small aerosol size enables low upper airway loss and efficient penetration to the lower regions of the lungs.[18] However, at this small aerosol size, a majority of the particles would typically not deposit and be exhaled,[53] especially with the quick respiration cycle of infants and test animals. A novel component of EEG delivery that enables hygroscopic growth, is inclusion of mannitol, or another hygroscopic excipient which absorbs water vapor in the warm and humid respiratory

airways rapidly increasing the size of the aerosol [16] as it travels to the deep lung and may foster enhanced deposition.[17], [18]

To study the efficacy of surfactant therapies, surfactant depletion (SD) animal models have been used previously.[54], [55] Successive lavage of the alveoli with warm saline solution is used for SD followed by delivery of the surfactant replacement therapies. In this study, we have used a modified SD model in order to evaluate the efficacy of delivering EEG Survanta powder aerosols in Sprague Dawley rats. *We hypothesized that EEG Survanta powder aerosol would improve lung mechanics compared to instilled liquid Survanta in surfactant depleted rats*.

Materials and Methods:

Novel dry powder inhaler:

The custom dry powder inhaler device (Figure 2.1) was created using Autodesk Inventor and exported as .STL files to be prototyped. The files were then prepared using Objet Studio preparation software and were built using an in-house Stratasys Objet24 3D Printer (Stratasys Ltd., Eden Prairie, MN, USA) using VeroWhitePlus material at a 32 μm resolution. Support material was cleaned away from the model material using a Stratasys waterjet and the devices were allowed to fully dry before use. The capillaries used in the DPI were custom cut from lengths of stainless steel (SAE 304) capillary tubing and epoxy was used to secure them in place. An o-ring was used to seal the two halves of the device to prevent leaks. A luer-lock style connection was used to seal the device to both the air syringe and the blunt needle used as the tracheostomy tube. Powder aerosol was delivered from the device using a 5 mL actuation air volume.

The aerosolization device separates into two parts with a twisting motion and powder is directly loaded into the powder chamber. Hand actuation of the 10 ml syringe supplies the necessary air volume to aerosolize the powder and deliver the aerosol into the rat lungs. Within the aerosolization device, the inlet capillaries form three high-velocity air jets that enter the powder chamber. These air jets initially fluidize the powder and then break apart the aggregates through particle interactions with turbulent eddies.[56] The aerosol is then carried through the outlet hollow capillary and to the trachea of the rat. Further description of the air-jet aerosolization concept and the effects of turbulence can be found in our previous work.[57], [58] The custom novel dry powder inhaler used in this study was developed by VCU College of Engineering [59], [60] for aerosolizing surfactant powders with low air volumes (3-10 mL). Aerosolization testing with surfactant powder indicated that emitted dose remains proportional to loaded dose through a fill mass of 10 mg.[59], [60] However, optimal aerosolization of the powder occurs at a 3 mg powder mass (producing the smallest MMAD) and aerosolization efficiency decreases with larger fill masses (producing larger MMADs).[59], [60] It is well known that smaller MMAD values will better penetrate the upper airways and thereby reach the deep lung at higher efficiencies.

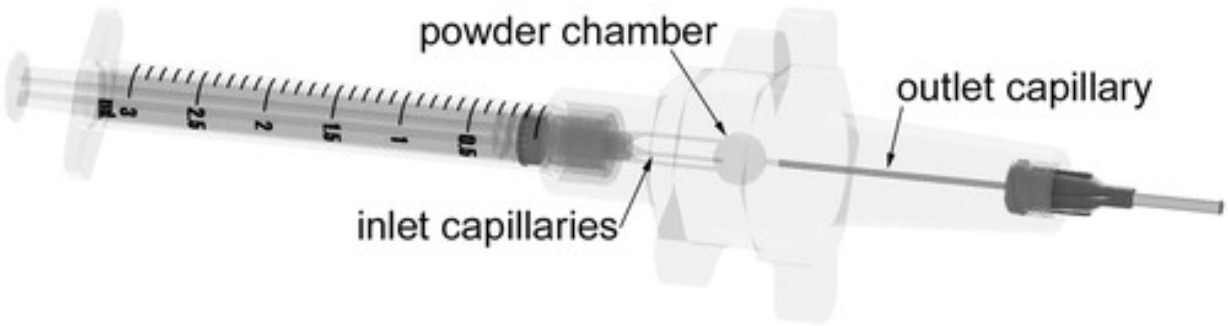

Figure 2. 1 Custom dry powder inhaler device used for EEG Survanta® delivery. EEG, excipient enhanced growth.

EEG formulation:

Survanta-EEG spray-dried powders were prepared from dispersions containing Survanta®, mannitol, and leucine in a ratio of 45:33:22 % w/w in a 5% ethanol in water mixture with a solids concentration of 0.125% w/v. Powders were spray-dried using the Büchi Nano Spray Dryer B-90 HP (Büchi Labortechnik AG, Flawil, Switzerland). Spray drying parameters were as follows: 70 °C inlet temperature (outlet temperatures of 37 - 41 °C), pump speed of 3%, spray intensity of 80%, and a gas inlet flow of 120 L/min (drying chamber pressure of 40 - 42 mbar). Powders were collected from the electrostatic particle collector into vials and stored in a desiccator at 2 to 4 °C when not in use. For the deposition visualization study, 0.5% w/w of Texas Red® dye (1,2-dihexadecanoyl-sn-glycero-3-phosphoethanolamine, triethylammonium salt; Texas Red® DHPE, ThermoFisher Scientific, Waltham, MA, USA) was added to the spray drying dispersion to enable labeling of the phospholipid powder aerosol.

Powder formulation particle size characterization:

The primary particle size of the spray-dried powder was determined using a laser diffraction method with a Sympatec ASPIROS dry dispersing unit and HELOS laser diffraction sensor (Sympatec GmbH, Clausthal-Zellerfeld, Germany). A pressure drop of 4.5 bar was used to disperse a small amount of powder for analysis.

Animal Use:

Sprague Dawley rats were purchased from Hilltop laboratory (Scottdale, PA, USA) and were housed at Virginia Commonwealth University (VCU) vivarium. The protocol was approved by the VCU Institutional Animal Care and Use Committee (IACUC) and all procedures were performed according to their guidelines.

IVIS Imaging:

To qualitatively assess the deposition of the EEG Survanta powder aerosol in the lungs, surfactant depletion was performed as described in the depletion and lung mechanics section below, surfactant depleted rats were then treated with 10 mg of EEG powder aerosol labeled with Texas Red dye as described in the treatment methods followed by 10 minutes mechanical ventilation. At the end of the mechanical ventilation, the lungs were isolated and image using an in vivo imaging system (IVIS) spectrum from VCU Cancer Mouse Models Core to determine the local distribution of aerosol. The IVIS spectrum uses 2D and 3D optical tomography to show 2D and 3D like structure of the location of the fluorescent dye in the lung.

Depletion and Lung Mechanics:

The rats (0.3 – 0.5 kg) were anesthetized with 60 mg/kg of sodium pentobarbital (Sigma, St. Louis, MO, USA) with 50% re-dosing when necessary. To assess the condition of the rats at baseline, initial lung mechanics were measured as healthy controls. Lungs mechanics were measured using a FlexiVent FX4 system and FlexiWare software (Scireq, Montreal, Quebec, Canada). The perturbations performed

included deep inflation for alveolar recruitment and Snapshot 150 for mechanics of the respiratory system. Flexiware then used Snapshot 150 to fit the data onto a single compartment math model to determine the lung mechanics of resistance (resistance assesses how constricted the lungs are to airflow), elastance (elastance is the elastic property of the lungs or the ease of the lungs to return to their original state after inflation), and compliance (compliance measures the ease of the respiratory system to stretch and expand). In the SD group, warmed phosphate buffer saline (PBS) (10 ml/kg) was perfused and quickly withdrawn from the lungs via the trachea and repeated once. Lung mechanics were normalized to individual rats. The SD mechanics were determined by normalizing to the healthy lung mechanics prior to depletion for each rat. Finally, the lung mechanics for each treatment (liquid Survanta® and EEG Survanta®) were determined by dividing mechanics taken following treatment of the surfactant depleted rats by the healthy ventilation mechanics of each rats taken at baseline.

Treatments:

Following depletion and ventilation mechanics measurements, the animals were taken off the mechanical ventilator to allow spontaneous breathing and were treated with EEG Survanta powder or liquid Survanta. Treatment arms consisted of liquid instillation of Survanta (Abbvie, North Chicago, IL, USA) at doses of 2 ml/kg and 4 ml/kg (18.6 and 34 mg PL, respectively). Dry powder aerosol delivery of EEG Survanta powder at nominal loaded doses of 3, 5, 10, and 20 mg (0.61, 0.97, 1.73, and 3.46 mg phospholipids (PL), respectively; see Table 1) was accomplished via the novel dry powder inhaler. Liquid treatments were administered via a syringe connected to a tracheal cannula while

aerosol treatments were loaded into the dry powder inhaler and were administered via a syringe connected to the dry powder inhaler (figure 2.2) and connected to a tracheal cannula. The inhaler was actuated using 5 ml of air delivered from a syringe connected to the inhaler. For the 20 mg dose, two inhalers were used each containing 10 mg of EEG Survanta. In separate studies, the delivered mass of powder emitted from the DPI was determined by measuring the weight of the inhaler before and after actuation. The mass of PL delivered was calculated from the measured DPPC content of the EEG Survanta powder. The DPPC content was determined by a validated LC-MS method.

Administration Method	Dose of Survanta or EEG Survanta	Aerosol Emitted Dose (%)	Phospholipid Dose (mg)
Instillation	0.75 (0.1) ml	NA	18.6 (2.6) mg
Instillation	1.36 (0.1) ml	NA	34.0 (2.0) mg
Aerosol	3.05 (0.03) mg	73.7 (9.3) %	0.61 (0.08) mg
Aerosol	5.02 (0.04) mg	71.4 (6.6) %	0.97 (0.09) mg
Aerosol	10.04 (0.04) mg	63.6 (6.3) %	1.73 (0.17) mg
Aerosol	20.08 mg*	NA	3.46* mg

Liquid and EEG Survanta aerosol doses are represented as mean and standard deviation (in parentheses) of loaded doses where applicable with their corresponding delivery percentage and PL content, $n = 5–7$.

* Calculated as 2 × 10.04 mg dose.

EEG, excipient enhanced growth, PL, phospholipid.

Table 1. 1 : Liquid and EEG Survanta aerosol doses

Mechanical Ventilation:

Treatments were followed by injection of a paralytic agent pancuronium bromide (MP Biomedicals, Santa Ana, CA, USA) at 1 mg/kg to prevent spontaneous breathing, and mechanical ventilation of the rats at 8 ml/kg, 90 bpm and 3 cm H2O positive end-expiratory pressure (PEEP) was performed. Lung mechanics were recorded after 10 minutes of ventilation. Five rats were used for liquid Survanta and 10 mg dose treatments groups each, while 3 rats each were used for other EEG Survanta groups.

Bronchoalveolar lavage:

Bronchoalveolar lavage (BAL) was performed as described before with minor modification and adapted for rats.[19] Briefly, at the end of mechanical ventilation, the rats were euthanized via the snipping of the inferior vena cava. A gravity assisted lavage was then performed by letting PBS flow into the lungs until full inflation and raising the rats to recover the fluid with no repeat. The BAL fluid (BALF) was then recovered for downstream processing.

BALF Cytology:

BALF cytology was performed as previously described with minor modifications.[19] Staining of the microscope slides was performed with a 3 Diff-Quik solutions staining kit. Neutrophils, monocytes and lymphocytes counts were then accessed by microscopy to assess inflammation.

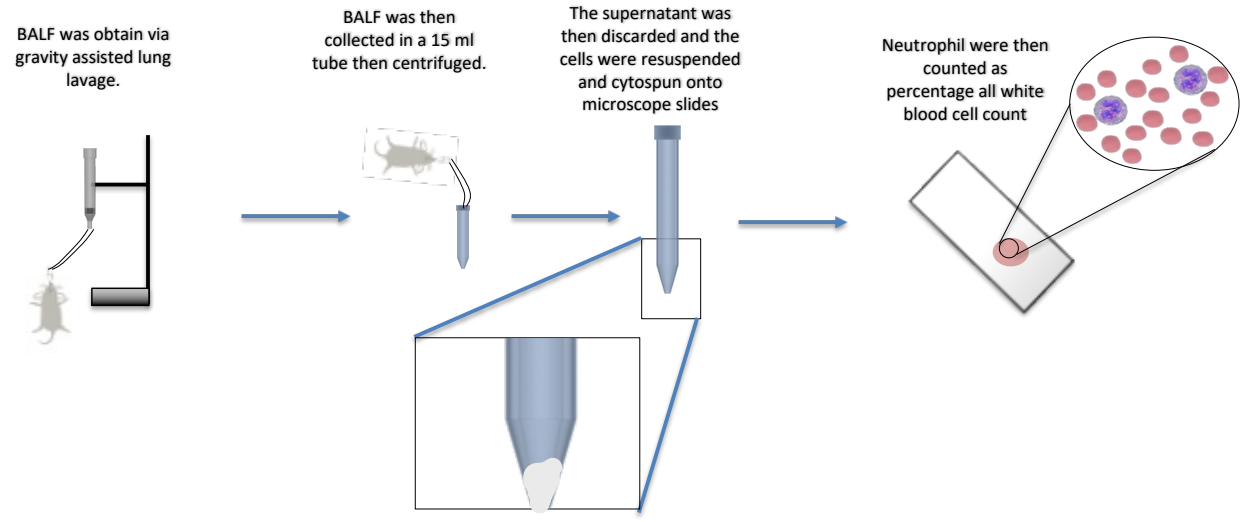

Figure 2. 2 Cytospin Method

Histology:

Lungs were fixed with a gravity assisted flow of 4% paraformaldehyde in the lungs via the trachea at the end of each procedure. Fixed lungs were dehydrated using increasing percentages of ethanol, after being placed in running tap water for 45 minutes, fixed lungs were placed in 50% ethanol overnight, then 70, 80, 90, 95 and 100% ethanol for 30 minutes each with a repeat of 100% followed by 30 minutes submersion in xylene. The lung tissues were then embedded into paraffin cassettes and 20 µm slices were made with a microtome and transferred onto microscope slides. The slides were then rehydrated and stained with hematoxylin and eosin stain (H&E). An Olympus microscope was then used to take color images of the slides with a 10X objective.

Statistics:

The power analysis was estimated based on our previous work in this model. Different treatment groups were compared by analysis of variance (ANOVA), followed by posthoc Tukey's multiple comparison test. GraphPad Prism 6 was used for statistical analyses. P-values less than 0.05 were considered significant and ≥3 replicates were performed for each experiment. The data were normally distributed.

Results:

Powder formulation particle size characterization: EEG Survanta powder aerosols from different spray dried batches used in this study were found to be monodisperse with an overall mean ± STDEV geometric diameter of 1.0 ± 0.04 μm at 4.5 bar dispersion pressure (Figure 2.3). This resulted in coefficients of variation of < 6% across the ten batches, indicating good reproducibility of the spray drying process.

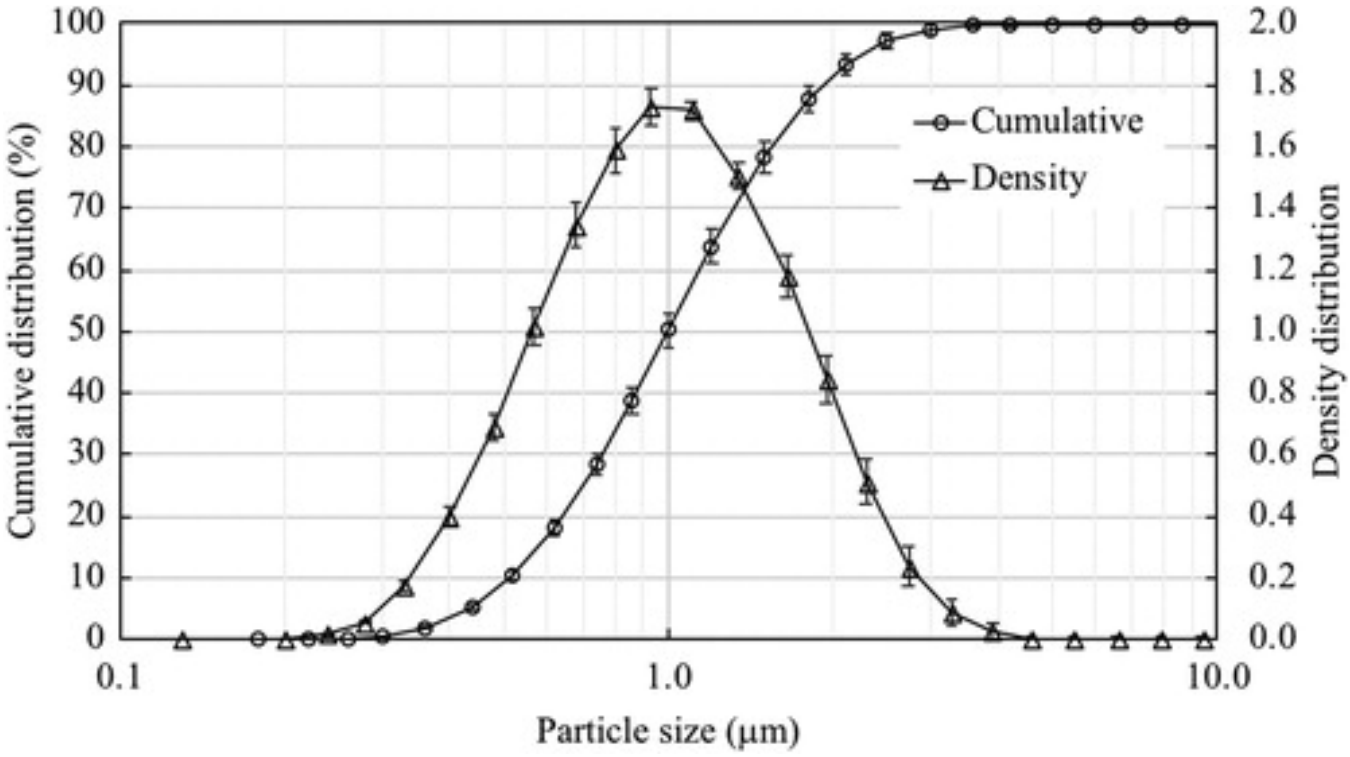

Figure 2. 3 Particle Size Characterization of EEG Survanta revealing significant fraction of particle <1.5 μm. Cumulative distribution percentage of particles less than the size reported on the y-axis. Density distribution shows the frequency of particles at each size reported on the x-axis. Error bars are standard deviation with n = 3.

Particle deposition: Figure 2.4 shows fluorescent IVIS images of the whole lung following deposition of the Texas Red labeled EEG Survanta powder aerosol. The distribution of the aerosol appears to be throughout almost the entire lung compared to control, which did not receive the fluorescent dye (Figure 2.4 A). Moreover, the image mixing which appears as a 3D like structure shows that the red fluorescent dye has reached the deep lung region (Figure 2.4 B).

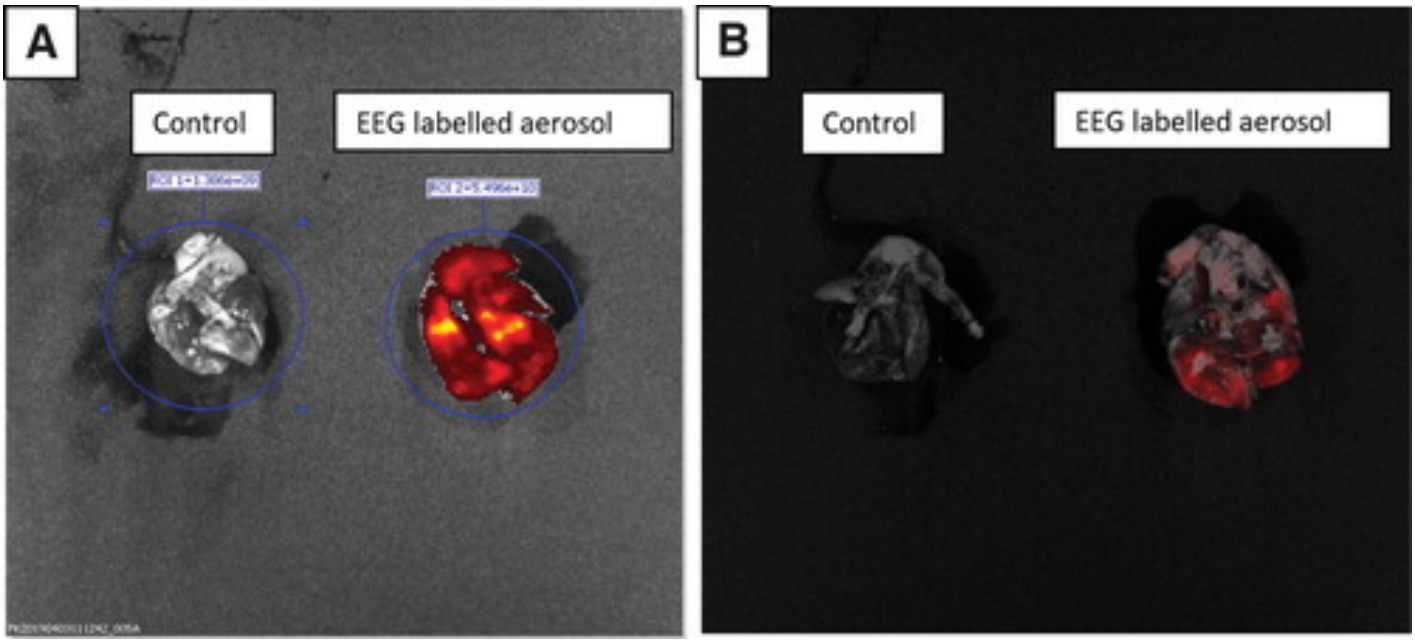

Figure 2. 4 Fluorescent images of EEG powder deposition (10 mg). (A) Fluorescence image for control and EEG Survanta powder-labeled aerosol and (B) 3D overlay of the fluorescence with light image mixed for control and EEG Survanta powder-labeled aerosol. Image mixing shows Quasi-complete deposition of EEG Survanta in the distal lung. 3D, three-dimensional.

Compliance: There was a significant decrease in the normalized compliance following SD compared to the healthy control. Figure 4 shows the normalized compliance values for the SD groups compared to the treatment groups. Each of the aerosol EEG-Survanta® treatment groups had significant increases in compliance compared to the SD group. There was no significant difference in compliance between the SD and liquid Survanta group. Dosing with 0.61 mg PL in the EEG Survanta® aerosol group produced the most improved compliance and was significantly greater than the SD and liquid Survanta® groups (Figure 4A). Each of the aerosol doses administered produced significantly greater compliance following treatment compared to the 18.6 mg PL liquid instillation. Importantly, this improved compliance was observed at PL doses that were ~10 fold lower compared to the liquid dosing. Within the aerosol EEG-Survanta® groups, an effect of administered dose was observed with a significant difference between dosing with 0.61 mg PL compared to 1.73 mg PL. There were no other differences between the 0.61 mg PL dose and the other aerosol EEG-Survanta® doses (0.97 mg of PL and 3.46 mg PL).

Elastance: There was a significant increase in the normalized elastance following SD. Figure 4B shows a significant difference between the groups that were treated with EEG Survanta® aerosol compared to the group that received liquid Survanta as treatment with the EEG Survanta group having a better elastance (Figure 4B). These results were confirmed with all the EEG Survanta groups being not statistically different from the healthy group whereas the group that received liquid Survanta as treatment was significantly different from the healthy. Moreover, there was no difference between the

liquid Survanta as treatment and the SD group while all EEG treatment groups were statistically different from the SD group. Lastly, there was a significant difference between the healthy and the SD group elastance. These results show the efficacy of the EEG Survanta at effectively improving elastance.

Resistance: The only groups that were statistically different from each other were the healthy and SD, SD and 1.73 mg of PL EEG Survanta, SD and 0.97 mg of PL EEG Survanta, SD and 0.61 mg of PL EEG Survanta (Figure 4C). Though there was not any significant statistical difference between the healthy, liquid and EEG Survanta, the groups that received EEG Survanta at different doses had a closer resistance to the healthy group compared to the ones that received liquid Survanta as treatment. The trend also shows a similar resistance among all EEG Survanta cases at different doses. Additionally, there was no significant difference between the SD group and the group that received liquid Survanta as treatment. Though we did not record any statistical difference in change of resistance between the two main treatment groups, EEG Survanta treatments at all dose levels appear to be better options in terms of reducing resistance than liquid Survanta.

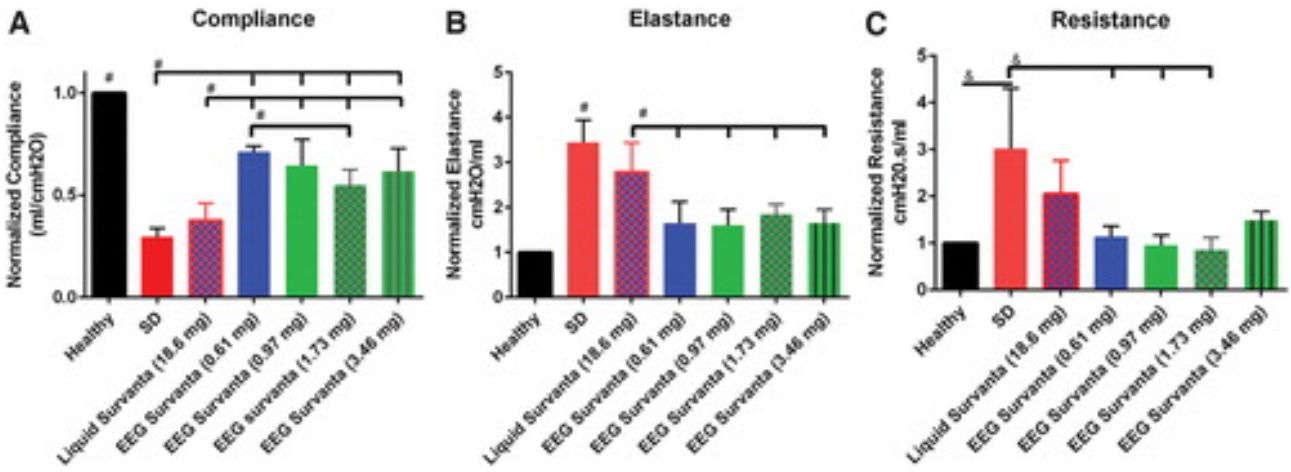

Figure 2. 5 Compliance, elastance, and resistance measurements for rats before and after treatments of 0.61, 0.97, 1.73, and 3.46 mg PL (3, 5, 10, and 20 mg EEG Survanta) and 2 mL/kg of liquid Survanta (18.6 mg PL). (A) Compliance: compliance of groups receiving EEG Survanta of 1.73 mg PL was higher than the compliance of groups receiving liquid Survanta treatment at 18.6 mg PL; EEG Survanta treatment of 0.61 mg PL had the highest compliance of all treatments. (B) Elastance: elastance for all EEG Survanta group was significantly lower than elastance of liquid Survanta. SD group had significantly higher elastance than other groups. (C) Resistance: no significant difference between the EEG Survanta group and liquid Survanta, although the trend of EEG Survanta was lower

Inflammatory Assessment: White blood cells (WBC) were counted in lavages obtained from different experimental groups. We specifically counted monocytes, lymphocytes, and neutrophils. There were similar percentages of monocytes (97 to 99 %) per 300 WBC count in cytospin slides of rats that received liquid Survanta and rats that received EEG Survanta. The same trend was observed when assessing the lymphocytes level. There was no statistically significant difference in the number of lymphocytes among any of the groups. Finally, the neutrophil count, which is characteristic of acute inflammation in the lungs did not significantly change among all experimental groups (Figure 2.6). Moreover, H&E stain yielded no visible signs of inflammation (Figure 2.7) though the group receiving liquid Survanta showed signs of alveoli collapse (Figure 2.7 B).

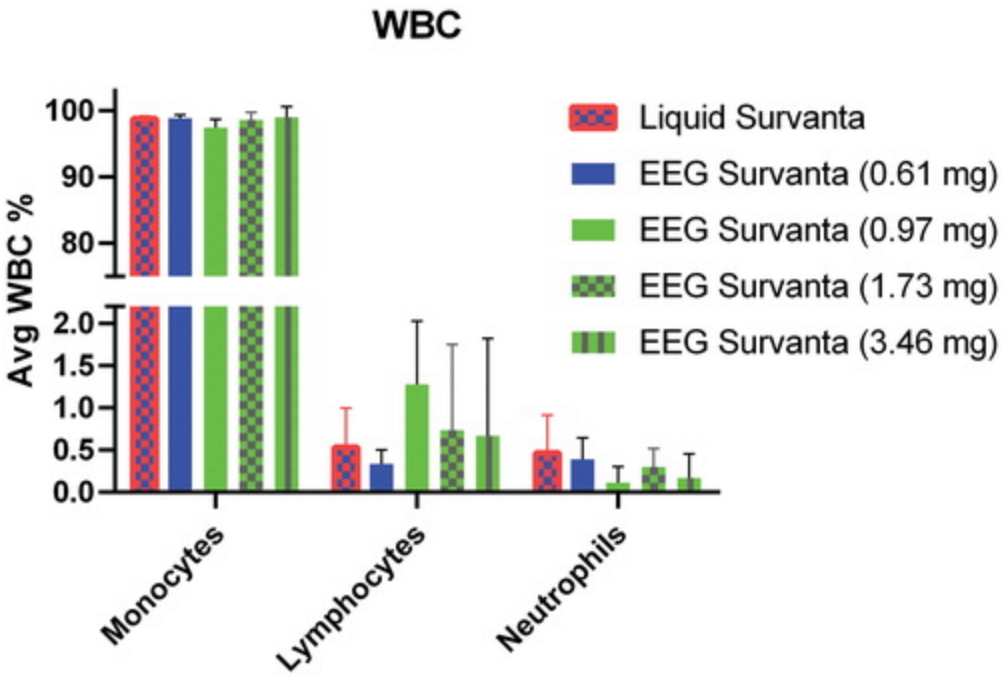

Figure 2. 6 White Blood Cell Count: Percent neutrophils, monocytes, and lymphocytes obtained per 300 WBC count of cytospin slides. No significant difference in all groups for all treatments. Bar graphs are mean ± standard deviation. n ≥ 4. WBC, white blood cell. Color images are available online.

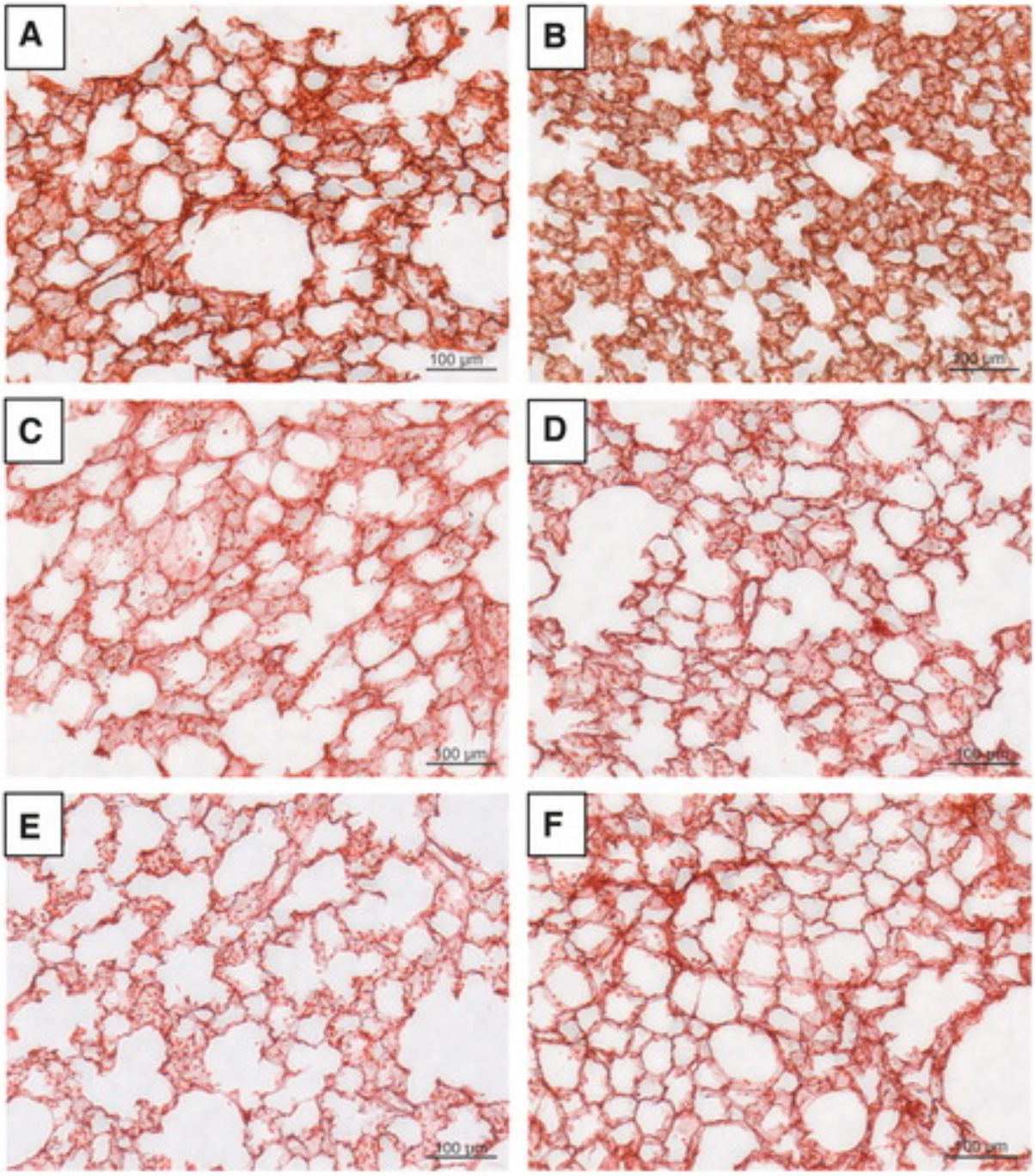

Figure 2. 7 Hematoxylin and eosin staining of (A) control rat with no treatment and no SD, (B) 18.6 mg PL liquid Survanta treatment, (C) 0.61 mg PL EEG Survanta, (D) 0.97 mg PL EEG Survanta, (E) 1.73 mg PL EEG Survanta treatment, and (F) 3.46 mg PL EEG Survanta showing no clear signs of neutrophils influx (i.e., inflammation), although liquid Survanta treatment group (B) shows signs of structural alveoli collapse. Color images are available online

Discussion:

This study has characterized the efficacy of a spray-dried powder aerosol formulation of Survanta. The spray-dried powder contained mannitol and leucine in addition to commercially available Survanta liquid and disperses into micrometer size particles upon aerosolization with a mass median aerodynamic diameter (MMAD) in the range of 1.0 μm. The small particle size allows for high-efficiency aerosol delivery to the lungs and enables the aerosol to reach the distal airways. Size increase during flight from the hygroscopic excipient helps target the site of deposition and prevents exhalation of the aerosol. A new aerosolization device, originally developed by Boc et al.[15], [59], [60] using an air-jet concept,[57], [58] was used that is capable of efficient lung delivery to a small animal model using only 5 ml of air. The study implemented a new rat lung SD model to compare the efficacy of liquid bolus surfactant instillation at a clinically implemented rate of 2 ml/kg of surfactant versus different doses of the surfactant EEG aerosol. The standard of care instillation method delivered a significantly higher dose of PL (18.6 mg) than the aerosol approach, which delivered a range of PL doses between 0.61 and 1.73 mg. Overall, the aerosolization approach significantly improved lung mechanics better than the standard-of-care liquid instillation. Little difference in lung mechanics was observed among the aerosol surfactant doses making the 0.61 mg dose the preferred dose in this model. The aerosolized surfactant formulation significantly improved lung mechanics compared with the standard-of-care liquid formulation and delivery approach at a PL dose (0.61 mg) that was a factor of 30-fold lower than with instillation.

Surfactant is composed of PL (mainly DPPC) and proteins, and this functions to reduce surface tension between the air and liquid interface in the alveoli.[61] The absence of surfactant is the underlying cause of RDS in premature neonates. To remedy RDS, surfactant replacement is available in both synthetic and natural formulations. Survanta is primarily a naturally-derived surfactant product that is formulated from minced porcine lungs with added DPPC [62] and is widely used in the treatment of RDS.[49] Survanta is administered by instillation as a liquid [63] in volumes of up to 7 mL/kg, which adds to the fluid burden already present in the alveolar space due to RDS and may not be efficiently distributed to the peripheral lung during instillation.

As an alternative to liquid instillation, a powder aerosol formulation of Survanta has been developed for high-efficiency lung delivery using the EEG approach.[14] For this method, excipients have been formulated with Survanta and spray dried into a powder containing micrometer-sized particles for inhalation. The EEG formulation contains mannitol as a hygroscopic excipient, which functions to absorb water during transit through the airways, turning the particles into droplets with increasing mass. This engineered size increase during flight can be controlled to target the region of deposition and prevent the exhalation of the aerosol, which is a significant problem when delivering small particles to infant airways. Leucine was used as a dry powder dispersion enhancer to facilitate aerosolization of the spray-dried particles.

Lung mechanics, especially the compliance of all animals receiving EEG Survanta aerosol were significantly improved compared to animals that received liquid Survanta containing 18.6 mg of PL. Initial studies using 4 mL/kg of liquid Survanta, the clinically

suggested dose in premature infants, resulted in the death of the animals during the post-dose mechanical ventilation. This was probably due to excess fluid in the alveoli that hindered the ability of the rats to effectively performed gas exchange. Subsequent control studies with liquid Survanta were performed at the 2 mL/kg dose level. We believe that this result confirms that liquid bolus instillation of surfactant, which is the current FDA approved method for all surfactant replacement therapies, may be in need of significant improvement and that aerosol delivery may be an effective alternative.

An important component of this study relates to the amount of PL that is delivered with each approach. The liquid surfactant formulation of 2 ml/kg contained 18.6 mg of PL whereas the EEG aerosol doses contained 0.61 to 3.46 mg of PL. The aerosol formulations delivered 5 to 30-fold less PL than the liquid formulation. Surprisingly, even with this significantly reduced dose of PL, the liquid surfactant was significantly better at improving lung mechanics than the liquid formulation. We theorize that this improved response at a lower administered dose is because of a combination of (i) improved targeting of PL dose to the alveolar region with the aerosol and (ii) the absence of the large liquid bolus and associated negative impacts on lung mechanics.

Of the aerosolized surfactant doses, the lowest dose of 0.61 mg was as effective as the higher dose levels. This is surprising because the response to surfactants is expected to be dose-dependent. The limited response to the escalated aerosol dose may be due to two reasons. First, the 0.61 mg of PL may be sufficiently high to restore lung mechanics as much as possible in the selected model. A dose-response relationship may be seen if lower doses are considered instead of higher. Second, we have observed that the aerosolization device is most efficient, producing the smallest

MMAD, with lower mass loadings of approximately 3 mg of powder.[15], [59], [60] Increasing the loaded mass in the range of 5 to 10 mg increases the MMAD size thereby limiting the amount of aerosol delivered to the distal airways. This limitation will require an improved design of the aerosol generation device for small animal experiments. However, for infants this problem may be more easily overcome as delivered air volumes are increased beyond what can be administered to a rat, which improves aerosolization of higher mass powders. For example, a reasonable tidal volume for a 1600 g infant is approximately 10 ml.[64] Our group has recently developed several inline DPIs that can effectively aerosolize 10 mg and higher doses of EEG powder with 10 ml of air producing aerosols with MMADs in the range of 1.5 μm.[57], [58], [65]

Liquid surfactant has also been used in the form of a nebulized solution to treat surfactant deficiency or lack of surfactant in preterm infants; however, those studies remain inconclusive due to the difficulty of getting the nebulized drug to the airways.[13], [66] Berggren et al.[66] saw no benefit in nebulized surfactant delivered to spontaneously breathing newborns with RDS despite the fact that 480 mg of surfactant was administered in each case. Potential reasons for the lack of response were cited as poor lung delivery efficiency, estimated to be <1% of the administered dose, and very long delivery times, on the order of hours. One recently published study (under evaluation in Phase II clinical trial) observed an equivalent response in terms of lung mechanics of rabbits that received nebulized poractant alfa (brand name Curosurf) at 200 mg/kg and 400 mg/kg to the ones that were treated with instilled surfactant at 200 mg/kg.[67] These results indicate that potential advantages of EEG powder as

surfactant replacement needs to be investigated further to unlock its full potential in the clinic.

Limitations: While the results of this study were promising, there were some limitations. As described above, the emitted aerosol size changes with the mass of loaded dose. Therefore, drug dose delivered to the lungs is not necessarily consistent with the loaded drug mass. Furthermore, it is currently not certain which powder mass formulation delivered the most PL mass to the alveolar region. The current washout model is different from experiments with preterm animal models that are naturally surfactant deficient. Rey-Santano et al.[68] considered both acute and sustained effects of surfactant delivery to premature lambs with RDS. While the preterm model may be more realistic, there is currently no evidence to prove that preterm animal models better predict efficacy in human neonates with RDS compared with SD models. In all animal models, the airway structure is significantly different from that of humans. The next recommended step is the application of the developed therapy in a larger animal closer to the size of a preterm infant, as with a ferret or rabbit model. Finally, we were not able to measure arterial partial pressure of oxygen (PaO2) to confirm a drop in PaO2 as some surfactant depleted methods have done in the past.[54] However, we observed a substantial decreased in compliance in the SD groups compared to the healthy group similar to RDS disease characteristic.[69]

Conclusion: We demonstrated that an EEG Survanta formulation can be effectively aerosolized with 5 ml of air and delivered to a rat SD model in a way that benefits lung

mechanics. The SD model was sensitive to different deliver approaches (instillation vs. aerosolization) and dosages of surfactant. Aerosol delivery significantly improved lung mechanics compared with no treatment in surfactant depleted rats. Aerosol delivery improved lung mechanics better than a 30-fold higher dose of PL administered through liquid bolus, which is the current standard-of-care method for administering surfactants to humans. Of the aerosol doses administered, there was little change in the lung mechanics, which may imply that the administered dose may be reduced below the lowest considered dose of 0.61 mg PL. Histology highlighted that liquid delivery resulted in some alveolar collapse, whereas this was not observed with aerosol delivery. Lastly, none of the treatments caused observable inflammation in the lungs. While these results are promising, longer studies need to be performed to evaluate the potential for side effects of the EEG powder delivery technique.

Chapter 3: A Review of Pulmonary Senescence: Acute Vs. Chronic Injury

INTRODUCTION: 49

LUNGS MECHANICS: COPD, IPF, AND ARDS 50

SENESCENCE: 52

History *52*

Cause *53*

HALLMARKS OF SENESCENCE: 53

DNA Damage: *53*

Cyclin-Dependent Kinase Inhibitors: *54*

Proliferation and Apoptosis: *56*

Senescence Associated Secretory Phenotype: *56*

Clearing Senescent cells: *57*

CONCLUSION AND FUTURE DIRECTIONS: 58

Introduction:

Diseases that affect the lungs can be classified into two main categories: acute and chronic. Chief among chronic lung diseases are chronic obstructive pulmonary disease (COPD) and idiopathic pulmonary fibrosis (IPF). COPD and IPF are very deadly diseases; in fact, COPD is the third leading cause of death [70] while the survival rate for IPF patients after diagnosis is less than 3 years [71]. COPD can be divided into 4 stages from mild to very severe depending on its severity [72]. The leading cause of COPD is smoking or inhaling other smoke-derived particles, such as workers in coal plants. These inhaled particles increase inflammation and cause structural lung changes, leading to airway obstruction [73] and emphysema. However, IPF is an interstitial lung disease of an unknown source (idiopathic) characterized by scarring of the lung tissue and increase scarring causes progressive chronic pulmonary fibrosis characterized by increased inflammation [74].

On the other hand, acute lung injury (ALI) in its most severe form can lead to acute respiratory distress syndrome (ARDS) [41]. ARDS is characterized by enhanced apoptosis of both alveolar endothelium and epithelium, which leads to the destruction of the alveolar barrier [75]. The loss of this barrier integrity leads to increase fluid (edema) and immune cells, namely neutrophil infiltration in the alveoli space. The neutrophils in the alveolar space secrete more cytokines recruiting even more immune cells to the injury site and exacerbating the injury [76]. The increased inflammation and edema hinder gas exchange, and patients may require mechanical ventilation to maintain lung function. However, it has been shown that mechanical ventilation leads to ventilation-

induced lung injury or VILI [77]. The physical force exerted by the air going in and out of the lungs causes structural damages at the cellular and tissue levels. Moreover, it has also been shown that VILI exacerbates the inflammatory environment that also ready exists in the lung of ARDS patients by directing the immune system [78].

These conditions created by both chronic and acute lung disease could lead to cellular senescence. Indeed, senescence has been reported in chronic and acute lung injuries listed above [79]–[81]. In this review, we are exploring the research done in both conditions, and we are also exploring their similarities and differences.

Lungs Mechanics: COPD, IPF, and ARDS

Though COPD and IPF are both chronic pulmonary lung diseases, the lung mechanics of these chronic diseases are different. In COPD, because of the narrowing and significant increase in airway resistance, patients have to take rapid and show breathing, resulting in hyperinflation of the lungs, increasing lung damage [82]. Generally, there is an increase in lung volume in COPD patients and a decrease in transpulmonary pressure. These changes in lung mechanics in COPD patients are due to the breakdown of elastin rendering the lungs less elastic and more compliant [83]. In IPF patients, the lung mechanics are almost opposite to in COPD. IPF patients exhibit increased proliferation of fibroblast and myofibroblast, which exponentially increase extracellular matrix (ECM) deposition in the lungs making the lungs more fibrotic [84]. Increased fibrosis leads to increase transpulmonary pressure decreased lung volume and compliance. In the case of ARDS, there is increased edema and alveolar barrier

destruction. These changes lead to increase resistance and decreased compliance of the lungs. Similar to IPF, there is increased ECM deposition with ARDS, though not as severe as in IPF. Indeed, prolonged ARDS leads to fibrosis.

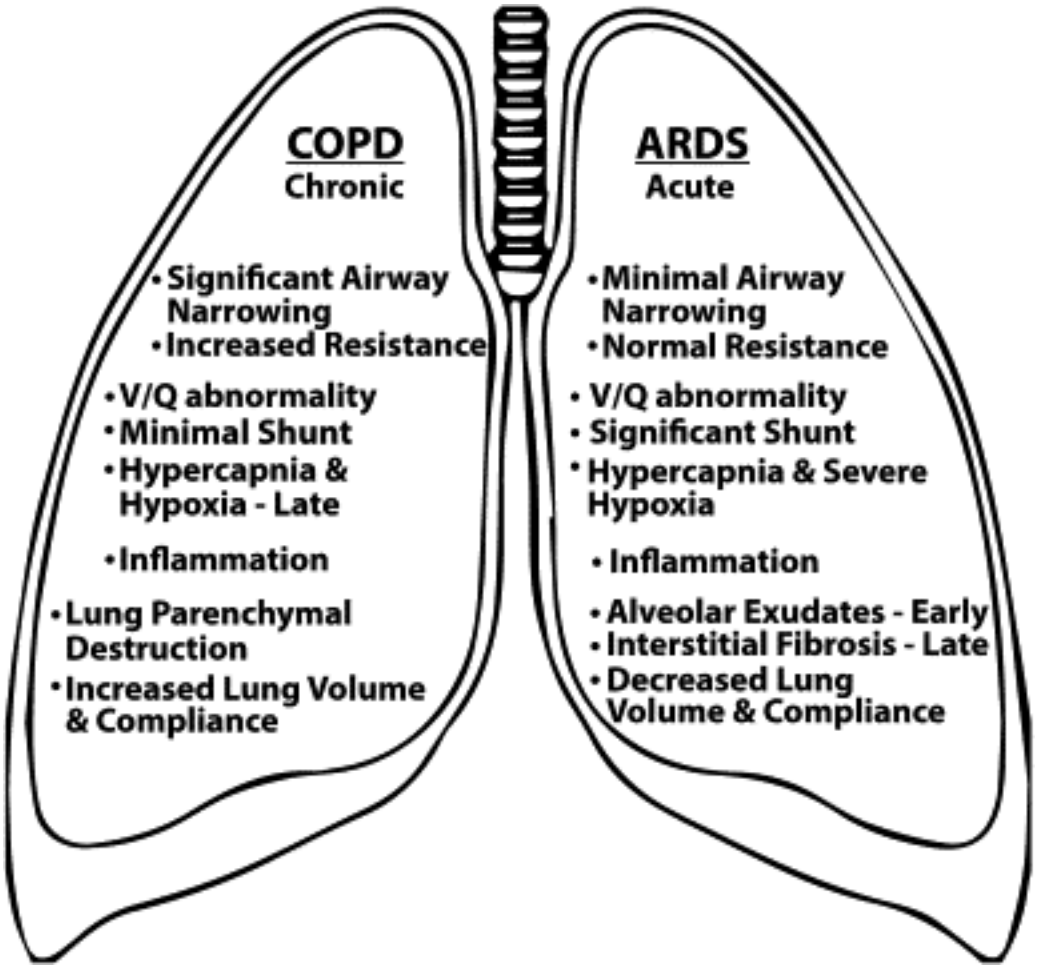

Figure 3. 1 Comparison of different effects brought by COPD and ARDS on the lungs. [85]

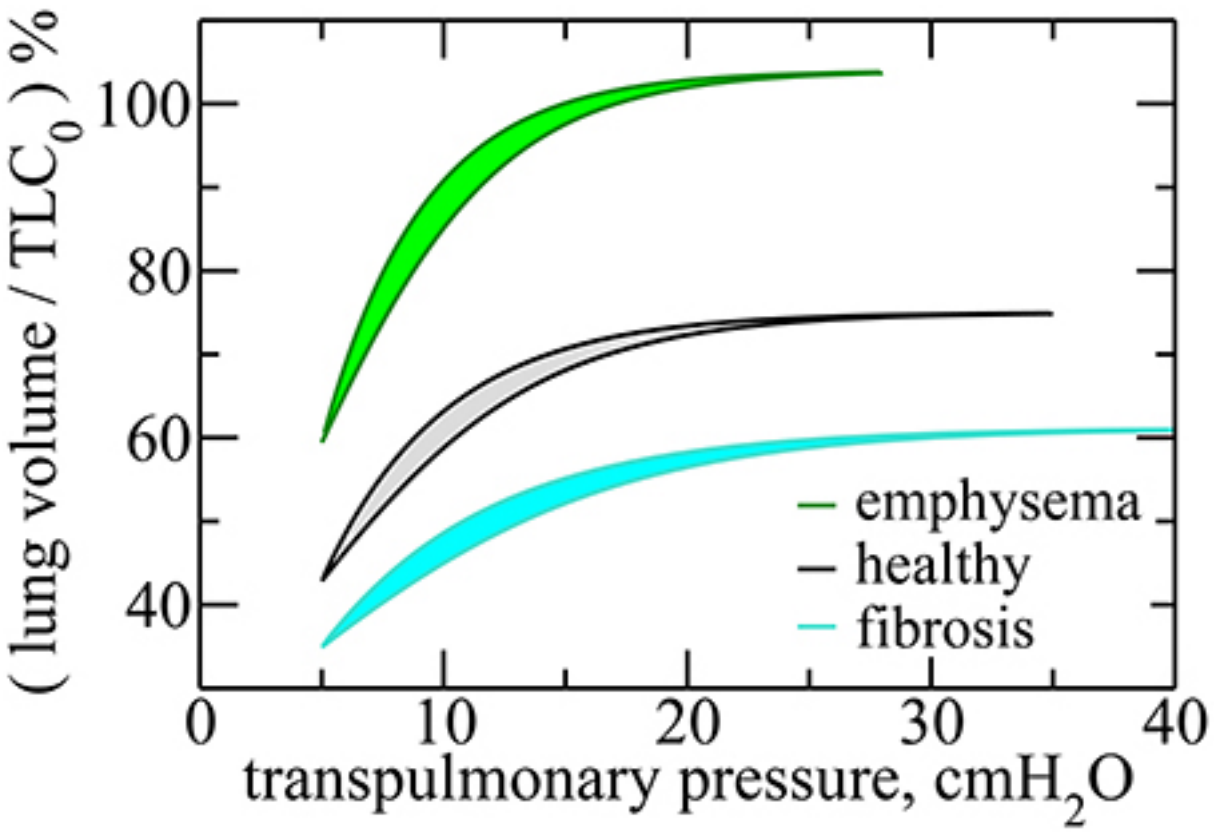

Figure 3.2: Emphysema vs healthy vs fibrotic transpulmonary P-V curves [86].

Senescence:

History

In the 1960s, while working with embryonic human fibroblast cells, Hayflick and Moorhead discovered that those cells ceased to replicate after a certain passage number [87]. However, Hayflick and Moorhead did not characterize this phenomenon as senescence. Later, the scientific community coined that early discovery of Hayflick as senescence from the Latin senex (the growth old). From its etymological definition,

senescence can occur naturally via a normal process of aging or prematurely via injury or diseases [88].

Cause

From its onset, senescence can be caused by multiple factors such as reactive oxygen species (ROS), oncogene, telomere dysfunction, DNA damage, epigenomic dysfunction, and mitogenic signals. Indeed, it has been shown that mitochondrial dysfunction drives the production of ROS which leads to senescence and activation of nuclear factor kappa-light-chain-enhancer of activated B cells (NF-κB) [89] which mediates SASP (senescence associated secretory phenotype), a collection of autocrine and paracrine signals secreted by senescent cells [90]. Meanwhile, the activation of an oncogene mutation can result in a robust and sustained antiproliferation signaling leading to senescence [91]. On the other hand, at the tail end of the chromosomes, telomeres dysfunction or attrition has been associated with cellular senescence [92]. Indeed, telomeres shortening or attrition can occur naturally via multiple cellular divisions [87] or prematurely due to injury and activating the DNA damage response [93].

Hallmarks of senescence:

DNA Damage:

In COPD, IPF, ARDS, and VILI, there has been reports of multiple agents causing DNA damage [94]–[97]. DNA replication stress occurs due to different stressors, intracellular or extracellular, that affect replication. Oxygen radicals, ionizing radiation, polyaromatic

hydrocarbons, UV lights, and chemotherapeutics are agents that can cause DNA damage. These agents can cause different types of DNA damages such as base pair mismatches due to insertion or deletion of nucleotides, DNA adducts due to the attachment of chemical moiety to the DNA, single and double-strand DNA breaks. When these damages occur, there are mechanisms to start the repair of the DNA. These mechanisms include mismatch, base-excision, nucleotide-excision, and double-stranded DNA break repair [98], [99].

DNA damage can also promote ER stress when there is an increased accumulation of misfolded proteins in the ER. These misfolded proteins lead to a cascade of events, including activation of unfolded proteins response (UPR) [100]. UPR is characterized by increased PERK, IRE1, and ATF6 [101]. Together, the accumulation of these latter proteins can lead to apoptosis [102], cell cycle arrest, and senescence-associated secretory phenotype (SASP) [103].

When DNA breaks, DNA damage response is activated. Activation of DNA damage response is sensed by ataxia-telangiectasia, mutated (ATM) and ATR (ATM and Rad3-related), which cause an increase in CHK2 and CHK1, respectively. The cell cycle is temporarily stopped during that process to repair the DNA. If the DNA repair is successful, the cell will return to normal function; if not successful, there are two routes the cell will take: apoptosis or permanent cell cycle arrest, which involve P53/P21 pathway or P16/pRB pathway, which are cyclin-dependent kinase inhibitors [104].

Cyclin-Dependent Kinase Inhibitors:

Cyclin-dependent kinases (CDKs) keep the cell cycle in check and allow its progression. CDKs regulate cell cycle checkpoints and transcriptional events to ensure DNA synthesis cell proliferation. P21, a cyclin-dependent kinase inhibitor, can inhibit CDK4,6/cyclin-D and CDK2/cyclin-E [105], thereby stopping the cell cycle and leading into a state of permanent cell cycle arrest or senescence. In their studies of ARDS, Blazquez-Prietro et al. showed that in the event of ALI, P21 is activated in response to DNA damage generated by mechanical overstretch to limit cellular apoptosis, rendering the effects of this essential cellular senescence pathway beneficial in acute lung injury. However, P16 was not upregulated with acute lung injury in the same study [81].

P16 is activated at a later senescence stage once the cell has established its senescence state. In contrast, P21 occurs in acute senescence at an early stage of senescence and starts fading away over time [106]. Like P21, P16 is also a cyclin-dependent kinase inhibitor that inhibits CDK4,6/cyclin-D, therefore, phosphorylating RB protein and inducing a cell cycle arrest [107]. Given that P16 occurs at the later chronic senescence stage, it has been associated with chronic lung diseases such as COPD and IPF [108], [109].

Indeed, there is increasing evidence that chronic injuries endured by the cells lead to acute inflammation and senescence. In their in vivo mouse model of IPF, Schafer et al. showed that epithelial and fibroblast cells become senescent via increased P21 and P16 in response to chronic lung injury induced by bleomycin. However, the endothelial cells did not exhibit these phenotypes when probed for the same standard senescent markers [24]. In the same train, multiple studies showed an increase of P16 in COPD

models. For instance, using a wild type and P16 knockout mice, Cottage et al. showed that when exposed to cigarette smoke (model of COPD), wild type mice had increased emphysema (a sign of COPD) and increase [109].

Proliferation and Apoptosis:

Senescent cells are strongly resistant to harsh environments and apoptosis. To achieve that, senescent cells have a high production of BCL-2 family proteins acting as antiapoptotic to increase the survival of the cells [110]. In addition to being resistant to apoptosis, senescent cells also lack Ki67, a proliferation marker [111]. In ARDS, VILI, COPD, and IPF models, there is evidence of increasing BCL-2 family proteins [112], [113] and decreasing Ki67 [114]–[116]. Case in point, multiple studies have used drugs such as Navitoclax to target BCL-2 family members by inhibiting them specifically to reduce senescence [24], [117], [118].

Senescence Associated Secretory Phenotype:

Once the cells have established their senescence fate, they do not remain idle as they secrete both autocrine and paracrine signaling to affect themselves and the cells around them. That signaling is collectively known as SASP (senescence-associated secretory phenotype). SASP includes a wide array of molecular signaling that can be categorized as soluble factors, soluble or shed receptors or ligands, nonprotein soluble factors, and insoluble factors. The soluble factors can also be subdivided into multiple groups, including interleukins such as IL6, IL7, and IL-1a and IL-1b. Chemokines such as IL8, MIP-1a, and MCP2. Growth factors and regulators such as KGF, VEGF, and bFGF.

Proteases and their regulators such as MMP1, 3, 10, 12, 13 and 14, TIMP1 and 2, and cathepsin B. Soluble or shed receptors or ligands include ICAM 1 and 3, EGF-R, and OPG. Nonprotein soluble factors include PGE2, nitric oxide, and ROS. Lastly, the insoluble factors include extracellular matrix proteins such as fibronectin, collagens, and laminin [43].

These SASP factors have been reported into both chronic and acute lung diseases. For instance, the exude present in ARDS is reached with activated macrophages secreting chemokines and cytokines such as IL6, IL8, MIP, and TNFa to recruit more immune cells to the injury site [119]. Amongst the first immune cells recruited are neutrophils which secrete more cytokines and chemokines, recruiting even more immune cells to the injury site. In addition to these inflammatory markers, proteases such as MMPs have also been reported in the exudate of ARDS patients [120]. In COPD and IPF, cytokines similar to those reported in SASP have also been reported [121]–[123].

Clearing Senescent cells:

Senescent cells are not entirely invincible. Indeed, immune cells can selectively target senescent cells, but these cells are very nimble at escaping immune cells clearance. [124]. Multiple avenues are used to clear out senescent cells, the so-called senolytic drugs. Senolytic drugs are used to target senescent cells selectively. In the case of COPD and IPF, there are multiple reports of the use of senolytic drugs to target senescent cells specifically. In the case of IPF, senolytic drugs such as dasatinib and quercetin cocktail have been successfully used to selectively clear out senescent cells in an IPF bleomycin mouse model and human clinical trial [24], [32]. In COPD, both

senolytic [125] and senostatics (drugs that inhibit cellular senescence) have been used to alleviate the effects of COPD [126]. However, attempts to remove senescent cells in ARDS and VILI yield a negative outcome for the mice. Moreover, P21 knockout mice had increased apoptosis and the worst histological score after mechanical ventilation [81].

Conclusion and Future Directions:

Though senescence occurs in acute and chronic lung diseases, its characteristics could not be more different. While in acute lung injury, the dominant senescence pathway is the P53-P21 pathway which occurs during early senescence, and in chronic lung diseases, it is P16-pRB. However, acute and chronic lung diseases share most of the SASP phenotypes. There are multiple studies about chronic lung diseases. As seen in this review, all those studies portray senescence as a harmful condition as it contributes to the deterioration of the disease and leads to worse outcomes in patients. Though there are few studies of senescence in acute lung diseases, early studies indicate that the body activates senescence as a mechanism to limit injury and promote healthy cell growth. Despite these findings, more studies need to be done to fully understand senescence in acute lung injury.

Chapter 4: Mechanical Ventilation Induced Senescence in an Acute Model of Lung Injury

INTRODUCTION: 61

METHODS: 62

Animal: *63*

Sample Collection: *63*

In vitro cell stretch: *63*

qPCR: *64*

Inflammatory Cytokine Analysis: *64*

Immunofluorescent staining: *65*

Tissue Protein extraction: *66*

Western Blot: *66*

TUNEL staining: *67*

Statistical analysis: *67*

RESULTS: 67

Mechanical Ventilation and Age Cause Structural Damage and Increased Polymorphonuclear in BALF *67*

Lung Mechanics: *70*

TUNEL: *70*

Presence of Senescence-like phenotypes in Mechanical Ventilation induced Acute Lung Injury *73*

Age and mechanical Ventilation lead to an Increase in Cells expressing keratin 8 (KRT8+): *76*

Cell stretch-induced senescence markers in human SAEC *78*

Inhibition of P38 Decreased KRT8+ Cells: *82*

DISCUSSION: 85

Damage due to MV *85*

DNA damage and P21 in VILI *86*

The potential role for P38 ..... *88*

Limitations: *88*

Conclusion: *90*

Introduction:

ARDS has a high mortality rate and disproportionally affects the elderly population with a higher mortality and incidence rate [127]. There are signs of hindered gas exchange amongst ARDS patients [2], leading to mechanical ventilation. Despite the benefits of mechanical ventilation at mitigating the effects of ARDS and facilitating the gas exchange, the constant strain and stress created by the former due to the air moving in and out of the alveoli may worsen the injury and lead to ventilation-induced lung injury, VILI [129]. VILI is characterized by biotrauma due to the increased inflammation; volutrauma due to the overextension of the alveoli caused by air going in and out of the lungs during ventilation; and atelectrauma caused by the constant collapse and reopening of the alveoli [130]. These characteristics of VILI, especially biotrauma and volutrauma, can result in cascades of events that can cause the alveoli cells to become damaged and change phenotype, therefore creating a hostile environment. The hostile environment created by VILI coupled with inflammation observed in ARDS may lead to senescence.

Senescence is an irreversible terminal cell cycle arrest process in which proliferating cells stop responding to replication-promoting stimuli. However, evidence suggests that senescence can occur prematurely in response to injury [131]. Because of its heterogenicity across different tissues and conditions, senescence is a complex phenomenon that is poorly understood. Furthermore, more is known about senescence in chronic lung diseases than acute. In senescence, cyclin-dependent kinase inhibitors such as P21 and P16 are upregulated. While P21 plays an essential role in early senescence, P16 is accumulated at a later stage of senescence [106]. There is also

evidence that P21, not P16, is upregulated with VILI [81]. Senescent cells also produce autocrine and paracrine signaling collectively known as senescence-associated secretory phenotype, SASP. SASP mediators include pro-inflammatory cytokines such as IL-6, which can exacerbate inflammation [132].

Though some parts of the senescence mechanism have been investigated, more still needs to be done to fully understand the mechanism of senescence in VILI and other diseases. One of the mechanisms of senescence is the DNA damage response pathway which could be activated via mechanotransduction. Cyclic stretch like the one generated by mechanical ventilation can break DNA strands down via MAPK activation [133], leading to upregulation of DNA damage proteins such as ɣH2AX [134]. Activation of ɣH2AX, in turn, will lead to the activation of P21 [135]. P38-MAPK is also known to activate the P53-P21 pathway resulting in cellular senescence [135]. However, this pathway has not been investigated in the context of senescence in acute diseases or VILI.

In this research, we are investigating whether mechanical ventilation promotes senescence-like phenotypes. We also examine whether stretch induces DNA damage response, leading to senescence. Finally, we are using a P38-MAPK inhibitor to understand the mechanism of senescence in VILI. We hypothesized that mechanical ventilation would lead to DNA damage and senescence-like phenotype via P38-MAPK activation and blocking it will reduce this phenotype.

Methods:

Animal: Male young (8-10 weeks) and old (20-22 months) C57BL/6 mice were acquired from the National Institute on aging and housed at the VCU vivarium. All procedures performed on the mice were approved by VCU Institutional Animal Care and Use Committee (IACUC). Mice were mechanically ventilated at 0 PEEP and 35 and 45 cmH2O for young and old mice, respectively, for 2 hours. Lung mechanics were measured at 30-minute increments for the duration of ventilation.

Sample Collection: At the end of the 2-hour mechanical ventilation, blood was collected from the vena cava and centrifuged to obtain plasma. As previously described, gravity-assisted bronchoalveolar lavage (BAL) was performed [45]. Briefly, PBS was instilled into the mice lungs and collected and repeated twice. The BAL fluid was then centrifuged, the supernatant was transferred onto a new tube for later processing. The cells were resuspended then cytospun onto a microscope slide. WBC analysis was performed by counting 300 cells while refraining from the peripheral edges of the microscopy region. The different immune cells were distinguished and quantified.

In vitro cell stretch: Human small airway epithelial cells (SAEC) were purchased from Promocell (C-12642) and cultured according to their recommendations with a supplied SAEC growth media. SAEC were plated on Bioflex culture plates (Flexcell international Corp., BF-3001) for 48 hours for acclimation. Then, media change was performed; some wells received DMSO vehicle and others SB203580 (a P38 inhibitor) for 30 minutes. Media change was performed again to rid the wells of the vehicle and inhibitor.

The cells were then stretched at 20% change in surface area for 24 hours and at 0.33 Hz to cause injury.

qPCR: For lung tissues, small lung fragments of about 50 mg were homogenized with Trizol (ThermoFisher, 15596026). RNA extraction was performed as recommended by the manufacturer. Briefly, after homogenization, 200 ul of chloroform was added per 1 ml of Trizol. Phase separation was performed via centrifugation, then the clear phase, which contained RNA, was then separated. *In vitro* experiments, cells were lysed using RLT buffer to obtain a cell lysate containing RNA. RNA isolation of both tissues extracted RNA, and cell lysate was performed using Qiagen RNeasy kit. cDNA conversion was performed using a Bio-Rad iScript cDNA synthesis kit (Bio-Rad, 1708891). cDNA and Bio-Rad SsoAdvanced universal SYBR green (Bio-Rad, 1725274) was used for gene amplification. Primers: human 18s F: 5'-TAACCCGTTGAACCCCATTC-3' R: 5'-TCCAATCGGTAGTAGCGACG-3', human P21 F: 5'-TGTCCGTCAGAACCCATGC-3' R: 5'-AAAGTCGAAGTTCCATCGCTC3', mouse 18s: F: 5'-GCAATTATTCCCCATGAACG-3' R: 5'-GGCCTCACTAAACCATCCAA-3', mouse P21 F: 5'-GACAAGAGGCCCAGTACTTC-3' R: 5'-GCTTGGAGTGATAGAAATCTGTC-3'

Inflammatory Cytokine Analysis: IL6 ELISA (R&D system, DY 406) was performed according to the manufacturer's protocol. Briefly, 96-well ELISA plates were coated using a captured antibody overnight. The next day, the plate was washed (0.05% Tween 20 in PBS) and blocked (R&D system, DY995) at room temperature using the

reagent diluent for 2 hours. Standards and samples were loaded into the plates and incubated at room temperature for 2 hours. The plates were then washed, and the detection antibody was added for 2 more hours. The plates were then incubated with Streptavidin-HRP and substrate solution solutions, respectively, for 20 minutes, each with washes in between. Diluted sulfuric acid at the concentration recommended by the manufacturer was used to stop the reaction. The plates were read at 450 nm with wavelength correction.

Immunofluorescent staining: Immunofluorescent staining was performed according to the antibody manufacturer protocol with modifications. Briefly, when stretch experiments concluded, the cells were fixed then permeabilized. When appropriate, the cells were blocked for 2 hours at room temperature using 10% normal goat serum or BSA. The slides were then incubated overnight at 4C in primary antibody. The next day, the slides were rinsed then incubated with a secondary fluorophore antibody for an hour. For tissue embedded sections, the slides were deparaffinized, and antigen retrieval was performed before the permeabilization. Primary antibodies: mouse anti-gamma H2AX (Novus Biologicals, NB100-74435), rabbit anti-Ki67/MKi67 (Novus Biologicals, NB500-170SS), rabbit anti-SP-C (Bioss, bs-10067R), rat anti-KRT8 (CreativeBiolabs, CBDH1469). Goat anti-Rat IgG (H+L) Alexa Fluor 555 (ThermoFisher scientific, A-21434), Goat anti-Rabbit IgG (H+L) Alexa Fluor 647 (ThermoFisher scientific, A-21245), Goat anti-Mouse IgG (H+L) Alexa Fluor 488 (ThermoFisher scientific, A-28175). Images were taken using a Nikon Eclipse Ti2 microscope or a Zeiss axioobserver Z1 fluorescence microscope; the images were then quantified using Fiji.

Tissue Protein extraction: cytoplasmic and nuclear proteins were extracted according to the Millipore sigma protocol with minor modifications. Briefly, tissues were lysed using hypotonic buffer (10 mM HEPES, pH 7.9, with 1.5 mM MgCl2 and 10 mM KCl) containing Dithiothreitol (DTT), protease and phosphatase inhibitors. Then the tissues were homogenized and centrifuged at 10,000 g for 20 minutes. The supernatant, which contained cytoplasmic proteins, was preserved. The crude nuclei pellet was resuspended in 140 ul of extraction buffer containing DTT, protease, and phosphatase inhibitors. The solution was gently shaken for 30 minutes then centrifuged for 5 minutes at 20,000 g. The supernatant was transferred to a new tube and chilled at -70 C for later processing.

Western Blot: Western blot was performed according to the manufacturer's protocol. Briefly, BCA was performed on the freshly isolated proteins using a Pierce BCA protein assay kit (Sigma, 23227) to determine the protein concentration. Electrophoresis was performed using 30 ug of proteins loaded into each 10-well gel; proteins were then transferred from the gel onto a membrane. The memiphbrane was blocked for 1 hour, followed by primary antibody incubation overnight at 4 C. The next day, the membrane was rinsed and incubated in a solution of HRP bound secondary antibody for 1 hour, followed by rinsing and incubation in Pierce ECL western blotting substrate (ThermoFisher, 32106) for 5 minutes and imaged. Bands densities were analyzed using BioRad Image Lab software. Rabbit anti-histone H3 (Novus Biologicals, NB500-171),

mouse anti-gamma H2AX (Novus Biologicals, NB100-74435), anti-rabbit IgG HRP-linked antibody (Cell Signaling Technology, 7074S), anti-mouse IgG HRP-linked antibody (Cell Signaling Technology, 7076S).

TUNEL staining: Click-iT™ Plus TUNEL assay for in situ apoptosis detection with Alexa Fuor™ 647 was performed according to the manufacturer protocol (ThermoFisher Scientific, C10619). Briefly, slides were deparaffinized using xylenes, decreasing percentages of ethanol, saline solution and PBS. The tissue slides were fix and permeabilize using 4% paraformaldehyde and proteinase K, respectively. Then TdT reaction was performed by incorporating EdUTP into dsDNA strand breaks. Finally, fluorescence Click-iT™ plus reaction was performed to detect EdUTP, the the slides were mounted using ProLong™ Gold Antifade Mountant with DAPI (ThermoFisher Scientific, P36931).

Statistical analysis: Subjects were randomly assigned to different groups. Power analysis was estimated based on previous work. A minimum of 3 mice per group was used. One-way and two-way ANOVA followed by posthoc Tukey's multiple comparison test were performed when appropriate to compare multiple groups. A T-test was also performed to compare two groups. GraphPad Prism 6 was used for statistical analysis.

Results:

Mechanical Ventilation and Age Cause Structural Damage and Increased Polymorphonuclear in BALF

To assess the effects of mechanical ventilation on the lung structure and physiology, lung histology, lung mechanics perturbation maneuvers, and PMN (Polymorphonuclear leukocytes) count were performed. H&E-stained lung sections showed that high-pressure MV caused increased structural damage on the lungs of both young and old mice. Furthermore, when considering age alone, old mice inherently showed more significant structural damage signs than young mice without mechanical ventilation (figure 4.1 A). BCA results showed increased protein in the BALF with age and ventilation. These results suggest that mechanical ventilation and age are cofactors for lung injury (figure 4.1 B).

Similarly, the count of PMN on BALF showed a significant increase in PMN intrusion in the alveoli space with mechanical ventilation in both age groups. At baseline, without mechanical ventilation, old mice showed a more significant amount of PMN in the BALF compared to the young non-ventilated. However, in the old group who did not receive mechanical ventilation, we did not see much increase in PMN compared to the young non mechanically ventilated (figure 4.1 C).

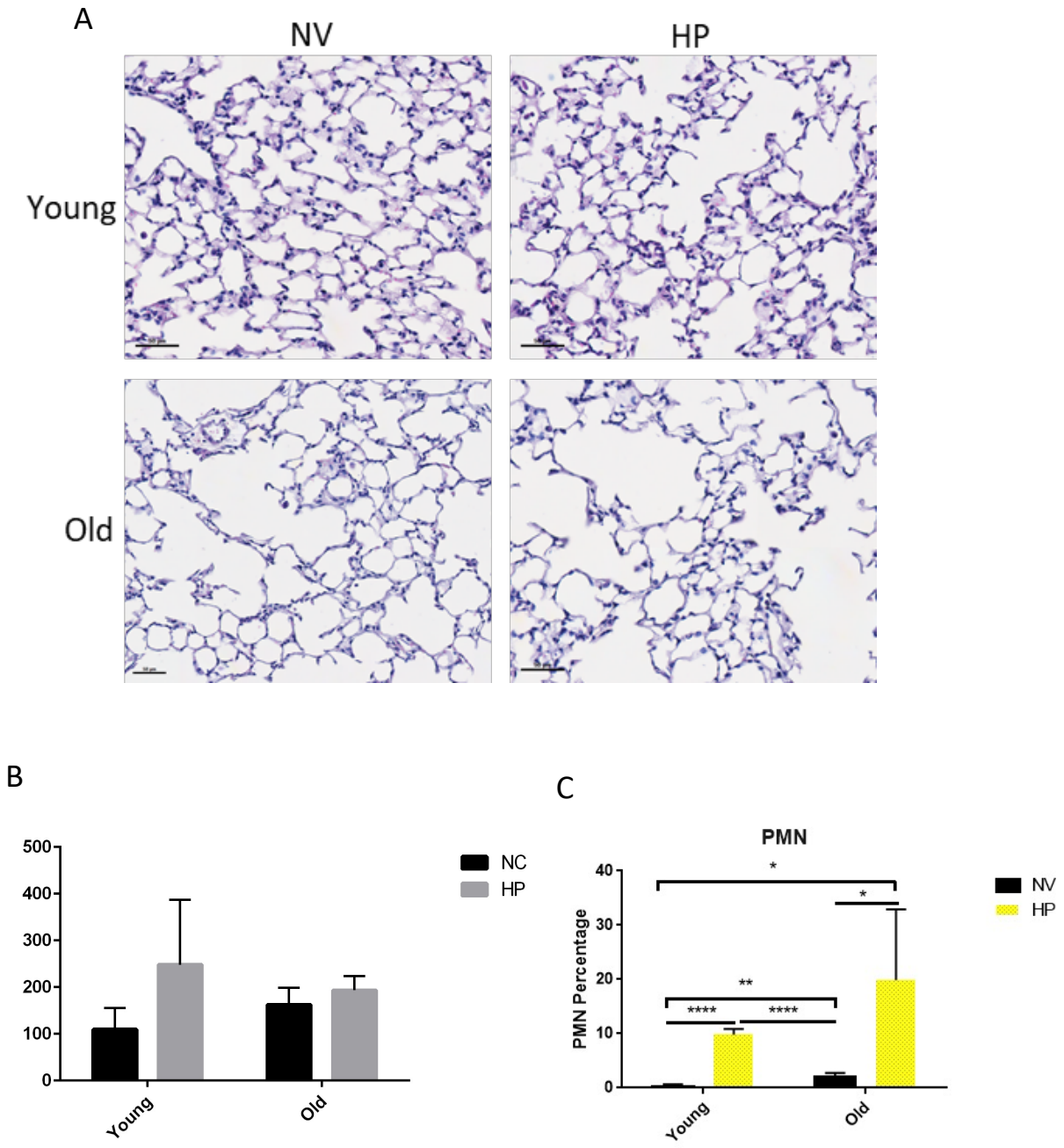

*Figure 4. 1 Lung Mechanics, BCA and White Blood Cell Count: A: Lung histology B: BCA (N=3-5) C: PMN (N=4-5) of mechanically ventilated mice showing increased lung injury with mechanical ventilation and age. * $p < 0.05$, ** $p < 0.01$ and **** $p < 0.0001$.*

Lung Mechanics:

From the PV-loops, we first noticed in both young and old mice that the loops have shifted up and a bit to the left after 30 minutes of ventilations, suggesting an increase in compliance. After one hour on the ventilator, both age group PV-loops were shifted back down and to the right, closer to the baseline's loop. However, two hours after mechanical ventilation, in the young mice group, there was a shift down and to the left compared to baseline compliance suggesting a decrease in compliance. After that initial increase in compliance, the loop returned to baseline in the old subjects (figure 4.2).

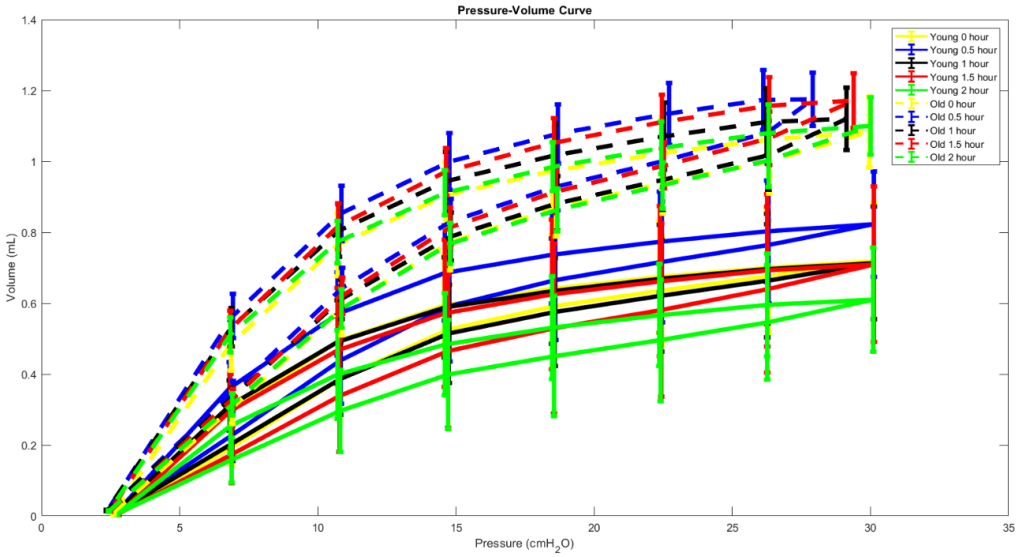

Figure 4. 2 Single compartment compliance showing changes in the lung mechanics of mechanically ventilated mice. N = 3-5 mice

TUNEL:

TUNEL was used to detect apoptosis in the fixed lung tissue postmortem. There was an increase in TUNEL positive cells with mechanical ventilation in the young mice group. Moreover, non-ventilated old mice showed signs of apoptosis though not in a considerable amount. However, old mice showed more apoptotic cells than any other groups when mechanically ventilated. These results suggest that the high-pressure mechanical ventilation settings used in this study caused damage at the tissue level, which changed the lungs' mechanics, and damage at the cellular level, which manifested by increased apoptosis in both you and old groups (figure 4.3).

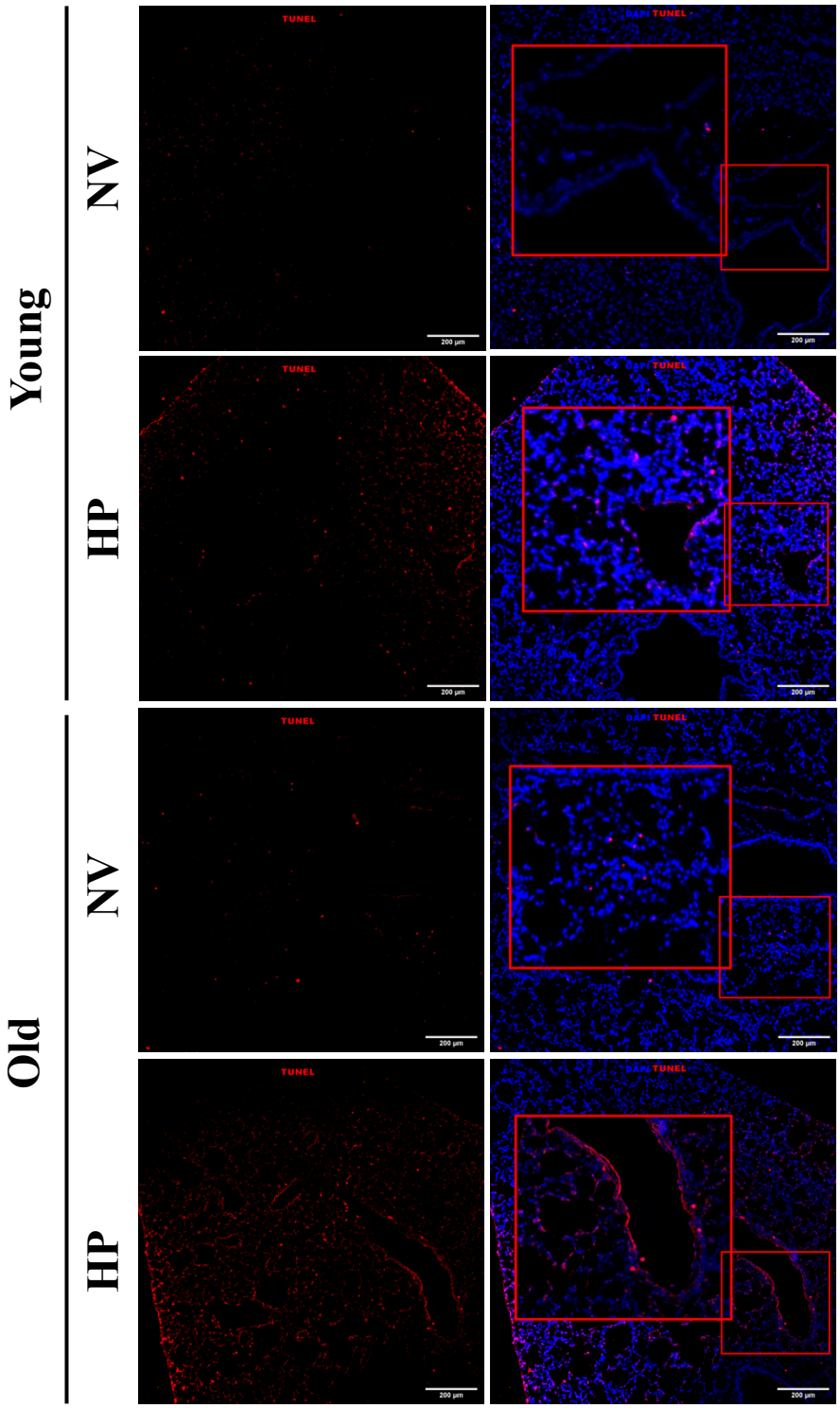

Figure 4. 3 TUNEL Staining showing increased apoptosis with mechanical ventilation and with age.

Scale bar 100 um

Presence of Senescence-like phenotypes in Mechanical Ventilation induced Acute Lung Injury

DNA Damage increases with age, and HP

One known pathway leading to cellular senescence is the DNA damage response pathway. In this experiment, after mechanical ventilation, we probed for ɣH2AX, a DNA damage marker in the homogenized bulk lung nuclear protein. Mechanical ventilation of both young and old mice yielded an increase of ɣH2AX, a sign that the mechanical force generated by the mechanical ventilator is transduced from the extracellular space in the cytoplasm and the nucleus of the cells causing damage to the nucleus. Moreover, in the old mice population, there was an increase in ɣH2AX with no mechanical ventilation compared to the young mice who were not mechanically ventilated, suggesting that old mice inherently show signs of DNA damage probably due to age (figure 4.4 A).

HP is correlated with P21 gene expression, SASP, and decreased proliferation:

P21, a protein involved in the cell cycle, was analyzed. There was an increase in P21 gene expression with mechanical ventilation. Young and old mice that were mechanically ventilated had a significant increase in P21 compared to the young non-ventilated. Mechanically ventilated old mice also showed a significant increase in P21 compared to the old non-ventilated. These results suggest that mechanical ventilation plays a role in P21 regulation. However, we did not observe a significant increase in P21 gene expression with age alone; this could be because P21 is an early marker of senescence (figure 4.4 B).

Ki67, a proliferation marker, did not increase with age or mechanical ventilation. Ki67 level was significantly lower in the young mice when mechanically ventilated compared

to the young non-ventilated. This is consistent with the P21 marker increase suggesting that mechanical ventilation and age initially lead to increased P21 gene expression and the lack of proliferation (figure 4.4 C).

IL6, a pro-inflammatory marker part of the SASP, was also probed in the BALF. It has been previously shown that when cells become senescent, they produce cytokines which include IL6 [132]. Mechanically ventilated mice showed an increase in IL6 level (figure 4.4 D); this is on par with P21 gene expression groups. In all, these results suggest that increased DNA damage, high P21 gene expression levels, and reduced Ki67 (proliferation), all hallmarks of cellular senescence, also lead to increase SASP.

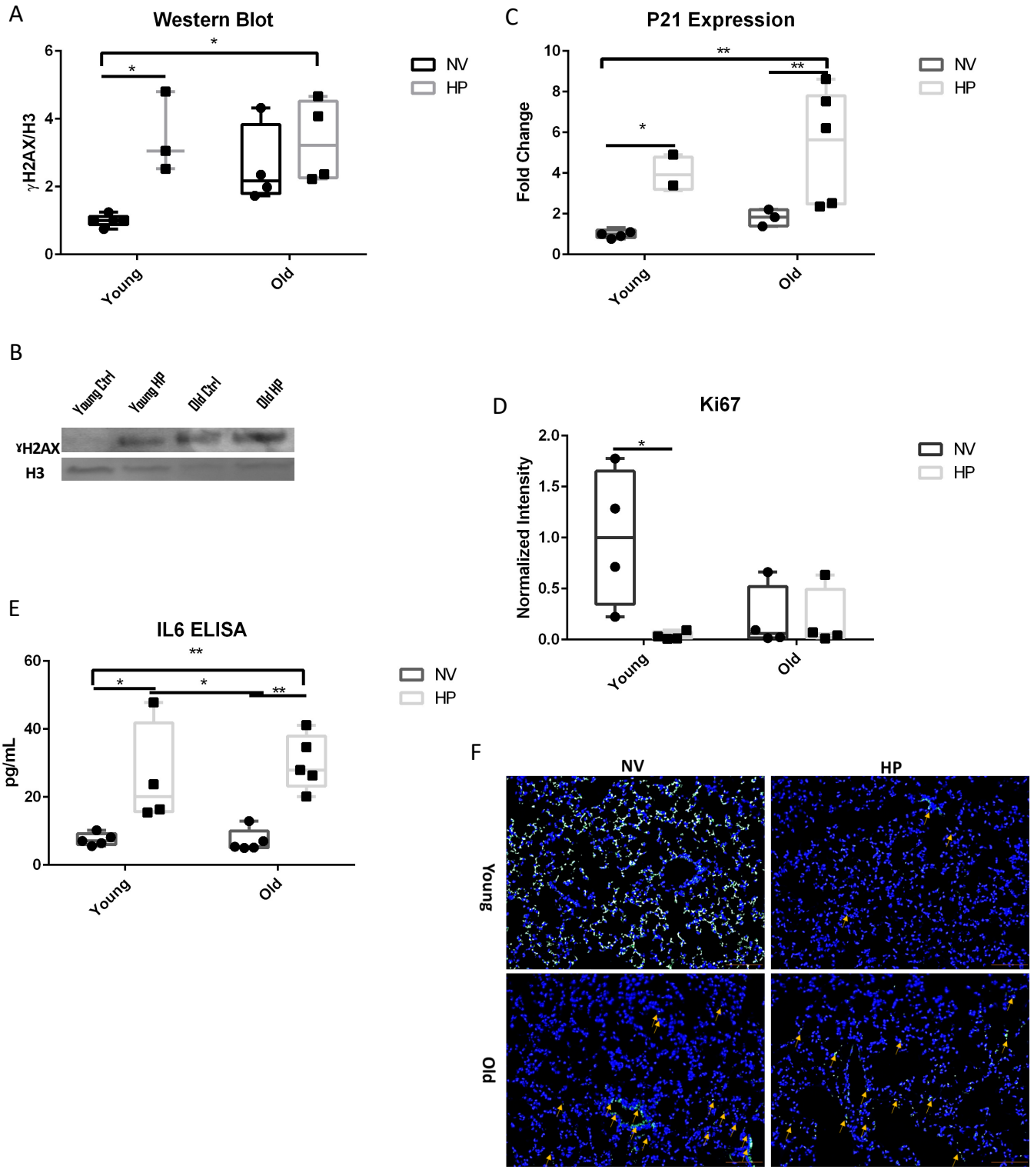

Figure 4. 4 Evidence of Senescence in VILI A: γH2AX increased with ventilation in both age groups. B: P21 increased with ventilation as well. C: Decreased Ki67 with age and

*with mechanical ventilation. D: IL6 increased as a result of mechanical ventilation. Scale bar 100 um. N = 3-5. * p < 0.05, ** p < 0.01.*

Age and mechanical Ventilation lead to an Increase in Cells expressing keratin 8 (KRT8+):

There are mainly two cell types in the alveolar epithelium, alveolar type 1 and type 2 (AT1 and AT2). It has been shown that due to mechanical cues and in certain diseases, AT2 differentiate into AT1[136]. It has also been shown that before differentiating to AT1 due to various stimuli, AT2 cells go through a transient state which is positive for Krt8 [137]. These transient Krt8+ cells are also more prone to DNA damage [138]. To test if mechanical ventilation resulted in increased Krt8+ cells, we stained the lungs of the mice with anti-krt8 antibodies. Compared to the young non-ventilated mice, there were an increase in Krt8+ cells in the young mechanically ventilated mice. Moreover, there was an increase in Krt8+ cells in the old mice group, regardless of ventilation status, compared to the young non-ventilated mice. The increase in Krt8+ cells (which are more prone to DNA damage) with age and mechanical ventilation could explain why there was an increase in DNA damage in those groups compared to the non-ventilated young mice (figure 4.5).

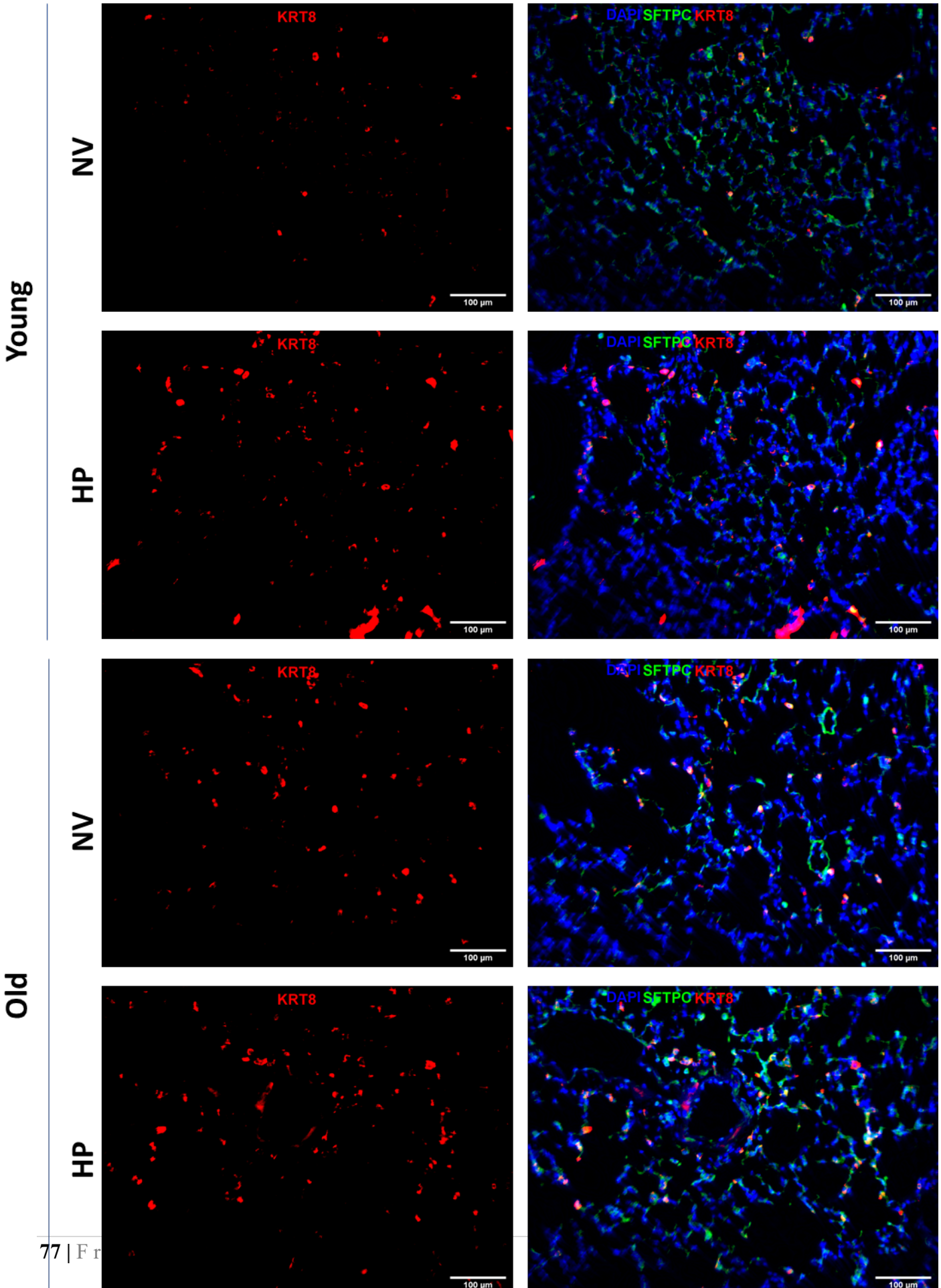
Young
Old
NV
HP
NV
HP
KRT8
DAPI SFTPC KRT8
100 µm

Figure 4. 5 Increase Krt8 positive cells with age and mechanical ventilation. Scale bar 100 μm

Cell stretch-induced senescence markers in human SAEC

We first wanted to know if human SAEC undergoes DNA damage in response to cyclic stretch, potentially leading to cellular senescence. Compared to the static group, there was more DNA damage manifested by an increase ɣH2AX in the stretch SAEC group (figure 4.7). Similarly, there was an increase in P21 in stretch SAEC compared to the static group (figure 4.6). This is consistent with the results obtained in the mechanically ventilated old mice; The SAEC were from patients aged 51-66 years. As in old mice, there was an increase in ɣH2AX with mechanical stretch compared to the static group. In addition, it was only when mechanically ventilated that the old mice showed an increase in P21.

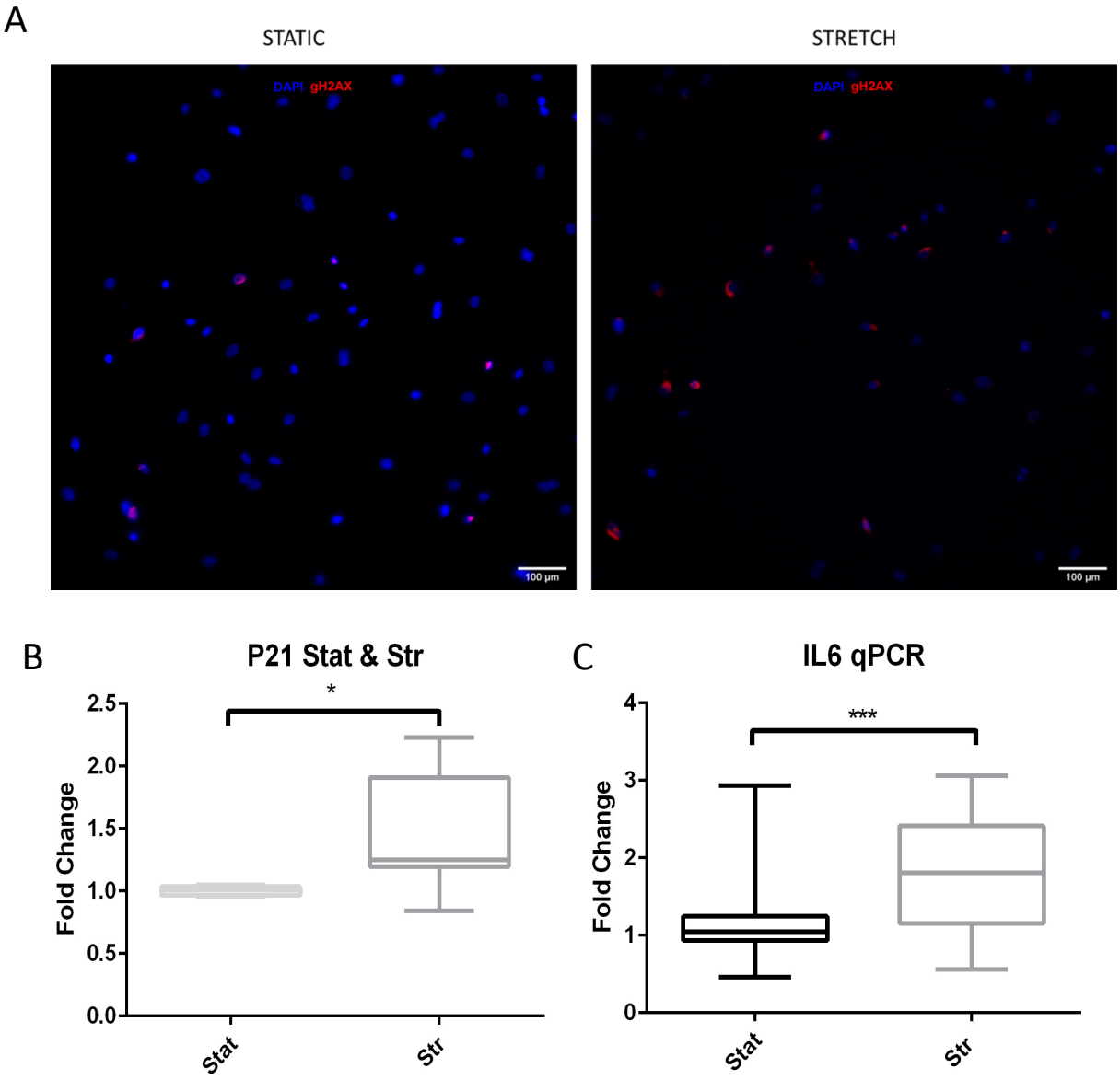

*Figure 4. 6 Gene expression and immunofluorescent staining of human SAEC cells at static and stretch conditions A, B & C: Stretch Caused DNA damage, a significant increase in P21, and an increase in IL6 in SAEC. Scale bar 100 µm. N = 4-5. * p < 0.05, *** p < 0.001, **** p < 0.0001.*

Since it had been reported that activation of P38-MAPK leads to an increase in P21, we inhibited P38-MAPK using a P38 inhibitor. However, when given the P38 inhibitor, there was a downregulation of P21 with stretch compared to the vehicle control (figure 4.8), suggesting that P38 is involved in cellular senescence pathways in this *in vitro* model VILI. Nevertheless, inhibition of P38 did not decrease ɣH2AX protein level in the stretched SAEC (figure 4.9), possibly due to DNA damage being upstream of P38-MAPK. It is also worth noting that there was decreased cell proliferation in all stretch groups, including stretch plus P38 inhibitor; this could be due to stretch causing DNA damage and regulating cell cycle via P21.

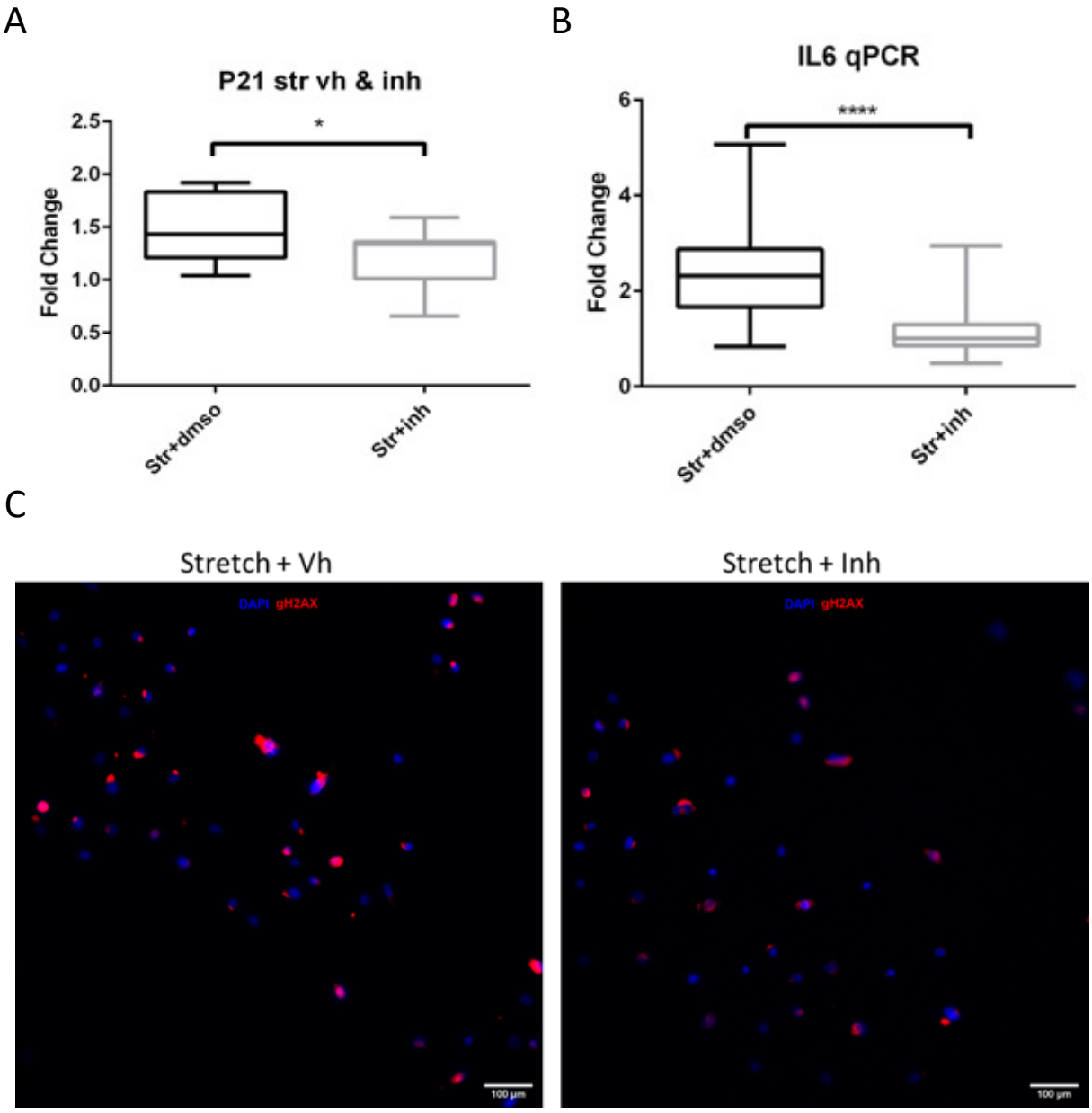

*Figure 4. 7 Gene expression and immunofluorescent staining of human SAEC cells at static and stretch conditions with DMSO and P38 inhibitor A, B & C: P38 inhibition reduces P21 and IL6 but does not affect DNA damage. Stat: static, str: stretch, Vh: vehicle and inh: P38 inhibitor. Scale bar 100 μm. N = 4-5. * $p < 0.05$, *** $p < 0.001$, **** $p < 0.0001$.*

Inhibition of P38 Decreased KRT8+ Cells:

Next, we investigated the effects of P38 inhibitor on distal alveoli cells. Static or stretch conditions both had a high amount of KRT8+ cells. This is perhaps due to the age of the donor (66 years old). However, when given the P38 inhibitor, there was a decreased in KRT8+ cells. Finally, we did not observe any noticeable changes in RAGE (receptor for advanced glycation end-products), an AT1 marker.

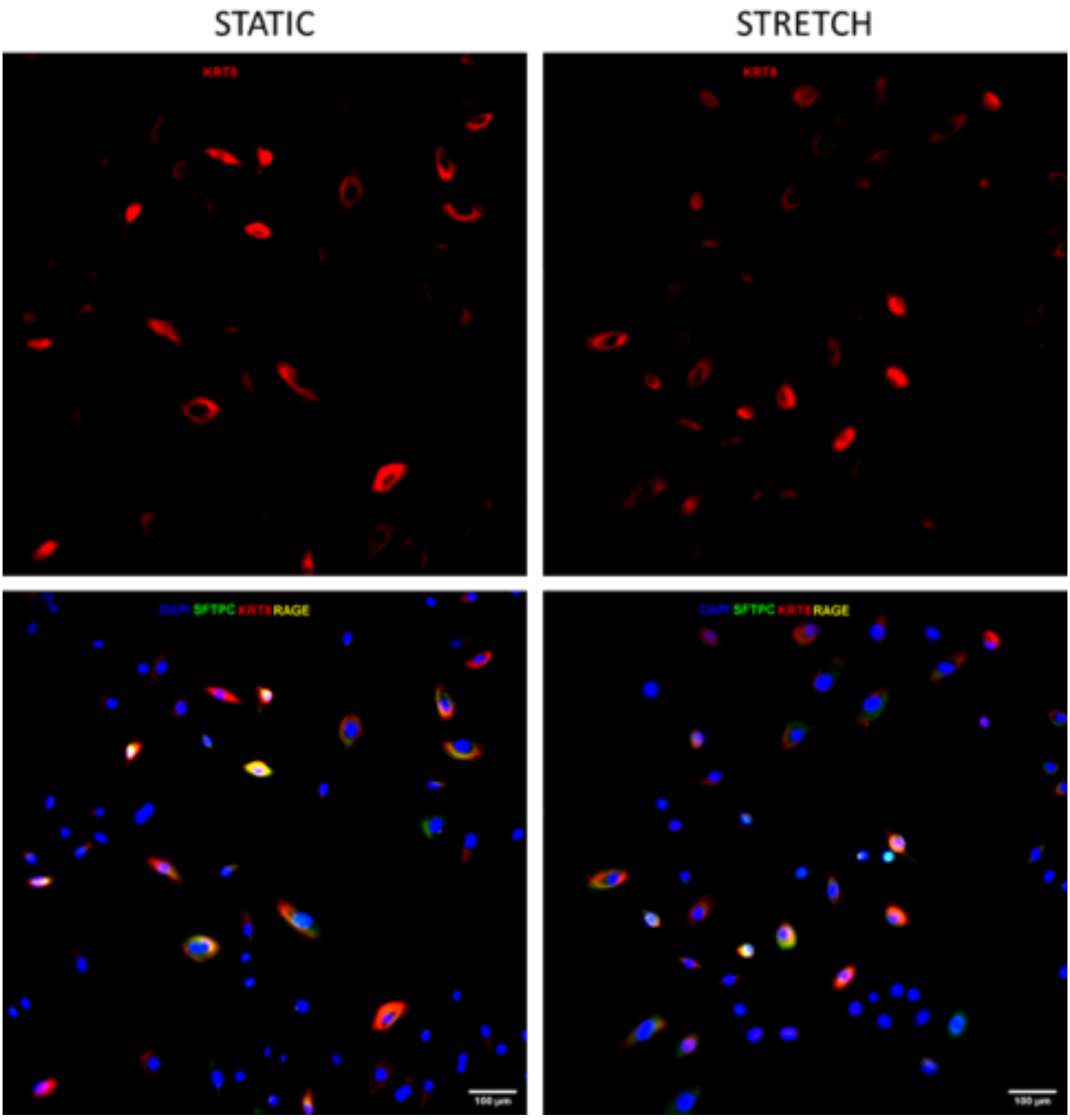

Figure 4. 8 Stretch SAEC Does not Increase KRT8. RAGE, an AT1 marker. Scale bar 100 μm.

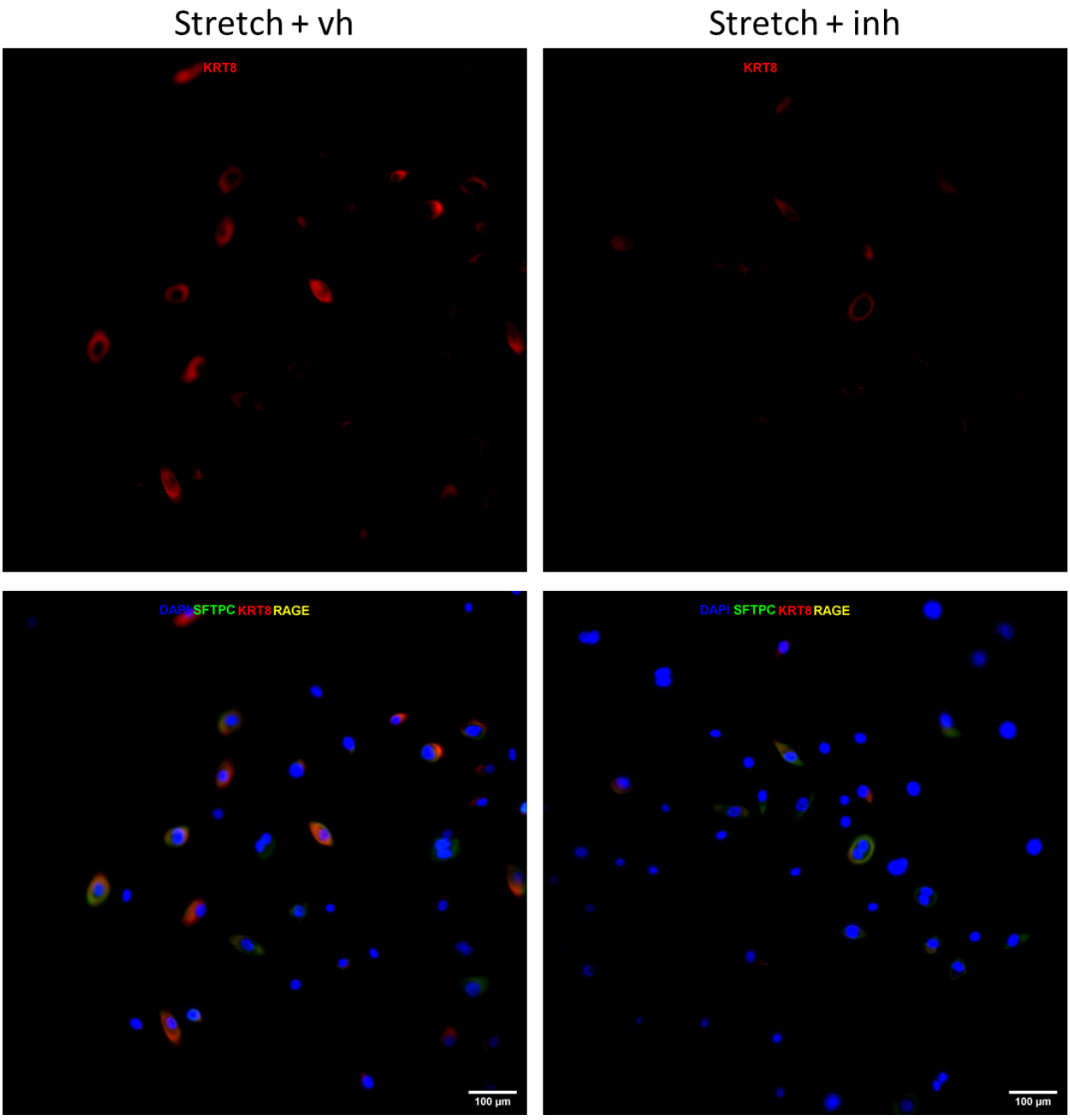

Figure 4. 9 P38 Inhibitor Decrease KRT8+ Cells. RAGE, an AT1 marker. *Scale bar 100 µm.*

Discussion:

With the advent of novel respiratory diseases, including the current pandemic caused by COVID-19, more and more patients are ending up on mechanical ventilators, which lead to further injuries such as VILI. Despite being a lifeline for some patients, mechanical ventilators can leave lifelong damages [139] that are still not fully understood. In this study, we have developed both in vitro and in vivo models to simulate different damages caused by mechanical ventilation. We used these models to study the different mechanisms potentially involved in VILI, which can better understand the disease for future therapies.

Damage due to MV

It has been extensively documented that the shear forces generated by mechanical ventilation exacerbate lung injury [140]. The characteristics of these lung injuries include the changes in lung structure. For instance, other studies, including ours, have shown that after mechanical ventilation, the airspace of mice becomes enlarged [141]–[143]. This is in line with what we observed in the lung histology of the mechanically ventilated mice. This airspace enlargement is also more pronounced in old mice generally, which is then exacerbated with mechanical ventilation (figure 4.1 A) due to the change in the lung's parenchyma and alveolarization with age [144]. These structural changes in the lung could also lead to a change in the lung's mechanics.

The structural damage and increased alveolarization, factors related to airspace enlargement, increase lung volume and compliance [145]. The increased alveolar space and the structural damage observed in their histology (figure 4.2) could explain why the

old mice have inherently a higher lung single compartment static compliance compared to the young mice. However, other studies have shown that mechanical ventilation leads to a decrease in compliance [146], as observed in the young group in this study. Multiple studies have shown that structural lung damage leads to fluid exudation in the alveolar space [147]–[150]. This exudative phase is the cause of acute inflammation and leads to the release of the pro-inflammatory cytokine, which will then recruit immune cells to the site of the injury [151]. Amongst the recruited immune cells, PMN appears always to be recruited at a higher amount with ventilation. Bobba et al. have shown that PMNs are mechanosensitive, and they release cytokines in response to barotrauma, increased pressure usually associated with mechanical ventilation that causes alveolar damage [152]. The presence of PMN with mechanical ventilation correlate to our data where there was a high rise of PMN with ventilation in both young and old group.

DNA damage and P21 in VILI

In addition to causing structural lung damage and recruitment of PMN, Blazquez-Prieto et al. have shown that when mechanically ventilated, mice exhibited a change in the nuclear envelope which coexisted with an increase ɣH2AX, a marker of DNA damage [81]. Moreover, increased accumulation of ɣH2AX has been associated with apoptosis [153] and cellular senescence [154]. Indeed, when cells sense DNA damage, they try to repair it by activating DNA damage response and increasing ɣH2AX, which could lead cells to cell cycle arrest and adapting senescence and a pro-inflammatory phenotype (SASP) [155] as a protective mechanism acutely to prevent further injury. However, activation of DNA damage response can also lead to apoptosis to clear out damaged

cells [156]. Together with our results, where there was an increase in DNA damage manifested by increased ɣH2AX in both *in vitro* and *in vivo* experiments, these findings suggest that mechanical ventilation leads to early signs of senescence.

Strunz et al. have shown that epithelial cells in the alveolar are amongst the cells that experience DNA damage and apoptosis due to ventilation [137]. Apoptosis was further confirmed by TUNEL staining (figure 4.3), where mechanically ventilated mice (young and old) had larger total TUNEL positive cells than those that were not. The alveolar epithelium comprises two main cell types: AT1 (RAGE positive) and AT2 (SFTPC positive) cells. During homeostasis and injury repair, AT2 cells are crucial to replacing AT1 cells which are terminally differentiated [136]. However, AT2 can also adopt a transient phenotype (which stain positive for KRT8) more susceptible to DNA damage. In this study, with mechanical ventilation and age, we observed an increase of KRT8 positive cells; but it was not until stretched that we had increased DNA damage with age. The susceptibility of these transient cells to DNA damage is evidence that mechanical ventilation can cause DNA damage, leading to a senescence-like phenotype.

P21 has been extensively linked to senescence and anti-proliferation [25], [157]–[159]. In our model, the increased P21 gene expression and SASP manifested by increased IL6 with ventilation in both age groups indicate that mechanical ventilation here could be causing early senescence. In fact, during early senescence, the P21 level picks and declines as the cells are more committed to the senescence fate [160]. Another characteristic of senescent cells is a lack of proliferation due to cell cycle arrest. With increased senescence markers, there is a decrease in Ki67 [111]. This is in line with our

findings where mechanical ventilation combined with age and age alone; there was a decrease in proliferation marked by a decrease in Ki67 (figure 4C); further signs that mechanical ventilation and age lead to senescence-like phenotype.

The potential role for P38

TGF-β, which is involved in multiple physiological functions and diseases [161]–[164], has been shown to play an important role in pulmonary senescence [165], [166]. The sequestered TGF-β on the extracellular matrix is released during a stretch. Due to that release compounded with the injurious state of the environment that already exists, TGF-β becomes activated [167]. The activated TGF-β will cause a cascade of events, including activating the P38-MAPK pathway [168]. Activation of the P38-MAPK pathway plays an essential role in regulating the cell cycle by increasing P53, increasing P21 [169]. Though some parts of this mechanism have been extensible studied, the role of p38 inhibition has not been examined in an aging model of VILI. In the quest to investigate the mechanism of these senescence-like phenotypes in VILI, we used a P38 inhibitor to control the level of P21 observed with mechanical stretch ventilation. Inhibiting P38 in this study led to a decrease in P21 but not ɣH2AX because cyclic stretch leads to DNA damage that activates the P38-MAPK pathway.

Limitations:

The markers of senescence are very heterogeneous dynamic. Though markers traditionally associated with senescence were upregulated, we cannot be certain this is a chronic or irreversible phenotype as these markers can be found at other cellular

states and conditions [170]. The hallmarks of senescence observed in this study could be a protective mechanism started by the cells to prevent further injuries [81]. They may revert when the acute injury is under control if the immune system has not already cleared out those cells. Further studies need to be done to confirm the state of senescence of the cells when stretched, such as survival study with long-term recovery. Though the study of the P38 mechanism performed on primary human lung cells isolated from the distal part of the alveoli provided some valuable information on how P21 is upregulated, more in vivo studies need to be performed t. We could not obtain cells isolated from young patients; this mechanism needs to be verified using cells from young patients to confirm if the mechanism holds with age.

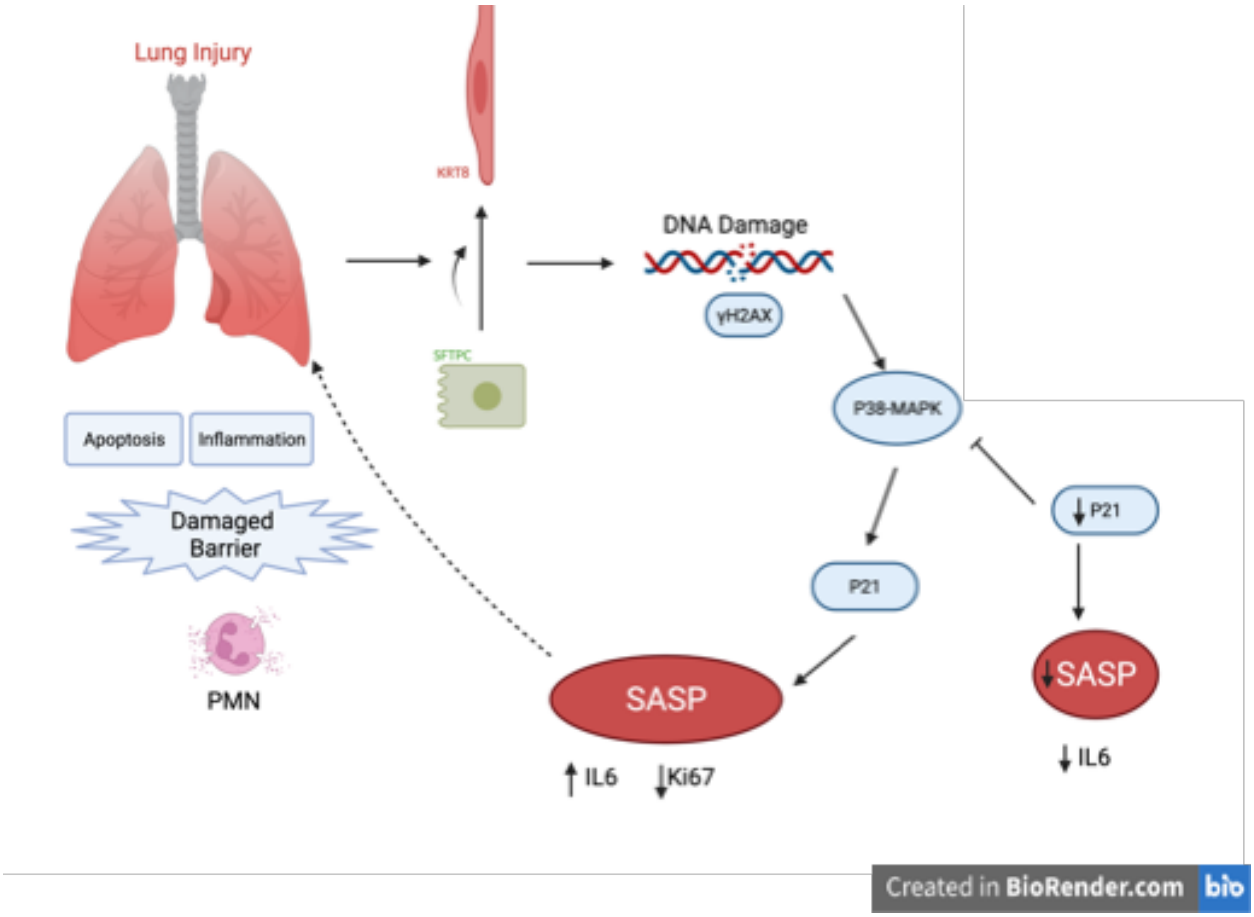

Figure 4. 10 Figure summary of VILI leading to lung damage and cellular senescence.

Conclusion:

In conclusion, we have shown that high-pressure mechanical ventilation and age lead to structural damage at tissue, cellular, and proteins levels. These damages were correlated with the increase of KRT8 positive cells, which are susceptible to DNA damage and could also play a vital role in senescence. We have also shown signs of senescence-like phenotypes with mechanical ventilation and with age. Finally, we have provided evidence that p38 may be a therapeutic target in stretch-induced senescence. These findings provide a better understanding of injuries resulting during mechanical

ventilation and VILI and could be used for better-targeted therapies from injuries created by ventilation.

Chapter 5: Senolytic Drugs as Therapy in an Aging Model of Acute Lung Injury

INTRODUCTION: 94

METHODS: 95

In vitro cell stretch: *95*

Animal: *96*

Sample Collection: *97*

qPCR: *98*

Inflammatory Cytokine Analysis: *98*

Immunofluorescent staining: *99*

Tissue Protein extraction: *100*

Western Blot: *100*

Statistical analysis: *101*

RESULTS: 101

Dimethyl sulfoxide (DMSO) does not cause Increase P21: *101*

SAEC can keep senescence P21 phenotype after recovery: *103*

Stretch causes Senescence and DQ decrease Senescent Cells. *105*

Increase dosing of LPS increase P21 positive cells. *108*

DQ improved lung compliance: *110*

DISCUSSION: 111

Establishing an In Vitro Two-hit VILI Model with Recovery: *111*

Mechanical stretch, DNA Damage and Senescence: *112*

ER Stress, DNA Damage and Senescence: *112*

Removal of Senescent Cells Causes Harm: *113*

LIMITATION: 113

CONCLUSION: 114

Introduction:

Senescence occurs naturally because of aging [171]. However, due to some injuries or stressors, senescence can occur prematurely [172]. Senescent cells secrete both autocrine and paracrine signaling to affect themselves and the cells around them [173]. Those signals include anti-apoptotic markers, pro-inflammatory cytokines and chemokines, growth factors, and matrix metalloproteinases (MMPs) to remodel the matrix around them [26]. These autocrine and paracrine signaling are collectively called SASP or senescence-associated secretory phenotype. The anti-apoptotic markers which make up the SASP include Bcl-xL proteins. TNF-a, Interleukins such as IL6 and IL8, and chemokines such as MCP1 (CCL2) make up the pro-inflammatory markers in SASP. The main growth factor observed in SASP is TGF-b. While the MMP-1, MMP-3, MMP-10, MMP-12, MMP-13, and MMP-14 have been reported to be elevated in senescence as part of the SASP [43].

Some of the earlier SASP factors were also reported in other diseases such as ARDS or acute respiratory distress syndrome [174]. ARDS is characterized by poor oxygenation, leaky alveolar barrier, and lung-filled fluid [128]. The leaky alveolar barrier allows for immune cells infiltration into the alveolar space. The first immune cells that infiltrated the alveolar space in ARDS are neutrophils [175]. These neutrophils exacerbate the inflammatory response which can damage the lung tissue [176]. Due to the conditions created by ARDS, some patients cannot breathe on their own; to remedy this issue; the patients are often put on mechanical ventilators. Despite the benefits of mechanical ventilators, they may exacerbate the injury causing a condition termed VILI or ventilation-induced lung injury [177]. In VILI, SASP markers such as pro-inflammatory

cytokines and chemokines have been observed. These SASP cause biotrauma that can also exacerbate inflammation [178].

Moreover, we previously showed how old mice are more prone to increases in inflammation markers and injury and decreased survival rate when ventilated at high tidal volume (25 ml/kg for young and 18 ml/kg for old) [143]. The hostile environment brought by ARDS and VILI can cause that premature aging in the cells or senescence [81]. However, it is unclear what role senescence plays in this acute lung injury.

In an ideal environment, the body has ways to get rid of senescent cells either via induced apoptosis or clearance by the immune system. Drugs known as senolytic drugs can also target senescent cells selectively [179]. The therapies used to alleviate the effects of VILI range from the adjustment of positive end-expiratory pressure (PEEP) [180] to anti-cytokine therapies to address the biotrauma [130]. However, more research still needs to be done to manipulate senescent cells that occur due to ARDS and VILI to understand the effects of these cells in these injuries and develop properly targeted therapies to remedy these conditions.

In this research, we are first developing both in vitro and clinically relevant in vivo aging models of VILI. We are using senolytic drugs to selectively target senescent cells that occur due to ARDS and VILI to understand their roles in these diseases. We hypothesized that the senolytic drugs would clear senescent cells and improve the outcome of the mice in our mouse model of VILI.

Methods:

In vitro cell stretch:

uman small airway epithelial cells (SAEC) were purchased from Promocell (C-12642) and cultured according to their recommendations with a supplied SAEC growth media. SAEC were plated on Bioflex culture plates (Flexcell international Corp., BF-3001) for 48 hours for acclimation. Then, media change was performed; some wells received lipopolysaccharide (LPS) at 1ug/ml to simulate ARDS; others received H2O2 or tunicamycin as a positive control to induce senescence. Media change was performed again to rid the wells of the LPS and senescence-inducing drugs. Before stretching, the cells were given DQ cocktail treatment at 500 and 750 nM, respectively. The cells were then stretched at 20% change in surface area for 24 hours and at 0.33 Hz to cause injury. DQ cocktail treatment was repeated on days 6 and 9. Conditioned media was collected, and the cells were fixed for later processing.

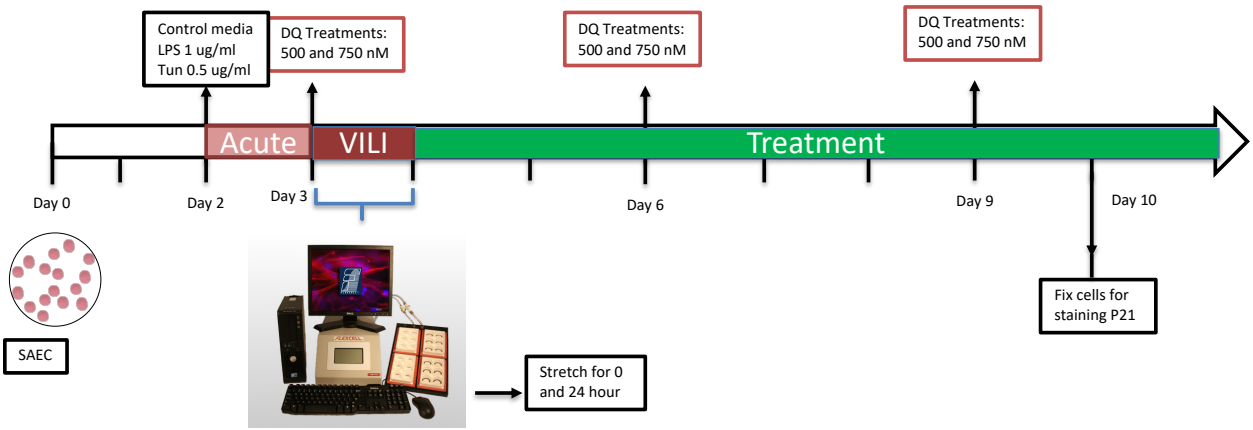

Figure 5. 1 In Vitro Experimental Setup

Animal:

Male young (8-10 weeks) and old (20-22 months) C57BL/6 mice were acquired from the National Institute on aging and housed at the VCU vivarium. All procedures performed

on the mice were approved by VCU Institutional Animal Care and Use Committee (IACUC). The mice were anesthetized using sodium pentobarbital. After anesthesia, mice were given the senolytic cocktail dasatinib quercetin (DQ) via oral gavage and 1N of HCl via instillation. The Mice were then mechanically ventilated at protective settings, 3 PEEP and 15 cmH2O, for 4 hours. Lung mechanics were measured at 30-minute increments for the duration of ventilation.

Figure 5. 2 In Vivo Experimental Setup

Sample Collection:

At the end of the 4-hour mechanical ventilation, blood was collected from the vena cava and centrifuged to obtain plasma. As previously described, gravity-assisted bronchoalveolar lavage (BAL) was performed [45]. Briefly, PBS was instilled into the

mice lungs and collected and repeated twice. The BAL fluid was then centrifuged, the supernatant was transferred onto a new tube for later processing. The cells were resuspended then cytospun onto a microscope slide. WBC analysis was performed by counting 300 cells while refraining from the peripheral edges of the microscopy region. The different immune cells were distinguished and quantified.

qPCR:

For lung tissues, small lung fragments of about 50 mg were homogenized with Trizol (ThermoFisher, 15596026). RNA extraction was performed as recommended by the manufacturer. Briefly, after homogenization, 200 ul of chloroform was added per 1 ml of Trizol. Phase separation was performed via centrifugation, then the clear phase, which contained RNA, was then separated. *In vitro* experiments, cells were lysed using RLT buffer to obtain a cell lysate containing RNA. RNA isolation of both tissues extracted RNA, and cell lysate was performed using Qiagen RNeasy kit. cDNA conversion was performed using a Bio-Rad iScript cDNA synthesis kit (Bio-Rad, 1708891). cDNA and Bio-Rad SsoAdvanced universal SYBR green (Bio-Rad, 1725274) was used for gene amplification. Primers: human 18s F: 5'-TAACCCGTTGAACCCCATTC-3' R: 5'-TCCAATCGGTAGTAGCGACG-3', human P21 F: 5'-TGTCCGTCAGAACCCATGC-3' R: 5'-AAAGTCGAAGTTCCATCGCTC3', mouse 18s: F: 5'-GCAATTATTCCCCATGAACG-3' R: 5'-GGCCTCACTAAACCATCCAA-3', mouse P21 F: 5'-GACAAGAGGCCCAGTACTTC-3' R: 5'-GCTTGGAGTGATAGAAATCTGTC-3'

Inflammatory Cytokine Analysis:

IL6 ELISA (R&D system, DY 406) was performed according to the manufacturer's protocol. Briefly, 96-well ELISA plates were coated using a captured antibody overnight. The next day, the plate was washed (0.05% Tween 20 in PBS) and blocked (R&D system, DY995) at room temperature using the reagent diluent for 2 hours. Standards and samples were loaded into the plates and incubated at room temperature for 2 hours. The plates were then washed, and the detection antibody was added for 2 more hours. The plates were then incubated with Streptavidin-HRP and substrate solution solutions, respectively, for 20 minutes, each with washes in between. Diluted sulfuric acid at the concentration recommended by the manufacturer was used to stop the reaction. The plates were read at 450 nm with wavelength correction.

Immunofluorescent staining:

Immunofluorescent staining was performed according to the antibody manufacturer protocol with modifications. Briefly, when stretch experiments concluded, the cells were fixed then permeabilized. When appropriate, the cells were blocked for 2 hours at room temperature using 10% normal goat serum or BSA. The slides were then incubated overnight at 4C in primary antibody. The next day, the slides were rinsed then incubated with a secondary fluorophore antibody for an hour. For tissue embedded sections, the slides were deparaffinized, and antigen retrieval was performed before the permeabilization. Primary antibodies: mouse anti-gamma H2AX (Novus Biologicals, NB100-74435), rabbit anti-Ki67/MKi67 (Novus Biologicals, NB500-170SS), rabbit anti-SP-C (Bioss, bs-10067R), rat anti-KRT8 (CreativeBiolabs, CBDH1469). Goat anti-Rat IgG (H+L) Alexa Fluor 555 (ThermoFisher scientific, A-21434), Goat anti-Rabbit IgG

(H+L) Alexa Fluor 647 (ThermoFisher scientific, A-21245), Goat anti-Mouse IgG (H+L) Alexa Fluor 488 (ThermoFisher scientific, A-28175)

Tissue Protein extraction:

cytoplasmic and nuclear proteins were extracted according to the Millipore sigma protocol with minor modifications. Briefly, tissues were lysed using hypotonic buffer (10 mM HEPES, pH 7.9, with 1.5 mM MgCl2 and 10 mM KCl) containing Dithiothreitol (DTT), protease and phosphatase inhibitors. Then the tissues were homogenized and centrifuged at 10,000 g for 20 minutes. The supernatant, which contained cytoplasmic proteins, was preserved. The crude nuclei pellet was resuspended in 140 ul of extraction buffer containing DTT, protease, and phosphatase inhibitors. The solution was gently shaken for 30 minutes then centrifuged for 5 minutes at 20,000 g. The supernatant was transferred to a new tube and chilled at -70 C for later processing.

Western Blot:

Western blot was performed according to the manufacturer's protocol. Briefly, BCA was performed on the freshly isolated proteins using a Pierce BCA protein assay kit (Sigma, 23227) to determine the protein concentration. Electrophoresis was performed using 30 ug of proteins loaded into each 10-well gel; proteins were then transferred from the gel onto a membrane. The membrane was blocked for 1 hour, followed by primary antibody incubation overnight at 4 C. The next day, the membrane was rinsed and incubated in a solution of HRP bound secondary antibody for 1 hour, followed by rinsing and incubation in Pierce ECL western blotting substrate (ThermoFisher, 32106) for 5

minutes and imaged. Bands densities were analyzed using BioRad Image Lab software. Rabbit anti-histone H3 (Novus Biologicals, NB500-171), mouse anti-gamma H2AX (Novus Biologicals, NB100-74435), anti-rabbit IgG HRP-linked antibody (Cell Signaling Technology, 7074S), anti-mouse IgG HRP-linked antibody (Cell Signaling Technology, 7076S).

Statistical analysis:

The results were analyzed using GraphPad prism. We used multiple two-way analysis of variance (2-way ANOVA) and post-hoc Tukey test to find significance. If p-value is less than the significance $\alpha = 0.05$, we will reject the null hypothesis that there are no differences in all the groups, otherwise, we will not reject it. We will need a total number of 240 mice for the study for each experimental condition requiring 5 mice based on a power of 0.8 assessed by G power with our prior data.

Results:

Dimethyl sulfoxide (DMSO) does not cause Increase P21:

Since the Senolytic cocktail was diluted with DMSO, we tested if DMSO alone at the dose used to dilute the DQ cocktail would induce an increase in P21. The control group that received growth media and the group that received DMSO were comparable in P21 positively stained cells (figure 5.3 A). The normalized fluorescence intensity also shows the same results as the cells count, where both control and DMSO groups had the same fluorescence intensity (figure 5.3 B). Moreover, when considering the cell density,

there were no differences between the DMSO group and the control group, suggesting that DMSO at the concentration used is does not cause increase P21.

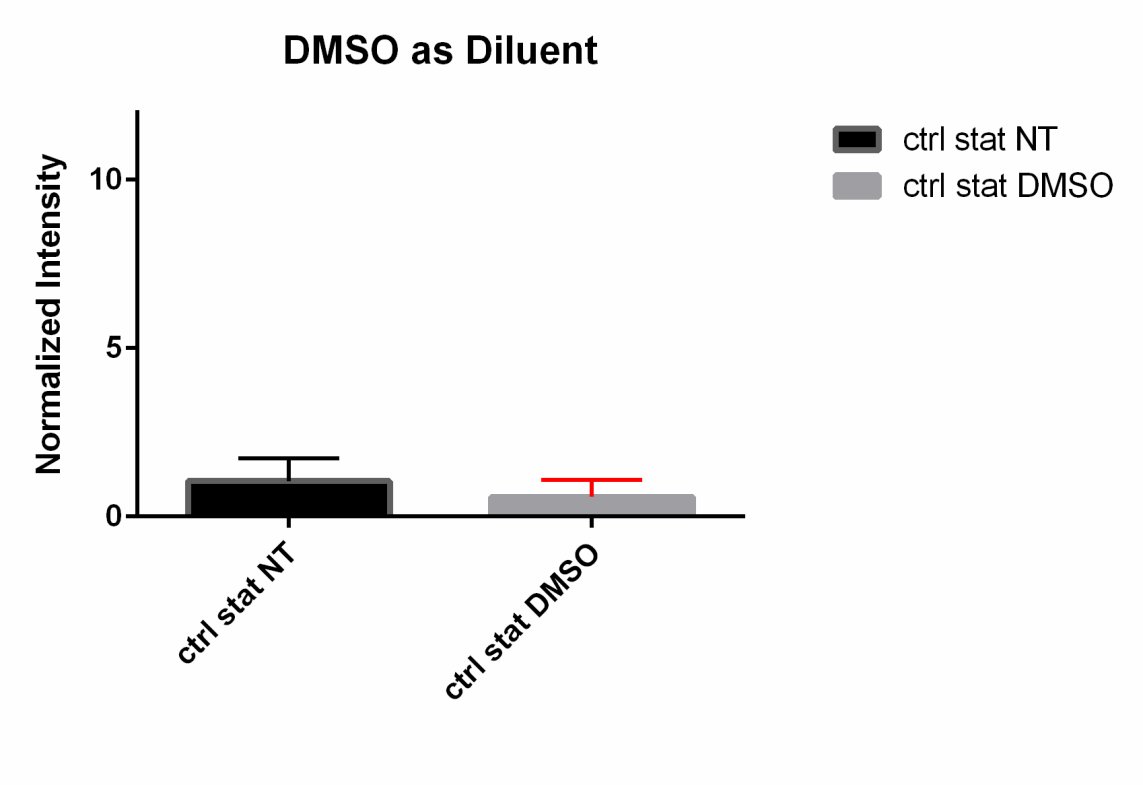

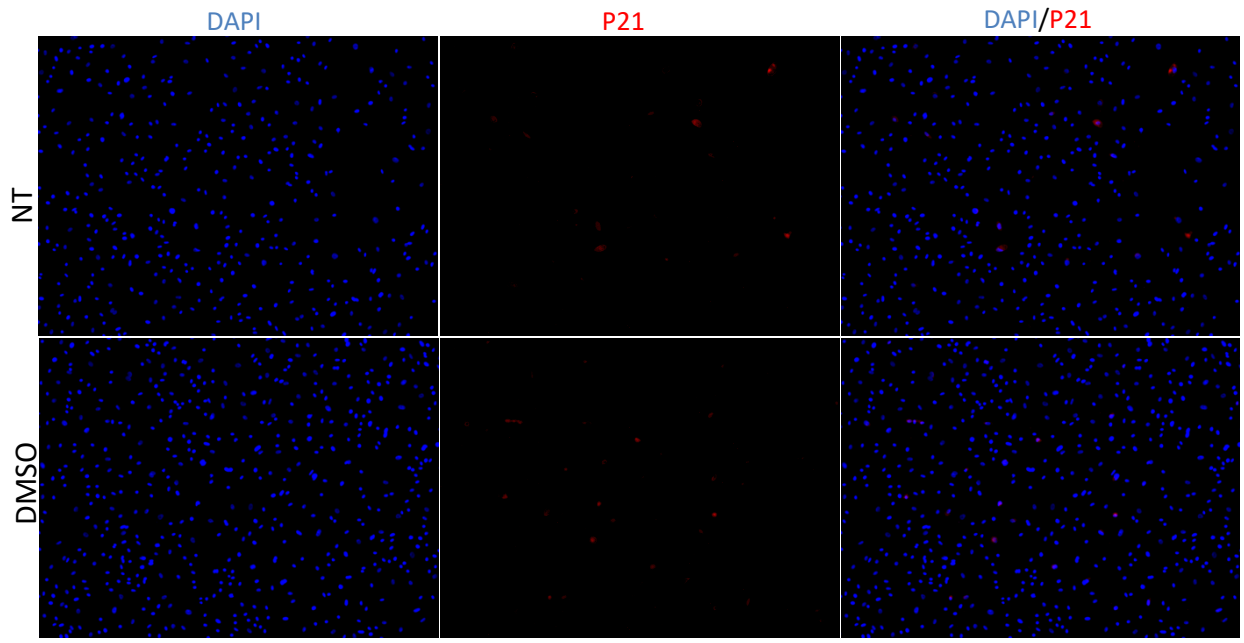

Figure 5. 3 DMSO is Non-Toxic to the SAEC: Graph of in vitro staining quantification and representative images showing DMSO at the dose used in this study is not toxic. N = 2-3

SAEC can keep senescence P21 phenotype after recovery:

Previous studies have shown that SAEC can have P21 gene expression upregulated after an acute injury (stretch) [81]. However, it is unclear if these SAEC cells will keep that P21 gene expression after recovery. Here, we used hydrogen peroxide and tunicamycin to induce senescence. After a ten-day culture, there was an increase of P21 positive cells in the groups that received hydrogen peroxide and tunicamycin. Moreover, there was a lack of cell proliferation in the hydrogen peroxide and tunicamycin groups, suggesting that cells in these could have undergone senescence.

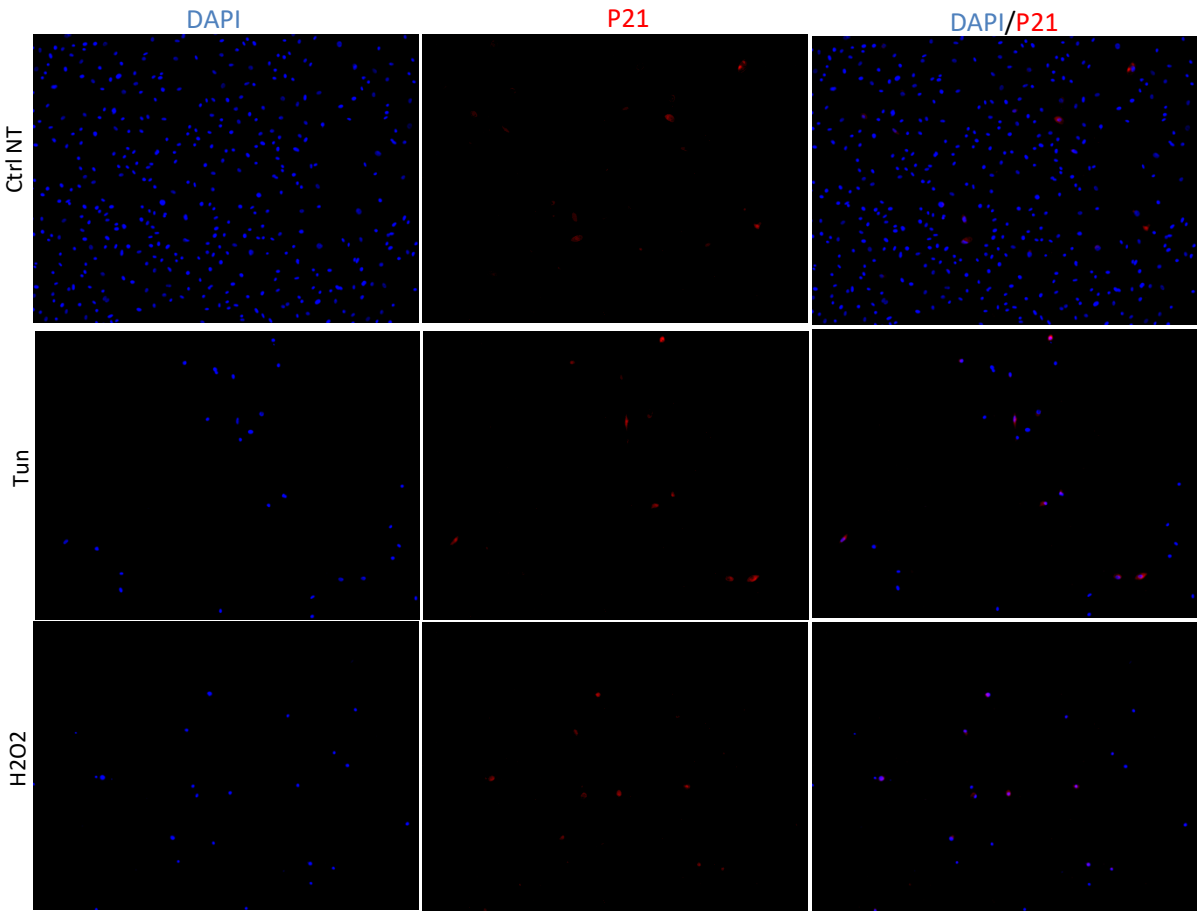
DAPI
P21
DAPI/P21
Ctrl NT
Tun
H2O2

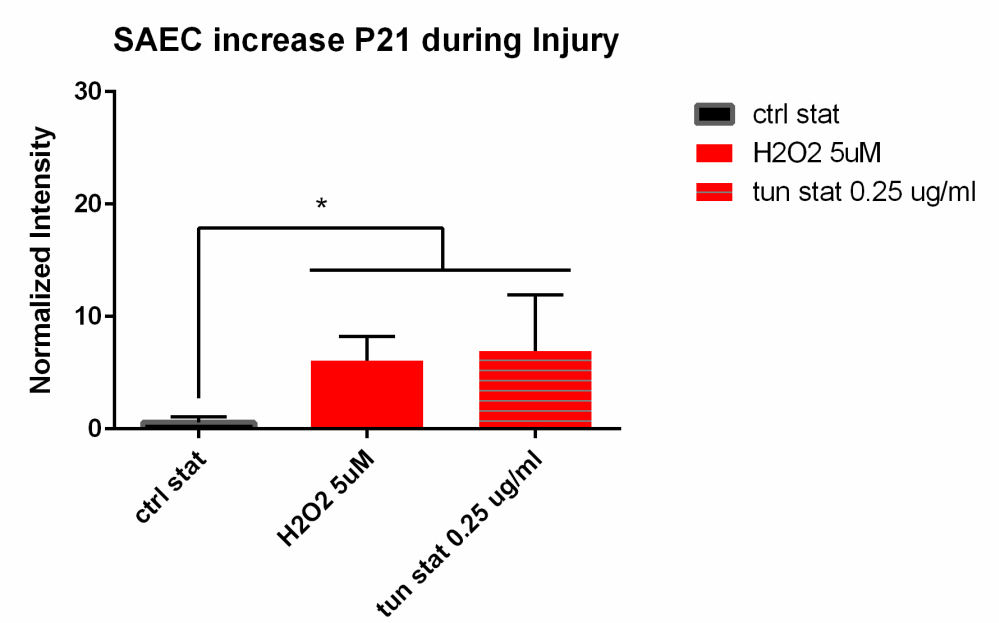

Figure 5. 4 Positive Control Experiment Representative images of H2O2 and tunicamycin positive control staining showing SAEC can undergo senescence. Representative images (top) and graph (bottom). N = 2-3

Stretch causes Senescence and DQ decrease Senescent Cells.

The goal of this experiment was to understand the role of stretch and stretch coupled with LPS on SAEC. The results show that stretch and stretch couples with LPS increase P21. These same latter groups also decreased cell density compared to the control. The widely reported dosing of LPS (1 ug/ml) from the literature did not cause an increase in P21 at the static condition, nor did it change the cells density. When treated with DQ, the stretch and stretch plus LPS groups decreased the P21, and cell density also seemed to increase. DQ did not have a visible effect on the static group.

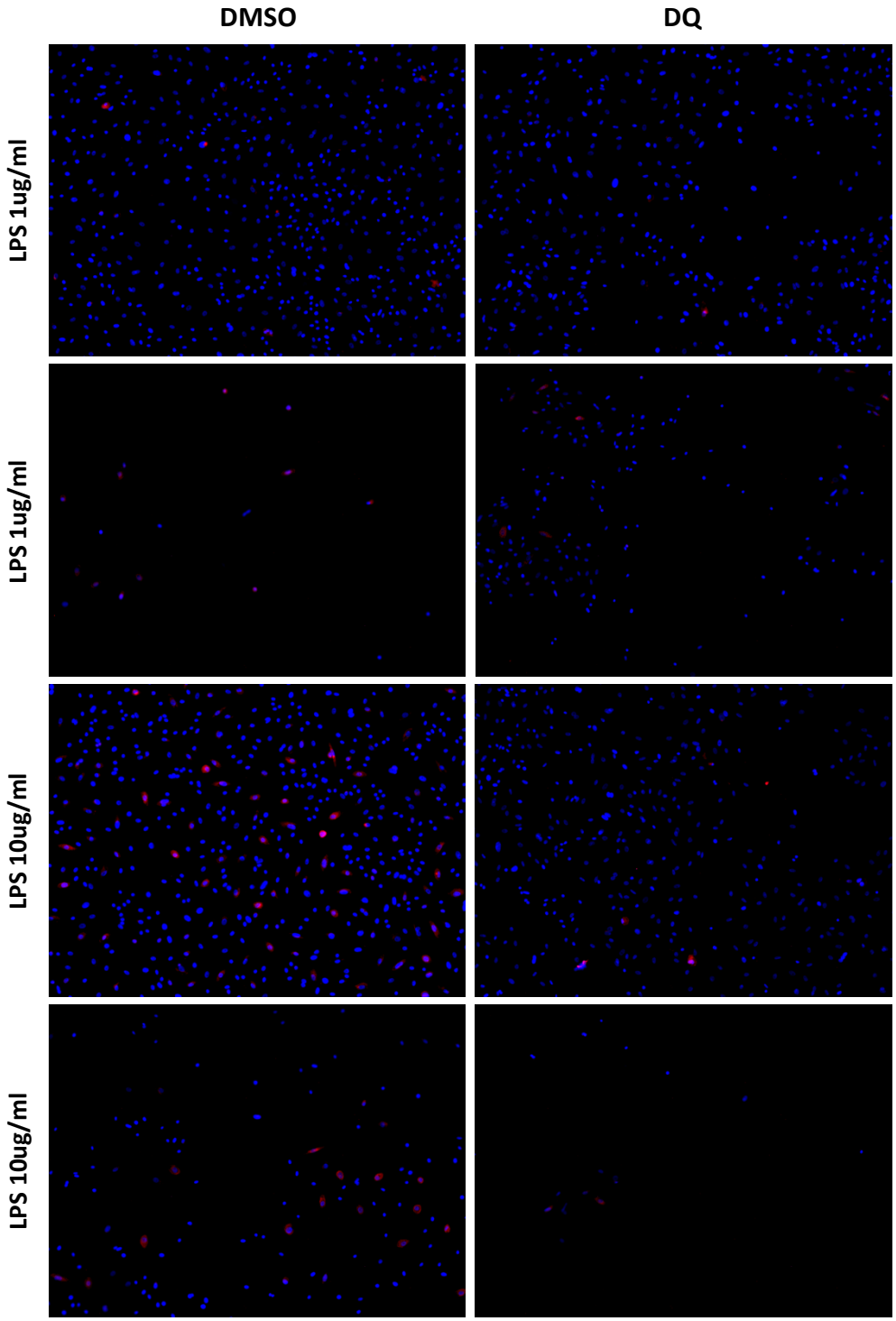
DMSO
DQ
LPS 1ug/ml
LPS 1ug/ml
LPS 10ug/ml
LPS 10ug/ml

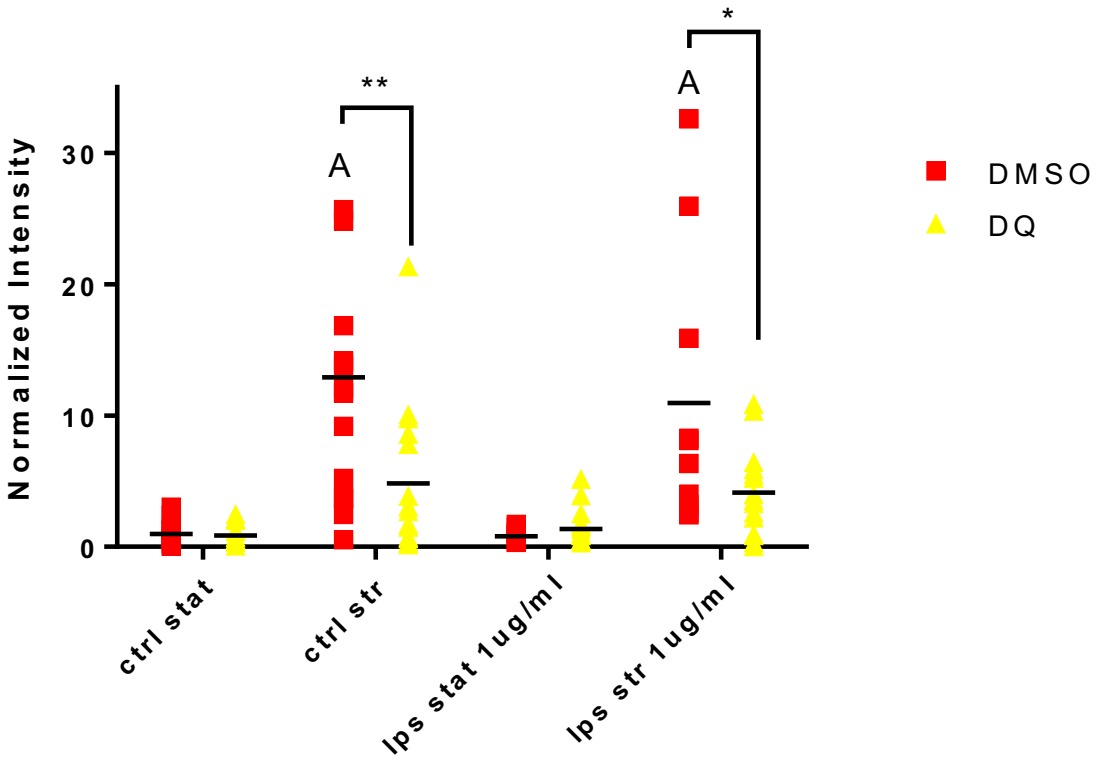

Figure 5. 5 In Vitro Stretch with Recovery Representative images and graph of different in vitro VILI model showing that stretch cause senescence and stretch coupled with LPS also causes senescence. DQ decrease the amount of P21. Representative images (top) and graph (bottom). N = 2-3

Increase dosing of LPS increase P21 positive cells.

We wanted to investigate if LPS alone could cause an increase in P21. This is crucial as we are trying to simulate ARDS by mimicking a bacterial infection before adding the stretch modeling the so-called 2-hit model of VILI. Since the reported dose of LPS used in the literature did not cause an increase in P21. We decided to increase the LPS dose by 10-fold. A 10-fold increase in LPS concentration caused an increase in P21 positive cells at the static condition. However, unlike in the stretch condition alone, there was no decrease in cell proliferation. When stretched, the 10-fold of LPS concentration group had increased in P21 positive cells compared to the 1 ug/ml LPS group. The treatment with DQ decreased the population of P21 positive cells in all the groups that a prior increase of it.

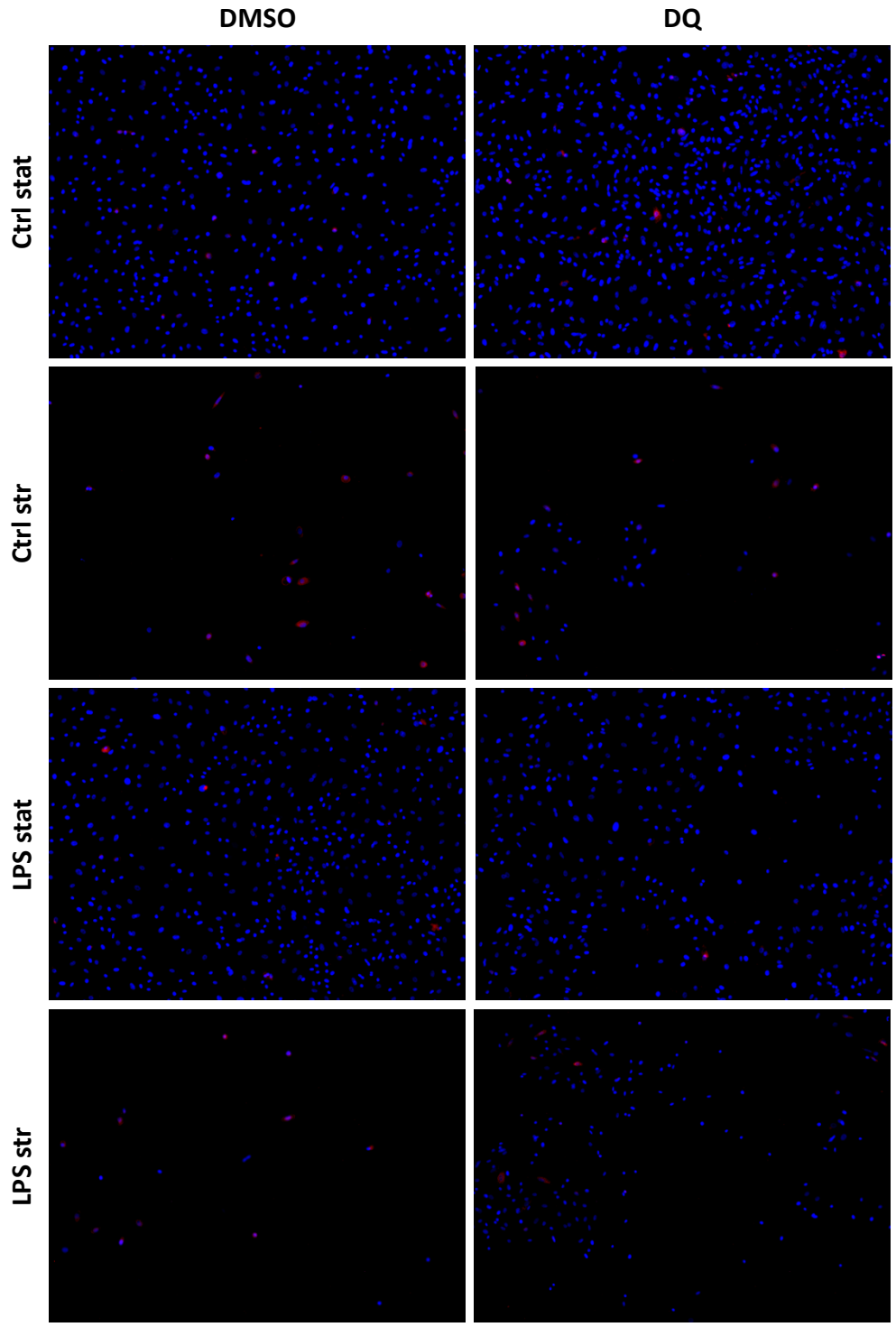
DMSO
DQ
Ctrl stat
Ctrl str
LPS stat
LPS str

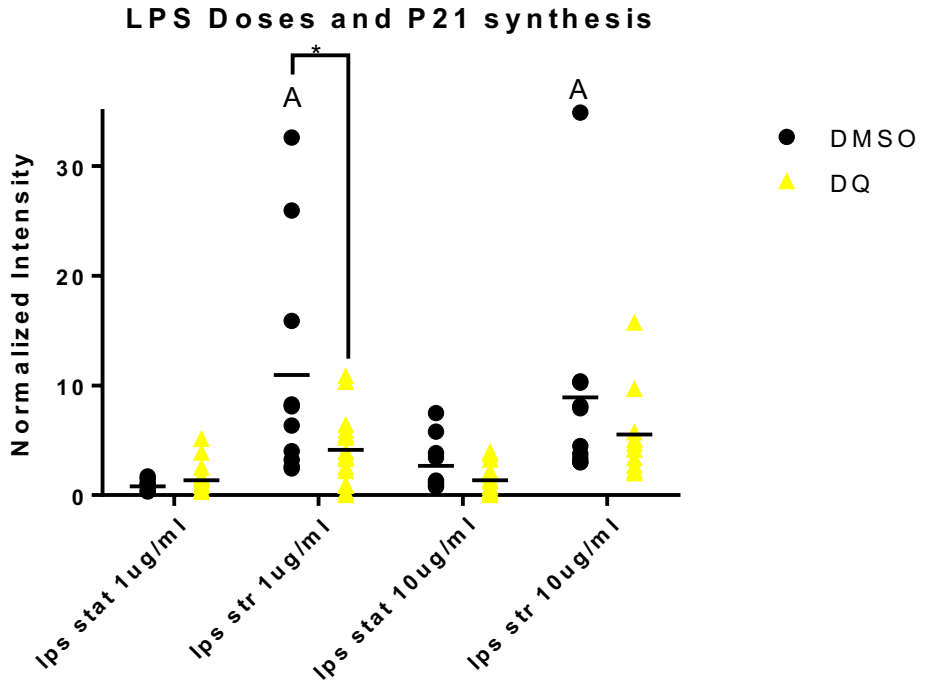

Figure 5. 6 In Vitro Stretch in Recovery with 10X LPS Representative images and graph of different in vitro VILI model showing that increased doses of LPS cause increase P21 however, DQ decreased the amount of P21 positive cells. N = 2-3

DQ improved lung compliance:

It is known that the increase in senescence cells decreases lung compliance. We treated the mice with a DQ cocktail prior to the two-hit VILI injury to test if the removal of senescent cells will decrease lung compliance. Initially, in both vehicle and DQ treated groups, the compliance was the same and lower than the non-injured control group; these same results were also observed at the 30 minutes post-injury. At the first 1-hour mark post injuries, the DQ group started to recover, and their compliance was almost closer to the non-injured control group at the two-hour mark. By 4-hour post-injury, the

DQ group had compliance almost comparable to the non-injured control group. In contrast, the group that received the vehicle had constant compliance from 30 minutes to 1-hour post-injury, which was lower than both the non-injured control group and the DQ group.

Discussion:

Senescence in chronic lung diseases has been extensively reported [24], [44], [165], [181], [182]. However, there is little evidence of senescence in an acute lung injury, especially in VILI. Attempts have been made in chronic lung diseases such as IPF to selectively target senescence cells to improve the patient's outcome [32]. However, it is unclear if similar so-called senotherapies will work in acute lung injury. Moreover, it is also unclear what role senescent cells play in acute lung injuries or if their removal will cause more harm than good. In this research, we are using senolytic drugs to selectively remove senescent cells in an acute model of lung injury; we are also investigating whether senescence is harmful or beneficial in an acute model of lung injury.

Establishing an In Vitro Two-hit VILI Model with Recovery:

Our previous studies have shown that SAEC can undergo senescence when stretched [116]. However, to the best of our knowledge, no one has ever shown that when injured acutely, with stretch, these cells will keep the senescence phenotype after recovery. Therefore, one of the study's goals was to develop a clinically relevant in vitro two-hit base model VILI. Previous studies have shown that when cells are exposed to

tunicamycin or hydrogen peroxide, they undergo senescence [183], [184]. As shown in multiple studies, oxidative stress is one of the causes of cellular senescence; hydrogen peroxide is used to achieve oxidative stress, therefore, causing senescence [185]. In contrast, tunicamycin induces endoplasmic reticulum (ER) stress [186], which has been shown cause to DNA damage response and senescence [187].

Mechanical stretch, DNA Damage and Senescence:

Other studies, including our own, have shown that mechanical ventilation or stretch leads to senescence [81], [116]. The mechanism of how stretch leads to senescence remains frustratingly elusive. However, some studies have shown that stretch leads to DNA damage [133]. DNA damage can lead to activation of DNA damage response; at this stage, the cell cycle momently stops to let the repair process take its course [135]. However, if the DNA is not salvageable, the cells undergo apoptosis, or the cell cycle stops permanently (senescence) [188]. This cell cycle arrest is characterized by increased P53-P21 pathway activation and or P16-pRB pathway activation [189]. The former is usually activated in early or acute senescence, and then the P16-pRB takes over once the cells have established their fate [106].

ER Stress, DNA Damage and Senescence:

Increased accumulation of misfolded proteins in the ER can lead to ER stress and ER stress can lead to DNA damage. These misfolded proteins lead to a cascade of events, including activation of unfolded proteins response (UPR). UPR is characterized by increased PERK, IRE1α, and ATF6α. Together, the accumulation of these latter

proteins can lead to apoptosis, cell cycle arrest, and senescence-associated secretory phenotype (SASP) [190].

Removal of Senescent Cells Causes Harm:

Though senescence is associated with DNA damage and ER stress, it is not clear what the role of senescence is in an acute model of VILI. we performed an in vivo experiment where we removed senescent cells using DQ in vivo albeit a sample size of one. Attempt to reduce senescence using the senolytic drug cocktail DQ yielded a decrease of P21 in the old mice but not in the young. This is probably due to the young and old not starting at the same level regarding the amount of senescent cells present. Indeed, since senescence is a condition related to aging, old organisms have a higher amount of senescence cells than their young counterparts, making the old animal more vulnerable to the worse outcome of an injury [191].

Removal of senescent cells caused more harm in both age groups suggesting that senescence could be protective in this two-hit model of VILI. In fact, in the old, though DQ cocktail reduced P21, there was a higher amount of damage manifested by increased BCA proteins than in the young group where there was a mild increase of BCA proteins and increase P21with DQ cocktail.

Limitation:

Though the results obtained in these experiments are groundbreaking and forward-thinking, more research needs to be done to confirm and to better understand the results obtained in these studies. Firstly, more experiments need to be performed to

verify if these results hold. Elsewhere, Though P21 has been associated with senescence, other markers associated with senescence need to be investigated to confirm that these cells are senescent and not in a temporary cell cycle arrest state. The markers associated with senescence that could be added include DNA damage markers such as gH2AX, which has been shown to the upregulated with senescence [81]. Since ER stress promotes DNA damage and ER stress has also been shown to be associated with senescence, markers of ER stress such as PERK, IRE1α, and ATF6α need to be investigated. Lastly, a more thorough analysis of SASP needs to be performed to better understand the consequences of senescence in this acute lung injury model.

Conclusion:

All in all, we have shown that after recovery from a two-hit VILI model, SAEC could keep their senescence via increased P21. We have also confirmed that senescence leads to a decrease in lung compliance, and when treated with senolytic drugs, the compliance recovers back to the healthy level. These findings help us understand the role of senescence in VILI, and these understandings could help tailor better therapies to remedy VILI and improve patients' outcomes when mechanically ventilated. Future studies could focus on two-hit in vivo models where young and old mice could be used to understand the role of senescent cells in these age groups with injury.

Chapter 6: Proof of Concept for In Vivo Survival Model of VILI

INTRODUCTION: 116

METHODS: 116

RESULTS: 117

Survival Injurious Mechanical ventilation and HCL lead to Neutrophil Influx: 119

DISCUSSION / CONCLUSION: 120

Introduction:

Patients that are mechanically ventilated must have had a prior lung injury that hinders gas exchange. Moreover, mechanical ventilation led to ventilator induced lung injury or VILI therefore it is critical to develop an animal model to decipher the mechanism of this injury. The most common model of VILI used is a two-hit model where LPS is used in conjunction with MV [129], [192]. The role of LPS is to simulate acute inflammation that is occurring with ARDS and MV shows the VILI side. During VILI, there is overexpression of inflammatory cytokines [193] and MMPs to remodel the matrix and change the lung's mechanics [194]. Aging is also issue in VILI as it exacerbates the injury. The consequences of aging in VILI have not been thoroughly investigated on a mechanistic level. One study examined VILI in senescent rats and found older rats were more susceptible to injury [20]. We previously showed how old mice are more prone to increases in inflammation markers and injury and decrease in survival rate when ventilated at high tidal volume (25 ml/kg for young and 18 ml/kg for old) [143]. Multiple therapies have been developed to alleviate the negative effects observed during VILI (biotrauma, volutrauma and atelectasis). These therapies range from the adjustment of positive end-expiratory pressure (PEEP) [180] to anti-cytokine therapies to address the biotrauma [130]; however, none of these strategies completely mitigate the effects of VILI.

In this study, we are simulating a two-hit model of VILI as a proof of concept to better understand the disease progression and its mechanism.

Methods:

Male young (8-10 weeks) C57BL/6 mice were acquired from the National Institute on aging and housed at the VCU vivarium. All procedures performed on the mice were approved by VCU Institutional Animal Care and Use Committee (IACUC). The mice were anesthetized using sodium pentobarbital. After anesthesia, some mice were given the 1N of HCl via instillation. These Mice were then mechanically ventilated at protective settings, 3 PEEP and 15 cmH2O, for 2 hours. For the injuries high pressure (HP) group, these mice mechanically ventilated at protective settings, 0 PEEP and 45 cmH2O, for 2 hours. The control group was ventilated at protective settings, 3 PEEP and 8 ml/kg for 2 hours. At the end of the mechanical ventilation, the mice were weaned off the ventilator and allowed to recover for 24 hours. Lung mechanics were measured before ventilation, at the end of ventilation and after recovery period just before the animals were euthanize.

At the end of the recovery period, blood was collected from the vena cava and centrifuged to obtain plasma. As previously described, gravity-assisted bronchoalveolar lavage (BAL) was performed [45]. Briefly, PBS was instilled into the mice lungs and collected and repeated twice. The BAL fluid was then centrifuged, the supernatant was transferred onto a new tube for later processing. The cells were resuspended then cytospun onto a microscope slide. WBC analysis was performed by counting 300 cells while refraining from the peripheral edges of the microscopy region. The different immune cells were distinguished and quantified.

Results:

One of the ways to assess VILI is via lung mechanics. Compared to the mechanically ventilated control group, there was a decrease in compliance and an increase in elastance in the group that was ventilated at injurious settings; these changes remained constant after recovery. However, the decrease in compliance and increase in elastance were not observed in the HCL group until after recovery. There was also no difference in resistance in all three groups, but after recovery, all groups had a drop in resistance.

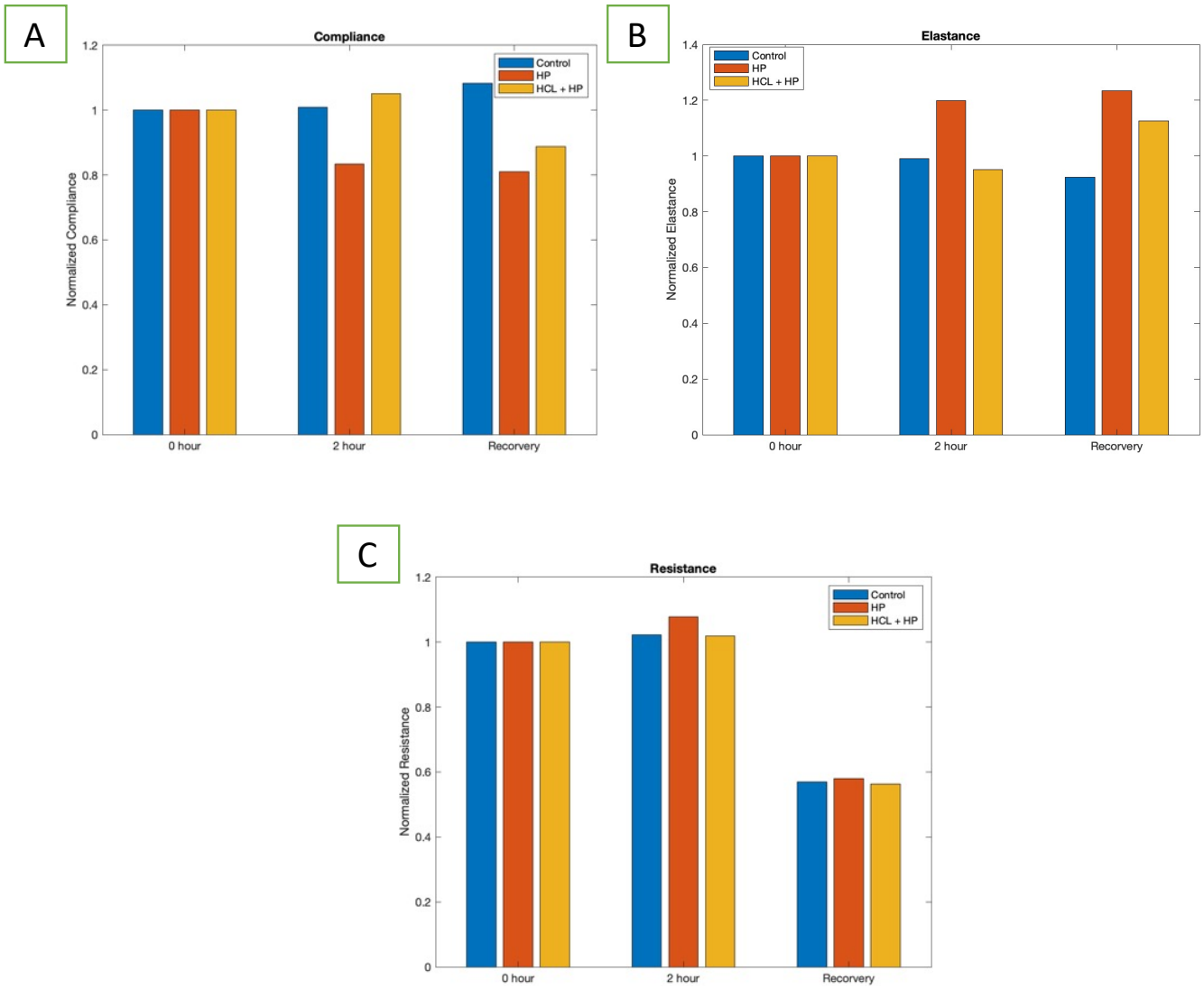

Figure 6. 1 Survival Study: Lung Mechanics A. Compliance, B. Elastance and C. Resistance graphs of survival study showing changes in these lung mechanics. N =1

Survival Injurious Mechanical ventilation and HCL lead to Neutrophil Influx:

To assess the damage caused by both HCL and the mechanical ventilator, we counted the number of neutrophils in the BALF. Neutrophils are the first immune cells that infiltrated the alveolar space in ARDS [175]. These neutrophils exacerbate the inflammatory response which can damage the lung tissue [176]. The group the control

group that received default settings mechanical ventilation had a slight increase of neutrophils in their lavage. The mechanically ventilated group at injurious settings had an astronomical increased in neutrophil influx after the 24-hour recovery. Lastly, the HCL group had a modest increase in neutrophil influx compared to the control non-ventilated group.

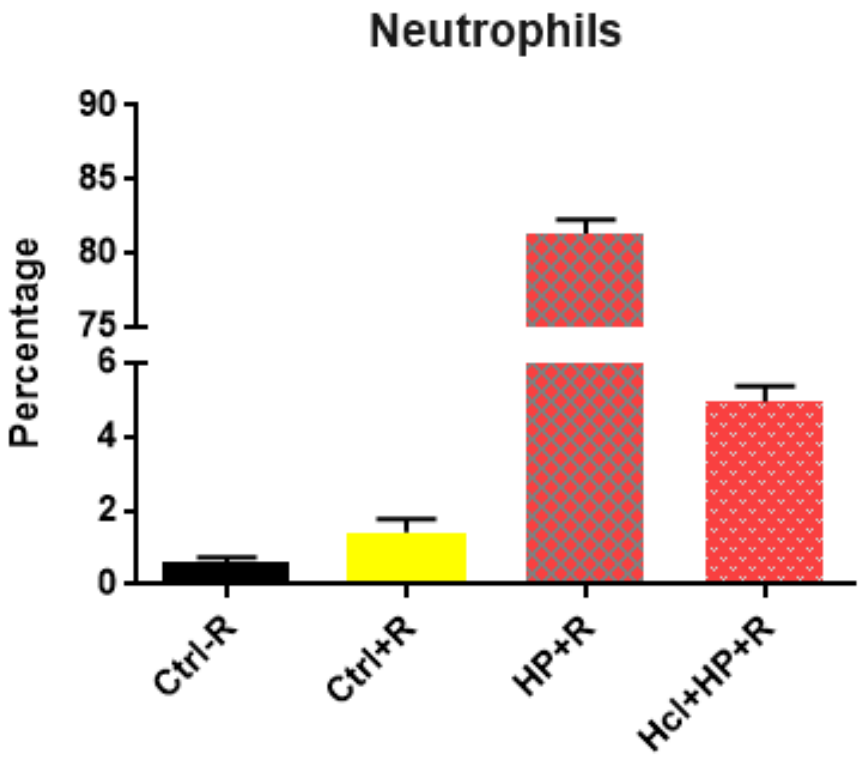

Figure 6. 2 Neutrophil count. Ctrl-R: control non-ventilated, and no recovery; Ctrl+R: control mechanically ventilated, with 24-hour recovery.

Discussion / Conclusion:

There are multiple in vitro and in vivo animal models of ARDS and VILI. Some use bacterial infection (or bacterial mimicking infection) [129], [192], and others use acid [195][196] to simulate the acid reflux that usually enters the lungs from the stomach. However, due to the complexity of mice anatomy and the size of these animals, most studies perform tracheotomy instead of oral intubation [22]. In this study, though with a sample size is one, we have used a survival in vivo two-hit mouse model of VILI to show to mimic ARDS and VILI.

Though these results are encouraging, more research still needs to be performed to confirm that all aspects of two-hit VILI are observed, such as inflammatory markers release in the BALF histology to confirm structural damage and barrier dysfunction. Despite these limitations, these experiments offer a proof of concept on creating a two-hit VILI model and potentially studying the mechanism of VILI that will lead to potential therapies.

Chapter 7: Conclusions and Future Directions

SURFACTANT REPLACEMENT THERAPY 123

VILI AND CELLULAR SENESCENCE: 124

Conclusion: 132

All in all, using different strategical approaches, we have tackled issues related to respiratory distress syndrome in both neonate and adult populations. We have used novel therapies and created new devices to deliver the therapy into the lungs of our animal models. Finally, we have shown that senescence is a key factor in VILI, and ARDS and we have also uncovered its mechanism in these injuries.

Surfactant Replacement Therapy

Surfactant plays an important role in the lungs, and it is composed of lipids and proteins and its purpose is to keep the airways open and prevent them from collapsing by reducing the surface tension of airway surface liquid [197]. The lungs are one of the last organs to develop, hence infant that are born prematurely may suffer from surfactant insufficiency. This lack of natural surfactant often leads to neonatal respiratory distress syndrome, NRDS, which is more prominent with preterm infant [198]. The gold standard to remedy NRDS, is to put neonates on breathing support and supply other therapies to keep the airways open. These therapies include surfactant replacement drugs such as Curosurf and Survanta [199], however these biologicals are given in liquid form, which requires a large liquid volume in order to reach the alveolar region. Instillation of a large volume of liquid into already injured lungs has been associated with several unwanted side effects [12] causing some to suggest the use of aerosolized surfactant . In this dissertation, we have developed an excipient enhanced growth (EEG) aerosolized surfactant approach for the rapid and high efficiency delivery of surfactant powders to the alveolar.

In order to test our EEG aerosolized surfactant, we have developed a rat surfactant depleted model. Since it has been shown that excessive phospholipids can hinder gas exchange [200], after surfactant depletion, rats were given different doses of EEG Survanta (3, 5, 10, and 20 mg). To deliver these EEG survanta, we customed built an aerosolization device. After surfactant administration and ventilation, lung ventilation mechanics were taken to assess the efficacy of the therapies. Inflammation was also assessed via cytospin of bronchioalveolar lavage fluid onto microscope slides.

Groups receiving EEG Survanta had lung ventilation mechanics that were closer to healthy conditions compared with the liquid Survanta groups. Moreover, lower doses of EEG Survanta (such as 3 mg) were better at improving mechanics than higher EEG Survanta doses, potentially due to better delivery to the deep lung from the custom device when delivering a lower powder dose and a lower amount of phospholipids. In addition, inflammation assessment using cytospin show no significant differences among all treatment groups and all groups also had a low neutrophil count. Overall, spray dried EEG Survanta significantly improved compliance and elastance of lungs compared to commercially available Survanta and did not lead to increase neutrophil count.

VILI and Cellular Senescence:

Acute respiratory distress syndrome is a form of acute lung injury that is characterized by shortness of breath amongst other symptoms which lead patients to require mechanical ventilation (MV) [201]. Despite the health benefits of MV, this latter can

exacerbate the injury in a condition termed ventilator-induced lung injury or VILI [202]. Moreover, it has been shown that the older adult population have the worst outcome of VILI [203]. VILI is characterized by biotrauma or increase in inflammation, volutrauma or overextension of alveoli, and atelectrauma or the collapse of the alveoli [204], [205]. This hostile environment created by VILI may lead to senescence, however, since the concept of senescence in VILI is poorly understood, we aimed to unmask the intricacies of senescence in VILI. Senescence is a permanent state of cell cycle arrest, and it is characterized by an increase in cyclin dependance kinase inhibitors [206]. Moreover, senescence cells secrete both autocrine and paracrine signaling including inflammatory cytokines termed senescence associated secretory phenotype (SASP) [207]. To clear out senescence cells, senolytic drugs are used [44], [208] however, the implications of removing senescence cells in an acute model of injury it is not well understood specially with age. We hypothesize that stretch caused by mechanical ventilator will induce senescence and this effect will be exacerbated with age and using senolytic drugs may improve outcome in both populations.

To test this hypothesis, young (2 months) and old (20 – 22 months) C57BL6 mice were mechanically ventilated at 35 and 45 cmH2O respectively for 2 hours. Bronchoalveolar lavage fluid (BALF) and lungs were collected at the end of MV. BALF was collected via a gravity assisted lung lavage. The right lobe of the lung was snap frozen and the left lobe was fixed for histology. Snap frozen lungs were homogenized, P21, IL6 and MCP1 gene expression was performed. Separately, the nuclear proteins were isolated from snap frozen lungs and western blot was performed to probe for γ-H2AX, a DNA

damaged protein. IL6 ELISA was perform on BALF. The previous animal experiment was repeated with both young and old mice receiving a cocktail of dasatinib and quercetin (DQ) and DMSO (vehicle) before HCl (to simulate ARDS) and 4-hour MV (17 cmH2O). Collection proceeded as stated earlier.

Mechanically ventilated mice had a significant increase in P21 gene expression compared to the non-ventilated old mice group. There was also a significant increase in IL6 expression in the ventilated group compared with non-ventilated group. IL6 was also upregulated in the BALF protein of both young and old ventilated groups compared to the non-ventilated groups. The results suggest that MV leads to increase senescence in the aging group and MV alone leads to inflammation.

Recently, it has been shown that AT2 differentiate to a transient state positive for KRT8 before becoming AT1 depending on the disease condition [137]. Analysis of this transiently differentiated state in our experiment showed an increase of KRT8+ cells in all groups but the young non-ventilated group. It is also worth noting that KRT8+ cells have been shown to be more prone to DNA damage [138]. Analysis of nuclear proteins showed an increase of DNA damage protein γ-H2AX in all the groups but the young non ventilated group suggesting that MV causes DNA damage and old mice inherently have sign of DNA damage.

We also analyzed the pathway that leads to senescence in VILI. It has been shown that accumulation of γ-H2AX leads to increase of P38-MAPK [209]. Moreover, it has also been shown that increase P38-MAPK leads to increase P21 [210]. To study the

mechanism of senescence in VILI, we inhibited P38-MAPK *in vitro*. Inhibition of P38-MAPK pathway decreased P21 but was not effective at reducing γ-H2AX, the DNA damage molecule. These results suggest that the pathway of senescence in VILI is P38-MAPK, but DNA damage is upstream of it, and it is required in order to activate this pathway.

Since we have previously shown that DQ was able to improve lung compliance, future studies could investigate the effect of DQ on the barrier damage. One method could be looking for total proteins in the BALF. Early results show that when given the vehicle, the two-hit injured groups in both young and old mice showed increased protein in their BALF. However, unlike positively impacting lung compliance, DQ treatment caused an increase of proteins in the BALF, suggesting that DQ could be harmful to the mice. This needs to be investigated further in the future.

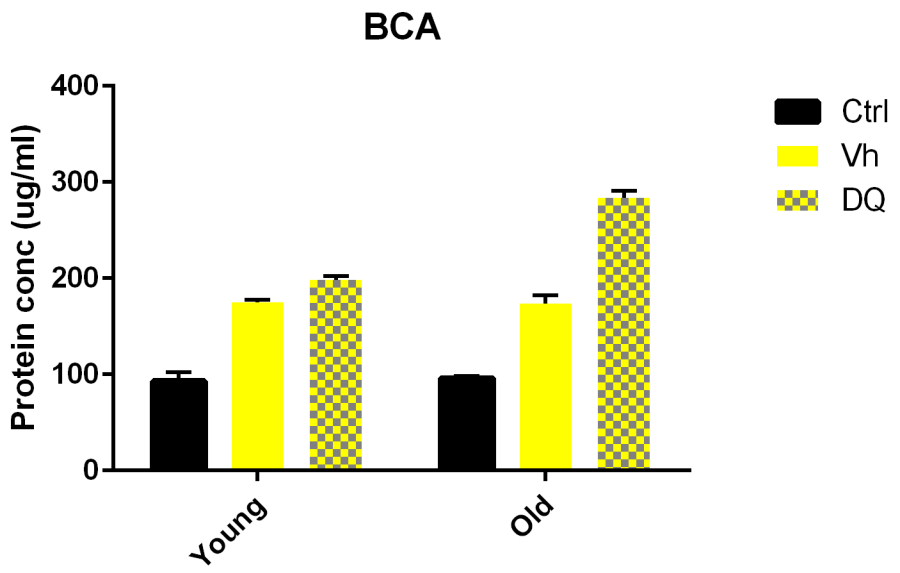

Figure 7. 1 BCA on BALF of two-hit VILI Showing increase in protein concentration in BALF with two-hit injury and with age. However, DQ treatment groups had the worst outcome in all the groups. N = 1

It is known that the increase in senescence cells decreases lung compliance. We treated the mice with a DQ cocktail prior to the two-hit VILI injury to test if the removal of senescent cells will decrease lung compliance. Initially, in both vehicle and DQ treated groups, the compliance was the same and lower than the non-injured control group; these same results were also observed at the 30 minutes post-injury. At the first 1-hour mark post injuries, the DQ group started to recover, and their compliance was almost closer to the non-injured control group at the two-hour mark. By 4-hour post-injury, the DQ group had compliance almost comparable to the non-injured control group. In contrast, the group that received the vehicle had constant compliance from 30 minutes

to 1-hour post-injury, which was lower than both the non-injured control group and the DQ group. This could be further evaluated in the future with the greater sample size and including the young mice.

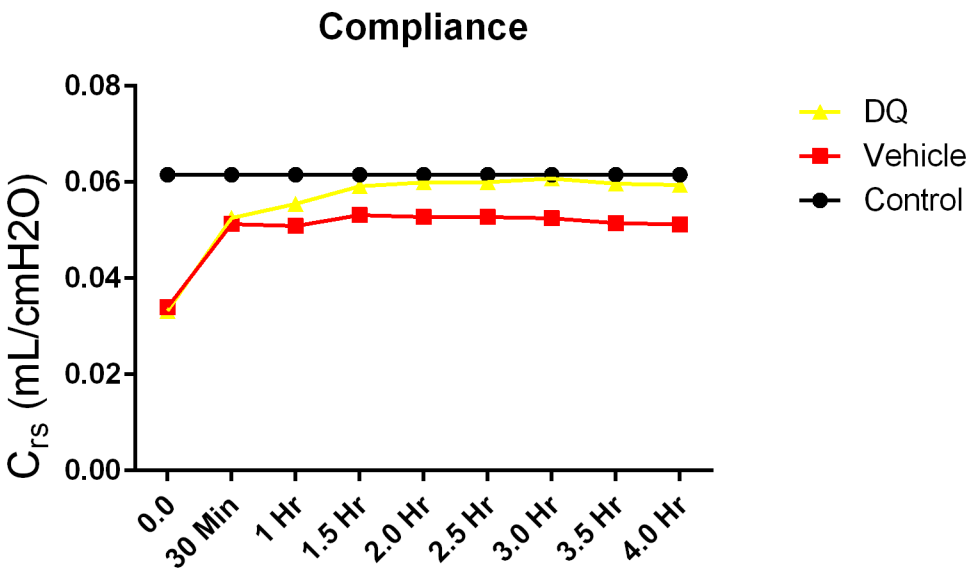

Figure 7. 2 DQ Lung Compliance of two-hit VILI old mice showing compliance of mice that received DQ treatment recover after injury. N = 1

Other studies could also look for P21 in in the two-hit VILI model mentioned earlier. We did one animal per group as a proof of concept for this study. Briefly, at the end of the 4-hour two-hit VILI model, both young and old mice showed an increase of P21 in the bulk lung gene expression of the vehicle group. The DQ cocktail failed to decrease the P21 gene expression level in the young. However, there was a decrease in P21 gene expression with DQ treatment in the old. These results were almost in tandem with the

inflammatory marker IL6. Bulk lung IL6 gene expression showed an increase in IL6 gene expression within the old with the two-hit VILI model, and DQ cocktail treatment decreased that IL6 gene expression level. However, in the young, the two-hit VILI model did not cause an increase in IL6 in the group that received the vehicle. Similar to the P21 gene expression, the young that received DQ treatment did not decrease IL6 level. These results suggest a difference in pathology in young and old mice and should be further investigated.

A

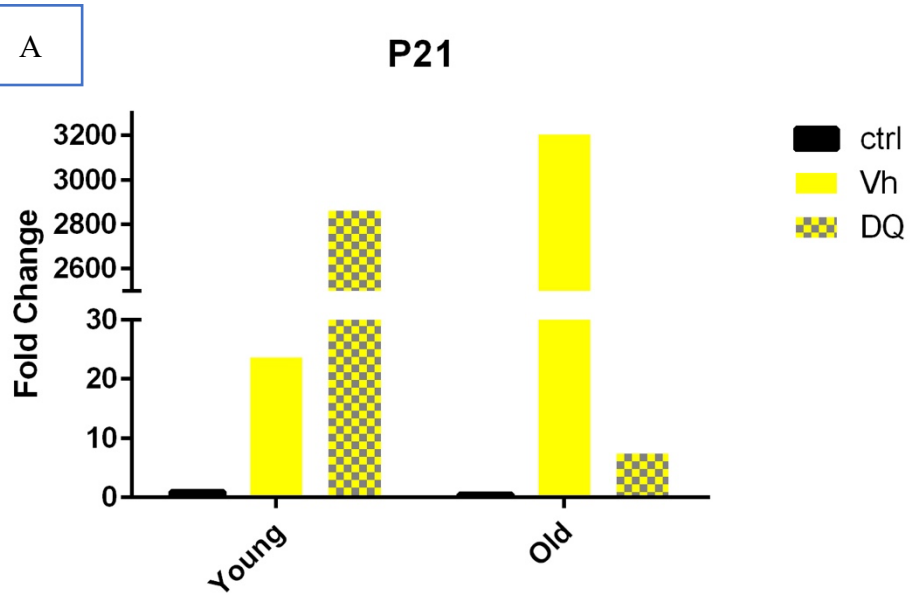

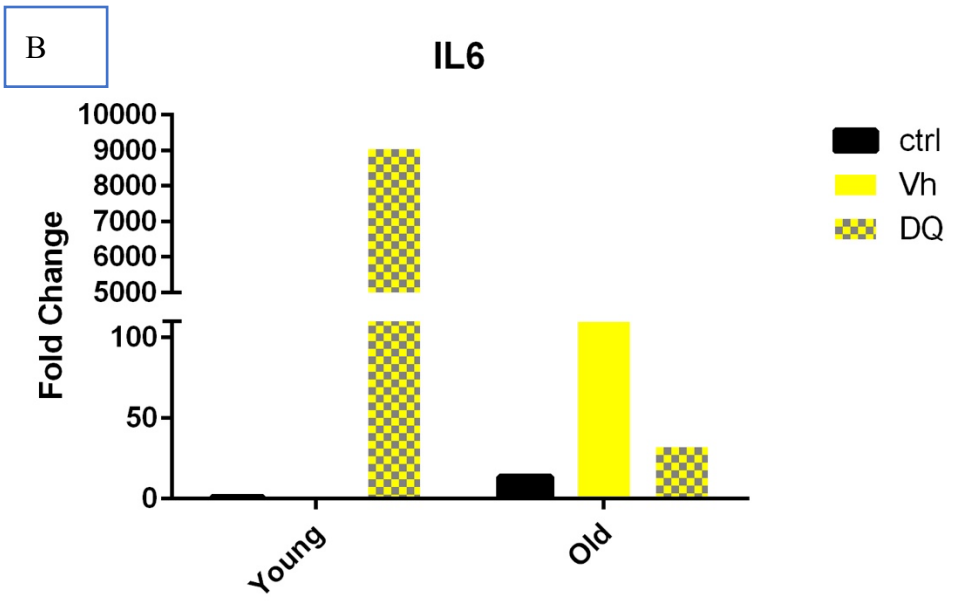

Figure 7. 3 P21 and IL6 In Vivo Gene Expression of young and old total lung lysate after a two-hit VILI injury. A: P21 increased with two-hit VILI and with age. DQ decrease P21 in old but failed to decrease it in the young. B. IL6 increased with age coupled with two-hit VILI. DQ decreases IL6 expression in old but not in the young. N = 1

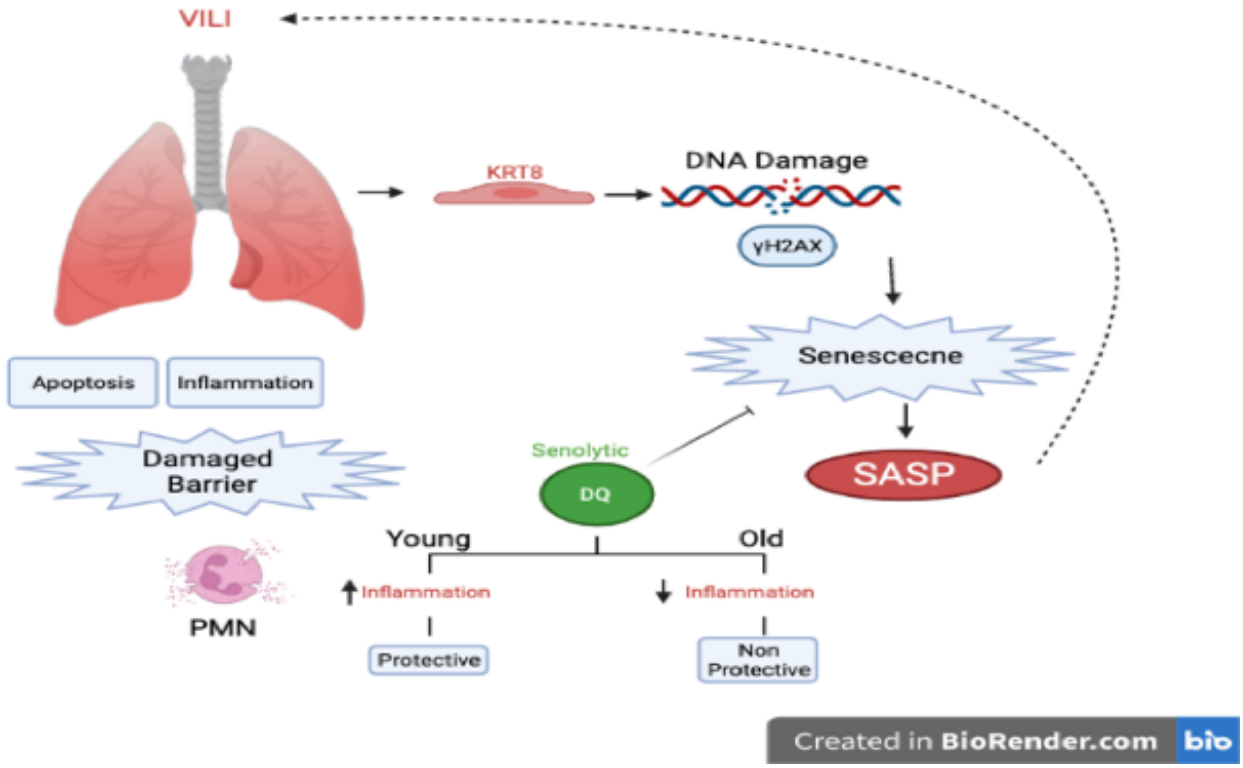

Figure 7. 4 Summary of the potential role of senescence in VILI.

Conclusion: In brief, the innovative aspect of this project highlights the role of senescence in VILI and sheds light in the different intricacy of VILI and aging. Finally, the results obtained in this study could in the future make us rethink different therapeutics to better target age related VILI.

Codes and Miscellaneous

IMAGEJ: CODE USED FOR ZOOMING IN IMAGES AND STACKS 135

MATLAB CODE: PV-LOOP VENTILATION MECHANICS 136

MATLAB CODE: LUNG COMPLIANCE 144

MATLAB CODE: LUNG ELASTANCE GRAPH 145

MATLAB CODE: LUNG RESISTANCE GRAPH 146

ImageJ: Code used for zooming in images and Stacks

```
Code from imagej.nih.gov

And

Instructions from

https://resources.finalsite.net/images/v1567624548/lsuhscshreveportedu/cr5rq8

iubnzgbayqqyoz/howtomakeinset.pdf


} [211]
```

Clearing Space

```
clear

close all

clc
```

Loading Data

```
excel_file_name='PV Loops (version 1).xlsx';

young_mean_sheet='Young';

old_mean_sheet='Old';

hour0='B82:E95';

hourhalf='B97:E110';

hour1='B112:E125';

hour1half='B127:E140';

hour2='B142:E155';

[young_hour0]=xlsread(excel_file_name,young_mean_sheet,hour0);
```

```
[young_hourhalf]=xlsread(excel_file_name,young_mean_sheet,hourhalf);

[young_hour1]=xlsread(excel_file_name,young_mean_sheet,hour1);

[young_hour1half]=xlsread(excel_file_name,young_mean_sheet,hour1half);

[young_hour2]=xlsread(excel_file_name,young_mean_sheet,hour2);

[old_hour0]=xlsread(excel_file_name,old_mean_sheet,hour0);

[old_hourhalf]=xlsread(excel_file_name,old_mean_sheet,hourhalf);

[old_hour1]=xlsread(excel_file_name,old_mean_sheet,hour1);

[old_hour1half]=xlsread(excel_file_name,old_mean_sheet,hour1half);

[old_hour2]=xlsread(excel_file_name,old_mean_sheet,hour2);

% [num_output,string_output,raw_output]=xlsread('filename','tab

% name','range'); Range goes from top left to bottom right. If you

only

% have one output, it defaults to number output.
```

Data Management

```
young_vol_hour0=[young_hour0(:,2);young_hour0(1,2)];
```

```
young_pres_hour0=[young_hour0(:,3);young_hour0(1,3)];

young_vol_hourhalf=[young_hourhalf(:,2);young_hourhalf(1,2)];

young_pres_hourhalf=[young_hourhalf(:,3);young_hourhalf(1,3)];

young_vol_hour1=[young_hour1(:,2);young_hour1(1,2)];

young_pres_hour1=[young_hour1(:,3);young_hour1(1,3)];

young_vol_hour1half=[young_hour1half(:,2);young_hour1half(1,2)];

young_pres_hour1half=[young_hour1half(:,3);young_hour1half(1,3)];

young_vol_hour2=[young_hour2(:,2);young_hour2(1,2)];

young_pres_hour2=[young_hour2(:,3);young_hour2(1,3)];

erry0 = [young_hour0(:,4);young_hour0(1,4)];

erryhalf = [young_hourhalf(:,4);young_hourhalf(1,4)];

erry1 = [young_hour1(:,4);young_hour1(1,4)];

erry1half = [young_hour1half(:,4);young_hour1half(1,4)];
```

1

```
erry2 = [young_hour2(:,4);young_hour2(1,4)];

old_vol_hour0=[old_hour0(:,2);old_hour0(1,2)];
```

```
old_pres_hour0=[old_hour0(:,3);old_hour0(1,3)];

old_vol_hourhalf=[old_hourhalf(:,2);old_hourhalf(1,2)];

old_pres_hourhalf=[old_hourhalf(:,3);old_hourhalf(1,3)];

old_vol_hour1=[old_hour1(:,2);old_hour1(1,2)];

old_pres_hour1=[old_hour1(:,3);old_hour1(1,3)];

old_vol_hour1half=[old_hour1half(:,2);old_hour1half(1,2)];

old_pres_hour1half=[old_hour1half(:,3);old_hour1half(1,3)];

old_vol_hour2=[old_hour2(:,2);old_hour2(1,2)];

old_pres_hour2=[old_hour2(:,3);old_hour2(1,3)];

errO0 = [old_hour0(:,4);old_hour0(1,4)];

errOhalf = [old_hourhalf(:,4);old_hourhalf(1,4)];

errO1 = [old_hour1(:,4);old_hour1(1,4)];

errO1half = [old_hour1half(:,4);old_hour1half(1,4)];

errO2 = [old_hour2(:,4);old_hour2(1,4)];
```

Plot

```
Title='Pressure-Volume Curve';

XLAB='Pressure (cmH_2O)';

YLAB='Volume (mL)';


figure


% plot(young_pres_hour0,young_vol_hour0,'y','LineWidth',4);

% hold on

% plot(young_pres_hourhalf,young_vol_hourhalf,'b','LineWidth',4);

% hold on

% plot(young_pres_hour1,young_vol_hour1,'k','LineWidth',4);

% hold on

% plot(young_pres_hour1half,young_vol_hour1half,'r','LineWidth',4);

% hold on

% plot(young_pres_hour2,young_vol_hour2,'g','LineWidth',4);

% hold on

% plot(old_pres_hour0,old_vol_hour0,'y --','LineWidth',4);

% hold on
```

```
% plot(old_pres_hourhalf,old_vol_hourhalf, 'b--','LineWidth',4);

% hold on

% plot(old_pres_hour1,old_vol_hour1,'k--','LineWidth',4);

% hold on

% plot(old_pres_hour1half,old_vol_hour1half,'r--','LineWidth',4);

% hold on

% plot(old_pres_hour2,old_vol_hour2,'g--','LineWidth',4);

% hold on

figure

errorbar(young_pres_hour0,young_vol_hour0,erry0,'y','LineWidth',4);

hold on

errorbar(young_pres_hourhalf,young_vol_hourhalf,erryhalf,'b','LineWidt

h',4);

hold on
```

2

```
errorbar(young_pres_hour1,young_vol_hour1,erry1,'k','LineWidth',4);
```

```
hold on

errorbar(young_pres_hour1half,young_vol_hour1half,erry1half,'r','LineW

idth',4);

hold on

errorbar(young_pres_hour2,young_vol_hour2,erry2,'g','LineWidth',4);

hold on

errorbar(old_pres_hour0,old_vol_hour0,errO0,'y --','LineWidth',4);

hold on

errorbar(old_pres_hourhalf,old_vol_hourhalf,errOhalf, 'b--

','LineWidth',4);

hold on

errorbar(old_pres_hour1,old_vol_hour1,errO1,'k--','LineWidth',4);

hold on

errorbar(old_pres_hour1half,old_vol_hour1half,errO1half,'r--

','LineWidth',4);

hold on

errorbar(old_pres_hour2,old_vol_hour2,errO2,'g--','LineWidth',4);
```

```
hold on



% figure

% plot(pres_y,vol_y,'y','LineWidth',8);

% hold on

% plot(pres_o,vol_y,'k','LineWidth',6);

% hold off

xlabel(XLAB)

ylabel(YLAB)

title(Title)

legend('Young 0 hour','Young 0.5 hour','Young 1 hour','Young 1.5

hour','Young 2 hour','
```

MATLAB Code: Lung Compliance

```
close all

clear all

clc

%%


X = categorical({'0 hour','2 hour','Recorvery'});

X = reordercats(X,{'0 hour','2 hour','Recorvery'});

Y = [1  1   1; 1.008818214  0.833873864 1.050286049; 1.083187291

0.810558401 0.888382294];

bar(X,Y)


ylabel 'Normalized Compliance';


title 'Compliance';


legend('Control','HP', 'HCL + HP');
```

MATLAB Code: Lung Elastance Graph

```
% Graph Elastance


X = categorical({'0 hour','2 hour','Recorvery'});

X = reordercats(X,{'0 hour','2 hour','Recorvery'});

Y = [1  1   1; 0.991258868  1.19922214  0.952121569; 0.923201378

1.233717396 1.125641525];

bar(X,Y)


ylabel 'Normalized Elastance';


title 'Elastance';


legend('Control','HP', 'HCL + HP');
```

MATLAB Code: Lung Resistance graph

```
% Graph Resistance


X = categorical({'0 hour','2 hour','Recorvery'});

X = reordercats(X,{'0 hour','2 hour','Recorvery'});

Y = [1  1   1; 1.021773539  1.077820339 1.01848264; 0.569434145 0.57914172

0.563200854];

bar(X,Y)


ylabel 'Normalized Resistance';


title 'Resistance';


legend('Control','HP', 'HCL + HP');
```

Curriculum Vitae

FRANCK KAMGA

401 Saybrook Dr., North Chesterfield, VA 23236
804-382-6118 kamgagninzefj@vcu.edu

EDUCATION:

Ph.D. Biomedical Engineering

Expected graduation 05/2022
Virginia Commonwealth University, Richmond, VA
Research topics:

- Ventilator-Induced Lung Injury
- Acute Respiratory Distress Syndrome
- Pulmonary Tissue Repair and Tissue Engineering
- Cellular Senescence
- Surfactant Replacement Therapies

Proposed thesis: ***Therapeutic Approaches for Respiratory Distress Syndrome***

Bachelor of Science in Biomedical Engineering

06/2017
Virginia Commonwealth University, Richmond, VA

Associate of Science in Engineering

12/2014
Reynolds Community College, Richmond, VA

EXPERIENCE:

Virginia Commonwealth University, Pulmonary Mechanobiology Lab
Richmond, VA

NIH/NIA R36 Graduate Principal Investigator

02/2020 – Present

- Obtained 2 years of funding support as the principal investigator through the National Institute of Health (NIH) National Institute on Aging (NIA) R36 grant
- Conceptualized and designed experiments to innovate within the field of aging-related acute lung injury
- Developed *in vivo* models to further uncover the mechanistic driver of cellular senescence of age model of ventilator-induced lung injury (VILI).
- Managed personnel and budgeted for each project phase per grants requirements

Teaching Assistant

- Assisted professors in multiple classes, including an introduction to biomedical engineering, biomedical instrumentation, biomedical signal processing
- Independently managed and designed lab sessions and activities for students
- Reached out to academic and industry partners to set up rounds and observations for introduction to biomedical engineering students

Graduate Research Assistant

08/2017 -- 2020

- Developed *in vitro* methods to investigate cellular senescence in an aging model of VILI using senolytic drugs to selectively target senescent cells (1 published peer-reviewed abstract).

- Successfully established novel surfactant depleted rat model and subsequently created treatments to replace surfactant for the treatment of neonatal respiratory distress syndrome. (1 publication)
- Cultured decellularized lungs within a negative pressure bioreactor to work towards establishing an ex vivo model for VILI.
- Frequently communicated research data within lab meetings, institute-wide meetings, and state and national conferences.
- Received multiple awards, including travel grants, a career development award from BMES.

Undergraduate Researcher
01/2016 – 08/2017

- Managed portions of NIH-funded research projects related to adjusting ventilator protocols to reduce inflammation caused by VILI under the supervision of a graduate student.
- Independently tested the effects of e-cigarettes and cigarette smoke combine with mechanical stretch on the alveoli epithelium.
- Learned skills such as mouse tracheostomy, mouse bone marrow-derived monocytes isolation, and mouse alveolar type ll cell isolation.

Volunteer
06/2015 – 08/2015

- Used histology techniques, Polymerase Chain Reaction (PCR), Enzyme-Linked Immunosorbent Assay (ELISA), Bicinchoninic Acid Assay (BCA assay), immunofluorescence staining, and western blot to analyze the

effects of VILI and aging within mice exposed to high or low tidal ventilation volumes.

John Tyler Community College
Midlothian, VA

Adjunct Anatomy and Physiology Instructor
01/2020 – Present

- Planned in-person and virtual lessons, lectures, and labs to engage students on diverse human anatomy and physiology topics.

Reynolds Community College, Academic Support Center
Richmond, VA

Tutor
01/2013 – 05/2016

- Tutor for multiple subjects, including calculus, biology and physiology, French, information technology, and developmental math.

Student Ambassador
04/2013 – 04/2014

- Helped students register for classes, provided advice to high school students, and led campus tours for parents and students.
- Assisted current students with information and welcome tables at the beginning of each semester.
- Hosted campus-wide event at the direction of the President's Office

ACHIEVEMENT:

VCU Graduate School Dissertation Assistantship 2022

GRC Carl Storm Underrepresented Minority Fellowship 2021

Koerner Family Foundation Supplemental Salary Fellowship	2021
NIH NIA R36: 1-R36-AG-065699-01	2020
BMES Career Development Award	2018
NextProf Pathfinder Participant	2018
Virginia Commonwealth University Sterheimer Senior Design Award	2016
Recipient of the Richard Reynolds Scholarship	2014
Reynolds Community College Excellence in Leadership Award	2013-2014
Reynolds Community College Excellence in Student Ambassador Award	2013-2014
Acceptance to Virginia Community College System Leadership Conference Virginia Beach	2013
Dean's List	Fall 2012, summer 2014
President's List	Spring 2013, Summer 2013, Fall 2013, Spring 2014

Related Skills:

Laboratory/Research Skills

- qPCR
- Cell Culture
- *In vitro* cytotoxicity
- Animal Handling and General Surgery
- Animal Mechanical Ventilation
- Animal Recovery
- Diseased Animal Model Design
- ELISA
- Western Blotting
- IF/IHC Staining
- Experimental Design
- Histology
- Tissue Engineering
- Cell Stretching Models
- IVIS Optical
- ImagingPulmonary
- Drug Delivery
- Pulmonary Drug Design
- Bioreactors
- Light Microscopy
- Animal Tissue Collection
- Rheometric and Tensile
- Biomechanical Testing
- MATLAB
- Rapid 3D Prototyping
- CellProfiler
- LabView
- SolidWorks
- AutoCAD
- Inventor
- ImageJ/FIJI Image Processing and Analysis
- GraphPad Prism
- Adobe Acrobat

- Microsoft Office
- Overleaf
- Creative and Critical Thinking
- Collaborative and Individual Grant Writing
- Public Speaking
- Networking

LEADERSHIP:

Mentor
01/2018 – Present

Virginia Commonwealth University, Richmond, VA

- Helped high school and undergraduate gain research experience through the dean's early research initiative (1 student) and the dean's undergraduate research initiative (2 students).
- Solely managed and guided more than four high school and undergraduate students within the laboratory, resulting in 6 mentee-led conference presentations.

Laboratory Chemical Safety Officer
06/2019 – Present

Virginia Commonwealth University, Richmond, VA

- Insured that all laboratory activities involving hazardous chemicals are conducted in a safe manner and compliance with OSHA regulation
- Worked with principal investigator to provide general chemical safety guidance to laboratory members
- Facilitated chemical laboratory safety training and ensured compliance for all laboratory personnel

Recruitment Co-Chair Biomedical Engineering Graduate Student Council
2017-2021

Virginia Commonwealth University, Richmond, VA

- Advocated for the choice and fair treatment of graduate teaching assistants as chair of the teaching assistant committee.
- Created recruitment events and fostered potential graduate student relationships alongside the Biomedical Engineering Department Director as Co-chair of the recruitment committee.
- Helped found the charter at VCU and established the constitution for the organization

Virginia Bio Statewide Non-Profit Life Science Trade Association
2017- Present

Virginia Biotechnology Research Park, Richmond, VA

- Attended networking events and industry seminars that allowed me to foster industry and academic relationships.

PROFESSIONAL MEMBERSHIP:

Phi Theta Kappa (Honor Society)	2013- present
Biomedical Engineering Society	2016- Present
Virginia Academy of Science	2017- Present
American Society of Mechanical Engineers	2019- Present

REVIEWING ACTIVITIES:

Journal: Translational Research (one article)

PEER-REVIEWED PUBLICATION:

S. Minucci, R.L. Heise, M.S. Valentine, **F.J. Kamga Gninzeko**, A.M. Reynolds. (2021). Mathematical modeling of ventilator-induced lung inflammation. Journal of Theoretical Biology

F.J. Kamga Gninzeko, M.S. Valentine, C.K. Tho, S.R. Chindal, S. Boc, S. Dhapare, M.A.M Momin, A. Hassan, M. Hindle, D.R. Farkas, P.W. Longest, R.L. Heise. (2020). Excipient Enhanced Growth Aerosol Surfactant Replacement Therapy in an In Vivo Rat Lung Injury Model. J. Aerosol Med. Pulm. Drug Deliv.

M.S. Valentine, P. A. Link, J. A. Herbert, **F. J. Kamga Gninzeko**, M. B. Schneck, K. Shankar, J. Nkwocha, A. M. Reynolds, and R. L. Heise. "Inflammation and Monocyte Recruitment Due to Aging and Mechanical Stretch in Alveolar Epithelium Are Inhibited by the Molecular Chaperone 4-Phenylbutyrate." Cellular and Molecular Bioengineering, June 19, 2018, 1–14. PMID: 30581495

R.A. Pouliot, P.A. Link, N.S. Mikhaiel, M.B. Schneck, Michael S. Valentine, **F.J. Kamga Gninzeko**, J.A. Herbert, M. Sakagami, and R.L. Heise. "Development and Characterization of a Naturally Derived Lung Extracellular Matrix Hydrogel." Journal of Biomedical Materials Research Part A 104, no. 8 (August 1, 2016): 1922–35. PMID: 27012815

Preprint:

S. B. Minucci, M. S. Valentine, **F. J. Kamga Gninzeko**, R. L. Heise, and A. M. Reynolds, "Understanding the Role of Macrophages in Lung Inflammation Through Mathematical Modeling," bioRxiv, p. 2020.06.03.132258, Jun. 2020, DOI: 10.1101/2020.06.03.132258.

MANUSCRIPTS IN PREPARATION:

F. J. Kamga Gninzeko, Michael S. Valentine, Cynthia Tho, Rebecca L. Heise. Stretch and Mechanical Ventilation induced senescence in an Acute Model of Lung Injury. Aging and Disease. (*In preparation*)

F. J. Kamga Gninzeko, Michael S. Valentine, Cynthia Tho, Rebecca L. Heise. Dasatinib and Quercetin Cocktail Decrease Senescence in an Aging Model of Ventilator Induced Lung Injury. Aging and Disease. (*In preparation*)

Michael S. Valentine, **Franck J. Kamga Gninzeko**, Cynthia Tho, Cynthia Weigel, Sarah Spiegel, Rebecca L. Heise. Macrophage Polarization and Sphingosine-1-Phosphate (S1P) Signaling in the Lung are Impaired by Aging and High Pressure-Controlled Mechanical Ventilation. Aging and Disease. (*In preparation*)

CONFERENCE PRESENTATIONS:

Kamga Gninzeko, F.J., C.K. Tho, K.K. Brown, R.L. Heise. Senolytic Treatment Reduces Mechanical Stretch-Induced Senescence in Pulmonary Epithelium. **Biomedical Engineering Society Conference**: Virtual (10/2020)

Kamga Gninzeko, F.J., C.K. Tho, K.K. Brown, R.L. Heise. Mechanically Induced Cell Senescence And Senolytic Drug Treatment In Pulmonary Epithelium. **Summer Biomechanics, Bioengineering and Biotransport Conference**: Virtual (06/2020) *Oral presentation*

Kamga Gninzeko, F.J., M.S. Valentine, C.K. Tho, S.R. Chindal, S. Boc, S. Dhapare, M.A.M Momin, A. Hassan, M. Hindle, D.R. Farkas, P.W. Longest, R.L. Heise. (2020). Excipient Enhanced Growth Aerosol Surfactant Replacement Therapy in an In Vivo Rat Lung Injury Model. **Summer Biomechanics, Bioengineering and Biotransport Conference**: Seven Springs, PA (06/2019) *Oral presentation*

Kamga Gninzeko, F.J., M. S. Valentine, S. R. Chindal, A. D. Cordero, R. L. Heise. Stretch and Mechanical Ventilator Induced-Senescence in Ventilator-Induced Lung Injury. **Biomedical Engineering Society Conference**: Atlanta, GA (10/2018)

Kamga Gninzeko, F.J., M. S. Valentine, S. R. Chindal, R. L. Heise. Stretch and Stiffness Induced-Senescence in Ventilator-Induced Lung Injury. **Virginia Academy of Science Conference**: Farmville, VA (05/2018)

Kamga Gninzeko, F. J., M. S. Valentine, J. A. Herbert, M. B. Schneck, R. L. Heise. Cellular Endoplasmic Reticulum Stress and Cytokine Response in Age-Associated Experimental Ventilator Induced Lung Injury. **Virginia Academy of Science Conference**: Richmond, VA (05/2017)

Kamga Gninzeko, F. J., M. S. Valentine, J. A. Herbert, M. B. Schneck, R. L. Heise. Cellular Endoplasmic Reticulum Stress and Cytokine Response in Age-Associated Experimental Ventilator Induced Lung Injury. **Biomedical Engineering Society Conference**: Minneapolis, MN (10/2016)

Kamga Gninzeko, F. J., M. S. Valentine, J. A. Herbert, M. B. Schneck, R. L. Heise**.** Cellular Endoplasmic Reticulum and Cytokine Response in an Aging Model of Ventilator Induced Lung Injury. **VCU Undergraduate Research Symposium**: Richmond, VA (05/2016)

REFEREED ABSTRACT:

R.L Heise, M. S. Valentine, S. R. Chindal, A. D. Cordero, **Kamga Gninzeko, F.J.** Stretch and Mechanical Ventilator Induced-Senescence in Ventilator-Induced Lung Injury. **American Thoracic Society – 2019.**

REFERENCES:

Rebecca Heise, Ph.D. (Advisor)
Associate Professor, Undergraduate Program Director
Department of Biomedical Engineering
Virginia Commonwealth University
Email: rlheise@vcu.edu

Henry J. Donahue, Ph.D. (Committee member)
Alice T. and William H. Goodwin, Jr. Endowed Professor and Chair
Department of Biomedical Engineering
Co-Director, Institute for Engineering and Medicine
Virginia Commonwealth University
Email: hjdonahue@vcu.edu

John Ryan, PhD
Professor, VCU Department of Biology
Associate Vice President for Research Development
VCU Office of Research and Innovation
Virginia Commonwealth University
Email: jjryan@vcu.edu

Christopher Lemmon, PhD
Associate Professor
Associate Department Chair, Biomedical Engineering
Inez Caudill, Jr. Distinguished Professor in Biomedical Engineering
Virginia Commonwealth University
Email: clemmon@vcu.edu

References:

[1] M. Kumar, W. Seeger, and R. Voswinckel, "Senescence-Associated Secretory Phenotype and Its Possible Role in Chronic Obstructive Pulmonary Disease," *Am J Respir Cell Mol Biol*, vol. 51, no. 3, pp. 323–333, Aug. 2014, doi: 10.1165/rcmb.2013-0382PS.

[2] S. R. Eachempati, L. J. Hydo, J. Shou, and P. S. Barie, "Outcomes of acute respiratory distress syndrome (ARDS) in elderly patients," *J Trauma*, vol. 63, no. 2, pp. 344–350, Aug. 2007, doi: 10.1097/TA.0b013e3180eea5a1.

[3] M. J. Sankar, N. Gupta, K. Jain, R. Agarwal, and V. K. Paul, "Efficacy and safety of surfactant replacement therapy for preterm neonates with respiratory distress syndrome in low- and middle-income countries: a systematic review," *J Perinatol*, vol. 36, no. Suppl 1, pp. S36–S48, May 2016, doi: 10.1038/jp.2016.31.

[4] S. Sardesai, M. Biniwale, F. Wertheimer, A. Garingo, and R. Ramanathan, "Evolution of surfactant therapy for respiratory distress syndrome: past, present, and future," *Pediatric Research*, vol. 81, no. 1–2, pp. 240–248, Jan. 2017, doi: 10.1038/pr.2016.203.

[5] H. Lu, W. Li, G. Shao, and H. Wang, "Expression of SP-C and Ki67 in lungs of preterm infants dying from respiratory distress syndrome," *Eur J Histochem*, vol. 56, no. 3, Jul. 2012, doi: 10.4081/ejh.2012.e35.

[6] C. Zhang and X. Zhu, "Clinical effects of pulmonary surfactant in combination with nasal continuous positive airway pressure therapy on neonatal respiratory distress syndrome," *Pak J Med Sci*, vol. 33, no. 3, pp. 621–625, 2017, doi: 10.12669/pjms.333.12227.

[7] J. Pérez-Gil, "Structure of pulmonary surfactant membranes and films: The role of proteins and lipid–protein interactions," *Biochimica et Biophysica Acta (BBA) - Biomembranes*, vol. 1778, no. 7, pp. 1676–1695, Jul. 2008, doi: 10.1016/j.bbamem.2008.05.003.

[8] J. R. Glasser and R. K. Mallampalli, "Surfactant and its role in the pathobiology of pulmonary infection," *Microbes Infect*, vol. 14, no. 1, pp. 17–25, Jan. 2012, doi: 10.1016/j.micinf.2011.08.019.

[9] J. M. Andersson, C. Grey, M. Larsson, T. M. Ferreira, and E. Sparr, “Effect of cholesterol on the molecular structure and transitions in a clinical-grade lung surfactant extract,” *Proc Natl Acad Sci U S A*, vol. 114, no. 18, pp. E3592–E3601, May 2017, doi: 10.1073/pnas.1701239114.

[10] K. Altirkawi, “Surfactant therapy: the current practice and the future trends,” *Sudan J Paediatr*, vol. 13, no. 1, pp. 11–22, 2013.

[11] M. Mussavi, K. Mirnia, and K. Asadollahi, “Comparison of the Efficacy of Three Natural Surfactants (Curosurf, Survanta, and Alveofact) in the Treatment of Respiratory Distress Syndrome Among Neonates: A Randomized Controlled Trial,” *Iran J Pediatr*, vol. 26, no. 5, Jul. 2016, doi: 10.5812/ijp.5743.

[12] C. Ruppert *et al.*, “Dry powder aerosolization of a recombinant surfactant protein-C–based surfactant for inhalative treatment of the acutely inflamed lung*,” *Critical Care Medicine*, vol. 38, no. 7, pp. 1584–1591, Jul. 2010, doi: 10.1097/CCM.0b013e3181dfcb3b.

[13] D. F. Willson, “Aerosolized Surfactants, Anti-Inflammatory Drugs, and Analgesics,” *Respiratory Care*, vol. 60, no. 6, pp. 774–793, Jun. 2015, doi: 10.4187/respcare.03579.

[14] P. W. Longest and M. Hindle, “Numerical Model to Characterize the Size Increase of Combination Drug and Hygroscopic Excipient Nanoparticle Aerosols,” *Aerosol Sci Technol*, vol. 45, no. 7, pp. 884–899, Jan. 2011, doi: 10.1080/02786826.2011.566592.

[15] S. Boc, “Aerosolized Surfactants: Formulation Development and Evaluation of Aerosol Drug Delivery to the Lungs of Infants,” *Theses and Dissertations*, Jan. 2018, [Online]. Available: https://scholarscompass.vcu.edu/etd/5577

[16] M. Hindle and P. W. Longest, “Condensational Growth of Combination Drug-Excipient Submicrometer Particles for Targeted High Efficiency Pulmonary Delivery: Evaluation of Formulation and Delivery Device,” *J Pharm Pharmacol*, vol. 64, no. 9, pp. 1254–1263, Sep. 2012, doi: 10.1111/j.2042-7158.2012.01476.x.

[17] P. W. Longest and G. Tian, “Development of a New Technique for the Efficient Delivery of Aerosolized Medications to Infants on Mechanical Ventilation,” *Pharm Res*, vol. 32, no. 1, pp. 321–336, Jan. 2015, doi: 10.1007/s11095-014-1466-4.

[18] G. Tian, P. W. Longest, X. Li, and M. Hindle, “Targeting aerosol deposition to and within the lung airways using excipient enhanced growth,” *Journal of Aerosol Medicine and Pulmonary Drug Delivery*, vol. 26, no. 5, pp. 248–265, 2013.

[19] J. A. Herbert *et al.*, “Conservative fluid management prevents age-associated ventilator induced mortality,” *Exp. Gerontol.*, vol. 81, pp. 101–109, Aug. 2016, doi: 10.1016/j.exger.2016.05.005.

[20] F. Setzer, K. Oschatz, L. Hueter, B. Schmidt, K. Schwarzkopf, and T. Schreiber, “Susceptibility to ventilator induced lung injury is increased in senescent rats,” *Crit Care*, vol. 17, no. 3, p. R99, 2013, doi: 10.1186/cc12744.

[21] M. S. Valentine *et al.*, “Inflammation and Monocyte Recruitment Due to Aging and Mechanical Stretch in Alveolar Epithelium are Inhibited by the Molecular Chaperone 4-Phenylbutyrate,” *Cel. Mol. Bioeng.*, vol. 11, no. 6, pp. 495–508, Dec. 2018, doi: 10.1007/s12195-018-0537-8.

[22] J. P. Joelsson, S. Ingthorsson, J. Kricker, T. Gudjonsson, and S. Karason, “Ventilator-induced lung-injury in mouse models: Is there a trap?,” *Laboratory Animal Research*, vol. 37, no. 1, p. 30, Oct. 2021, doi: 10.1186/s42826-021-00108-x.

[23] A. Biran *et al.*, “Quantitative identification of senescent cells in aging and disease,” *Aging Cell*, vol. 16, no. 4, pp. 661–671, Aug. 2017, doi: 10.1111/acel.12592.

[24] M. J. Schafer *et al.*, “Cellular senescence mediates fibrotic pulmonary disease,” *Nat Commun*, vol. 8, Feb. 2017, doi: 10.1038/ncomms14532.

[25] H. J. Jin *et al.*, “Senescence-Associated MCP-1 Secretion Is Dependent on a Decline in BMI1 in Human Mesenchymal Stromal Cells,” *Antioxid. Redox Signal.*, vol. 24, no. 9, pp. 471–485, Mar. 2016, doi: 10.1089/ars.2015.6359.

[26] T. Tchkonia, Y. Zhu, J. van Deursen, J. Campisi, and J. L. Kirkland, “Cellular senescence and the senescent secretory phenotype: therapeutic opportunities,” *J Clin Invest*, vol. 123, no. 3, pp. 966–972, Mar. 2013, doi: 10.1172/JCI64098.

[27] K. Aoshiba, T. Tsuji, and A. Nagai, “Bleomycin induces cellular senescence in alveolar epithelial cells,” *European Respiratory Journal*, vol. 22, no. 3, pp. 436–443, Sep. 2003, doi: 10.1183/09031936.03.00011903.

[28] D. J. Baker *et al.*, “Clearance of p16Ink4a-positive senescent cells delays ageing-associated disorders,” *Nature*, vol. 479, no. 7372, pp. 232–236, Nov. 2011, doi: 10.1038/nature10600.

[29] B. M. Fischer *et al.*, “Increased expression of senescence markers in cystic fibrosis airways,” *Am J Physiol Lung Cell Mol Physiol*, vol. 304, no. 6, pp. L394–L400, Mar. 2013, doi: 10.1152/ajplung.00091.2012.

[30] G. P. Dimri *et al.*, “A biomarker that identifies senescent human cells in culture and in aging skin in vivo.,” *Proc Natl Acad Sci U S A*, vol. 92, no. 20, pp. 9363–9367, Sep. 1995.

[31] M. J. Yousefzadeh *et al.*, “Fisetin is a senotherapeutic that extends health and lifespan,” *EBioMedicine*, vol. 36, pp. 18–28, Sep. 2018, doi: 10.1016/j.ebiom.2018.09.015.

[32] J. N. Justice *et al.*, “Senolytics in idiopathic pulmonary fibrosis: Results from a first-in-human, open-label, pilot study,” *EBioMedicine*, Jan. 2019, doi: 10.1016/j.ebiom.2018.12.052.

[33] A. F. Naeimi and M. Alizadeh, “Antioxidant properties of the flavonoid fisetin: An updated review of in vivo and in vitro studies,” *Trends in Food Science & Technology*, vol. 70, pp. 34–44, Dec. 2017, doi: 10.1016/j.tifs.2017.10.003.

[34] N. Khan, D. N. Syed, N. Ahmad, and H. Mukhtar, “Fisetin: A Dietary Antioxidant for Health Promotion,” *Antioxid Redox Signal*, vol. 19, no. 2, pp. 151–162, Jul. 2013, doi: 10.1089/ars.2012.4901.

[35] J. C. Montero, S. Seoane, A. Ocaña, and A. Pandiella, “Inhibition of Src Family Kinases and Receptor Tyrosine Kinases by Dasatinib: Possible Combinations in Solid Tumors,” *Clin Cancer Res*, vol. 17, no. 17, pp. 5546–5552, Sep. 2011, doi: 10.1158/1078-0432.CCR-10-2616.

[36] Y. Zhu *et al.*, "The Achilles' heel of senescent cells: from transcriptome to senolytic drugs," *Aging Cell*, vol. 14, no. 4, pp. 644–658, Aug. 2015, doi: 10.1111/acel.12344.

[37] T. Oyaizu *et al.*, "Src tyrosine kinase inhibition prevents pulmonary ischemia–reperfusion-induced acute lung injury," *Intensive Care Med*, vol. 38, no. 5, pp. 894–905, May 2012, doi: 10.1007/s00134-012-2498-z.

[38] B. Zhou, G. Weng, Z. Huang, T. Liu, and F. Dai, "Arctiin Prevents LPS-Induced Acute Lung Injury via Inhibition of PI3K/AKT Signaling Pathway in Mice," *Inflammation*, vol. 41, no. 6, pp. 2129–2135, Dec. 2018, doi: 10.1007/s10753-018-0856-x.

[39] A. R. Froese *et al.*, "Stretch-induced Activation of Transforming Growth Factor-β1 in Pulmonary Fibrosis," *Am J Respir Crit Care Med*, vol. 194, no. 1, pp. 84–96, Jan. 2016, doi: 10.1164/rccm.201508-1638OC.

[40] J. Kwong, L. Hong, R. Liao, Q. Deng, J. Han, and P. Sun, "p38α and p38γ Mediate Oncogenic ras-induced Senescence through Differential Mechanisms," *J Biol Chem*, vol. 284, no. 17, pp. 11237–11246, Apr. 2009, doi: 10.1074/jbc.M808327200.

[41] M. Ragaller and T. Richter, "Acute lung injury and acute respiratory distress syndrome," *J Emerg Trauma Shock*, vol. 3, no. 1, pp. 43–51, 2010, doi: 10.4103/0974-2700.58663.

[42] A. Rufini, P. Tucci, I. Celardo, and G. Melino, "Senescence and aging: the critical roles of p53," *Oncogene*, vol. 32, no. 43, pp. 5129–5143, Oct. 2013, doi: 10.1038/onc.2012.640.

[43] J.-P. Coppé, P.-Y. Desprez, A. Krtolica, and J. Campisi, "The Senescence-Associated Secretory Phenotype: The Dark Side of Tumor Suppression," *Annu Rev Pathol*, vol. 5, pp. 99–118, 2010, doi: 10.1146/annurev-pathol-121808-102144.

[44] M. Lehmann *et al.*, "Senolytic drugs target alveolar epithelial cell function and attenuate experimental lung fibrosis ex vivo," *Eur. Respir. J.*, vol. 50, no. 2, 2017, doi: 10.1183/13993003.02367-2016.

[45] F. J. Kamga Gninzeko *et al.*, “Excipient Enhanced Growth Aerosol Surfactant Replacement Therapy in an In Vivo Rat Lung Injury Model,” *Journal of Aerosol Medicine and Pulmonary Drug Delivery*, May 2020, doi: 10.1089/jamp.2020.1593.

[46] F. Ricci *et al.*, “Physiological, Biochemical, and Biophysical Characterization of the Lung-Lavaged Spontaneously-Breathing Rabbit as a Model for Respiratory Distress Syndrome,” *PLoS One*, vol. 12, no. 1, Jan. 2017, doi: 10.1371/journal.pone.0169190.

[47] M.-E. I. Tsitoura, E. F. Stavrou, I. A. Maraziotis, K. Sarafidis, A. Athanassiadou, and G. Dimitriou, “Surfactant Protein A and B Gene Polymorphisms and Risk of Respiratory Distress Syndrome in Late-Preterm Neonates,” *PLoS One*, vol. 11, no. 11, Nov. 2016, doi: 10.1371/journal.pone.0166516.

[48] M. V. Kinney, J. E. Lawn, C. P. Howson, and J. Belizan, “15 million preterm births annually: what has changed this year?,” *Reprod Health*, vol. 9, p. 28, Nov. 2012, doi: 10.1186/1742-4755-9-28.

[49] M. Mussavi, K. Mirnia, and K. Asadollahi, “Comparison of the Efficacy of Three Natural Surfactants (Curosurf, Survanta, and Alveofact) in the Treatment of Respiratory Distress Syndrome Among Neonates: A Randomized Controlled Trial,” *Iran J Pediatr*, vol. 26, no. 5, Jul. 2016, doi: 10.5812/ijp.5743.

[50] A. Moen, X.-Q. Yu, R. Almaas, T. Curstedt, and O. D. Saugstad, “Acute effects on systemic circulation after intratracheal instillation of Curosurf or Survanta in surfactant-depleted newborn piglets,” *Acta Paediatrica*, vol. 87, no. 3, pp. 297–303, 1998, doi: 10.1111/j.1651-2227.1998.tb01441.x.

[51] Y.-J. Son, P. W. Longest, and M. Hindle, “Aerosolization Characteristics of Dry Powder Inhaler Formulations for the Excipient Enhanced Growth (EEG) Application: Effect of Spray Drying Process Conditions on Aerosol Performance,” *Int J Pharm*, vol. 443, no. 1–2, pp. 137–145, Feb. 2013, doi: 10.1016/j.ijpharm.2013.01.003.

[52] Y.-J. Son, P. W. Longest, G. Tian, and M. Hindle, “Evaluation and Modification of Commercial Dry Powder Inhalers for the Aerosolization of a Submicrometer Excipient Enhanced Growth (EEG) Formulation,” *Eur J Pharm Sci*, vol. 49, no. 3, pp. 390–399, Jun. 2013, doi: 10.1016/j.ejps.2013.04.011.

[53] C. S. Kim, “Deposition of aerosol particles in human lungs: in vivo measurement and modeling,” *Biomarkers*, vol. 14(S1), no. Journal Article, pp. 54–58, 2009.

[54] F. Ricci *et al.*, “Surfactant replacement therapy in combination with different non-invasive ventilation techniques in spontaneously-breathing, surfactant-depleted adult rabbits,” *PLoS One*, vol. 13, no. 7, Jul. 2018, doi: 10.1371/journal.pone.0200542.

[55] M. Russ, S. Kronfeldt, W. Boemke, T. Busch, R. C. E. Francis, and P. A. Pickerodt, “Lavage-induced Surfactant Depletion in Pigs As a Model of the Acute Respiratory Distress Syndrome (ARDS),” *J Vis Exp*, no. 115, Sep. 2016, doi: 10.3791/53610.

[56] P. W. Longest, Y.-J. Son, L. Holbrook, and M. Hindle, “Aerodynamic Factors Responsible for the Deaggregation of Carrier-Free Drug Powders to form Micrometer and Submicrometer Aerosols,” *Pharm Res*, vol. 30, no. 6, pp. 1608–1627, Jun. 2013, doi: 10.1007/s11095-013-1001-z.

[57] W. Longest and D. Farkas, “Development of a New Inhaler for High-Efficiency Dispersion of Spray-Dried Powders Using Computational Fluid Dynamics (CFD) Modeling,” *AAPS J*, vol. 21, no. 2, p. 25, Feb. 2019, doi: 10.1208/s12248-018-0281-y.

[58] W. Longest, D. Farkas, K. Bass, and M. Hindle, “Use of Computational Fluid Dynamics (CFD) Dispersion Parameters in the Development of a New DPI Actuated with Low Air Volumes,” *Pharm Res*, vol. 36, no. 8, p. 110, May 2019, doi: 10.1007/s11095-019-2644-1.

[59] S. T. Boc, D. R. Farkas, P. W. Longest, and M. Hindle, “Spray Dried Pulmonary Surfactant Powder Formulations: Development and Characterization,” *RDD*, vol. 2, pp. 635–638, 2018.

[60] S. T. Boc, D. R. Farkas, P. W. Longest, and M. Hindle, “Aerosolization of spray dried pulmonary surfactant powder using a novel low air volume actuated dry powder inhaler,” *RDD*, vol. 2, pp. 639–642, 2018.

[61] P. O. Nkadi, T. A. Merritt, and D.-A. M. Pillers, “An Overview of Pulmonary Surfactant in the Neonate: Genetics, Metabolism, and the Role of Surfactant in Health and Disease,” *Mol Genet Metab*, vol. 97, no. 2, pp. 95–101, Jun. 2009, doi: 10.1016/j.ymgme.2009.01.015.

[62] C. C.-H. Ma and S. Ma, “The Role of Surfactant in Respiratory Distress Syndrome,” *Open Respir Med J*, vol. 6, pp. 44–53, Jul. 2012, doi: 10.2174/1874306401206010044.

[63] B. T. Bloom and R. H. Clark, “Comparison of Infasurf (Calfactant) and Survanta (Beractant) in the Prevention and Treatment of Respiratory Distress Syndrome,” *Pediatrics*, vol. 116, no. 2, pp. 392–399, Aug. 2005, doi: 10.1542/peds.2004-2783.

[64] B. K. Walsh and R. M. Diblasi, “Mechanical Ventilation of the Neonate and Pediatric Patient,” in *Perinatal and Pediatric Respiratory Care. B. K. Walsh, M. P. Czervinske and R. M. DiBlasi*, St. Louis: Saunders Elsevier, 2010, pp. 325–347.

[65] D. Farkas, M. Hindle, and P. W. Longest, “Development of an Inline Dry Powder Inhaler That Requires Low Air Volume,” *J Aerosol Med Pulm Drug Deliv*, vol. 31, no. 4, pp. 255–265, Aug. 2018, doi: 10.1089/jamp.2017.1424.

[66] E. Berggren *et al.*, “Pilot study of nebulized surfactant therapy for neonatal respiratory distress syndrome,” *Acta Paediatrica*, vol. 89, no. 4, pp. 460–464, 2000, doi: 10.1111/j.1651-2227.2000.tb00084.x.

[67] F. Bianco *et al.*, “From bench to bedside: in vitro and in vivo evaluation of a neonate-focused nebulized surfactant delivery strategy,” *Respir Res*, vol. 20, no. 1, p. 134, Jul. 2019, doi: 10.1186/s12931-019-1096-9.

[68] C. Rey-Santano, V. E. Mielgo, L. Andres, E. Ruiz-del-Yerro, A. Valls-i-Soler, and X. Murgia, “Acute and sustained effects of aerosolized vs. bolus surfactant therapy in premature lambs with respiratory distress syndrome,” *Pediatric Research*, vol. 73, no. 5, pp. 639–646, May 2013, doi: 10.1038/pr.2013.24.

[69] F. Caminita *et al.*, “A preterm pig model of lung immaturity and spontaneous infant respiratory distress syndrome,” *American Journal of Physiology-Lung Cellular and Molecular Physiology*, vol. 308, no. 2, pp. L118–L129, Nov. 2014, doi: 10.1152/ajplung.00173.2014.

[70] J. Vestbo *et al.*, “Global Strategy for the Diagnosis, Management, and Prevention of Chronic Obstructive Pulmonary Disease,” *Am J Respir Crit Care Med*, vol. 187, no. 4, pp. 347–365, Feb. 2013, doi: 10.1164/rccm.201204-0596PP.

[71] C. Vancheri, M. Failla, N. Crimi, and G. Raghu, “Idiopathic pulmonary fibrosis: a disease with similarities and links to cancer biology,” *Eur Respir J*, vol. 35, no. 3, pp. 496–504, Mar. 2010, doi: 10.1183/09031936.00077309.

[72] J. F. Devine, “Chronic Obstructive Pulmonary Disease: An Overview,” *Am Health Drug Benefits*, vol. 1, no. 7, pp. 34–42, Sep. 2008.

[73] J. C. Hogg, “Lung structure and function in COPD [State of the Art Series. Chronic obstructive pulmonary disease in high- and low-income countries. Edited by G. Marks and M. Chan-Yeung. Number 4 in the series],” *The International Journal of Tuberculosis and Lung Disease*, vol. 12, no. 5, pp. 467–479, May 2008.

[74] S. L. Barratt, A. Creamer, C. Hayton, and N. Chaudhuri, “Idiopathic Pulmonary Fibrosis (IPF): An Overview,” *J Clin Med*, vol. 7, no. 8, p. 201, Aug. 2018, doi: 10.3390/jcm7080201.

[75] R. Lucas, A. D. Verin, S. M. Black, and J. D. Catravas, “Regulators of endothelial and epithelial barrier integrity and function in acute lung injury,” *Biochem Pharmacol*, vol. 77, no. 12, pp. 1763–1772, Jun. 2009, doi: 10.1016/j.bcp.2009.01.014.

[76] J. K. Juss *et al.*, “Acute Respiratory Distress Syndrome Neutrophils Have a Distinct Phenotype and Are Resistant to Phosphoinositide 3-Kinase Inhibition,” *Am J Respir Crit Care Med*, vol. 194, no. 8, pp. 961–973, Oct. 2016, doi: 10.1164/rccm.201509-1818OC.

[77] G. F. Nieman, J. Satalin, P. Andrews, H. Aiash, N. M. Habashi, and L. A. Gatto, “Personalizing mechanical ventilation according to physiologic parameters to stabilize alveoli and minimize ventilator induced lung injury (VILI),” *Intensive Care Med Exp*, vol. 5, p. 8, Feb. 2017, doi: 10.1186/s40635-017-0121-x.

[78] H. Imanaka, M. Shimaoka, N. Matsuura, M. Nishimura, N. Ohta, and H. Kiyono, “Ventilator-Induced Lung Injury Is Associated with Neutrophil Infiltration, Macrophage Activation, and TGF-β1 mRNA Upregulation in Rat Lungs,” *Anesthesia & Analgesia*, vol. 92, no. 2, pp. 428–436, Feb. 2001, doi: 10.1213/00000539-200102000-00029.

[79] R. R. Woldhuis *et al.*, “Link between increased cellular senescence and extracellular matrix changes in COPD,” *American Journal of Physiology-Lung Cellular and Molecular Physiology*, vol. 319, no. 1, pp. L48–L60, Jul. 2020, doi: 10.1152/ajplung.00028.2020.

[80] C. Yao *et al.*, “Senescence of Alveolar Type 2 Cells Drives Progressive Pulmonary Fibrosis,” *Am J Respir Crit Care Med*, vol. 203, no. 6, pp. 707–717, Mar. 2021, doi: 10.1164/rccm.202004-1274OC.

[81] J. Blázquez-Prieto *et al.*, “Activation of p21 limits acute lung injury and induces early senescence after acid aspiration and mechanical ventilation,” *Transl Res*, vol. 233, pp. 104–116, Jul. 2021, doi: 10.1016/j.trsl.2021.01.008.

[82] M. Thomas, M. Decramer, and D. E. O’Donnell, “No room to breathe: the importance of lung hyperinflation in COPD,” *Prim Care Respir J*, vol. 22, no. 1, pp. 101–111, Mar. 2013, doi: 10.4104/pcrj.2013.00025.

[83] M. Sellami *et al.*, “Induction and regulation of murine emphysema by elastin peptides,” *American Journal of Physiology-Lung Cellular and Molecular Physiology*, vol. 310, no. 1, pp. L8–L23, Jan. 2016, doi: 10.1152/ajplung.00068.2015.

[84] L. K. Senavirathna *et al.*, “Hypoxia induces pulmonary fibroblast proliferation through NFAT signaling,” *Sci Rep*, vol. 8, no. 1, Art. no. 1, Feb. 2018, doi: 10.1038/s41598-018-21073-x.

[85] F. J. Jacono, “Control of ventilation in COPD and lung injury,” *Respiratory Physiology & Neurobiology*, vol. 189, no. 2, pp. 371–376, Nov. 2013, doi: 10.1016/j.resp.2013.07.010.

[86] C. L. N. Oliveira, A. D. Araújo, J. H. T. Bates, J. S. Andrade, and B. Suki, “Entropy Production and the Pressure–Volume Curve of the Lung,” *Frontiers in Physiology*, vol. 7, 2016, Accessed: Mar. 02, 2022. [Online]. Available: https://www.frontiersin.org/article/10.3389/fphys.2016.00073

[87] L. Hayflick and P. S. Moorhead, “The serial cultivation of human diploid cell strains,” *Experimental Cell Research*, vol. 25, no. 3, pp. 585–621, Dec. 1961, doi: 10.1016/0014-4827(61)90192-6.

[88] P. Parikh, S. Wicher, K. Khandalavala, C. M. Pabelick, R. D. Britt, and Y. S. Prakash, “Cellular senescence in the lung across the age spectrum,” *American Journal of Physiology-Lung Cellular and Molecular Physiology*, vol. 316, no. 5, pp. L826–L842, May 2019, doi: 10.1152/ajplung.00424.2018.

[89] G. Nelson, O. Kucheryavenko, J. Wordsworth, and T. von Zglinicki, “The senescent bystander effect is caused by ROS-activated NF-κB signalling,” *Mechanisms of Ageing and Development*, vol. 170, pp. 30–36, Mar. 2018, doi: 10.1016/j.mad.2017.08.005.

[90] R. Salama, M. Sadaie, M. Hoare, and M. Narita, “Cellular senescence and its effector programs,” *Genes Dev.*, vol. 28, no. 2, pp. 99–114, Jan. 2014, doi: 10.1101/gad.235184.113.

[91] C. Chandeck and W. J. Mooi, “Oncogene-induced Cellular Senescence,” *Advances in Anatomic Pathology*, vol. 17, no. 1, pp. 42–48, Jan. 2010, doi: 10.1097/PAP.0b013e3181c66f4e.

[92] J. Birch *et al.*, “Telomere Dysfunction and Senescence-associated Pathways in Bronchiectasis,” *Am J Respir Crit Care Med*, vol. 193, no. 8, pp. 929–932, Apr. 2016, doi: 10.1164/rccm.201510-2035LE.

[93] H. Jiang *et al.*, “Proteins induced by telomere dysfunction and DNA damage represent biomarkers of human aging and disease,” *Proceedings of the National Academy of Sciences*, vol. 105, no. 32, pp. 11299–11304, Aug. 2008, doi: 10.1073/pnas.0801457105.

[94] J. M. Helena *et al.*, “Deoxyribonucleic Acid Damage and Repair: Capitalizing on Our Understanding of the Mechanisms of Maintaining Genomic Integrity for Therapeutic Purposes,” *International Journal of Molecular Sciences*, vol. 19, no. 4, Art. no. 4, Apr. 2018, doi: 10.3390/ijms19041148.

[95] K. Aoshiba, F. Zhou, T. Tsuji, and A. Nagai, “DNA damage as a molecular link in the pathogenesis of COPD in smokers,” *European Respiratory Journal*, vol. 39, no. 6, pp. 1368–1376, Jun. 2012, doi: 10.1183/09031936.00050211.

[96] M. Schuliga *et al.*, “Self DNA perpetuates IPF lung fibroblast senescence in a cGAS-dependent manner,” *Clinical Science*, vol. 134, no. 7, pp. 889–905, Apr. 2020, doi: 10.1042/CS20191160.

[97] L. P. da S. Sergio, A. M. C. Thomé, L. A. da S. N. Trajano, A. L. Mencalha, A. de S. da Fonseca, and F. de Paoli, “Photobiomodulation prevents DNA fragmentation of alveolar epithelial cells and alters the

mRNA levels of caspase 3 and Bcl-2 genes in acute lung injury," *Photochem. Photobiol. Sci.*, vol. 17, no. 7, pp. 975–983, Jul. 2018, doi: 10.1039/C8PP00109J.

[98] L. B. PhD, "DNA Damage Response (DDR)." https://blog.crownbio.com/dna-damage-response (accessed Feb. 28, 2022).

[99] N. Chatterjee and G. C. Walker, "Mechanisms of DNA damage, repair and mutagenesis," *Environ Mol Mutagen*, vol. 58, no. 5, pp. 235–263, Jun. 2017, doi: 10.1002/em.22087.

[100] J. Deng, X. Bai, H. Tang, and S. Pang, "DNA damage promotes ER stress resistance through elevation of unsaturated phosphatidylcholine in Caenorhabditis elegans," *Journal of Biological Chemistry*, vol. 296, Jan. 2021, doi: 10.1074/jbc.RA120.016083.

[101] A. Gupta, M. M. Hossain, D. E. Read, C. Hetz, A. Samali, and S. Gupta, "PERK regulated miR-424(322)-503 cluster fine-tunes activation of IRE1 and ATF6 during Unfolded Protein Response," *Sci Rep*, vol. 5, no. 1, Art. no. 1, Dec. 2015, doi: 10.1038/srep18304.

[102] J. Y. Chan, J. Luzuriaga, E. L. Maxwell, P. K. West, M. Bensellam, and D. R. Laybutt, "The balance between adaptive and apoptotic unfolded protein responses regulates β-cell death under ER stress conditions through XBP1, CHOP and JNK," *Molecular and Cellular Endocrinology*, vol. 413, pp. 189–201, Sep. 2015, doi: 10.1016/j.mce.2015.06.025.

[103] H. S. Kim, Y. Kim, M. J. Lim, Y.-G. Park, S. I. Park, and J. Sohn, "The p38-activated ER stress-ATF6α axis mediates cellular senescence," *The FASEB Journal*, vol. 33, no. 2, pp. 2422–2434, 2019, doi: 10.1096/fj.201800836R.

[104] A. Maréchal and L. Zou, "DNA Damage Sensing by the ATM and ATR Kinases," *Cold Spring Harb Perspect Biol*, vol. 5, no. 9, p. a012716, Sep. 2013, doi: 10.1101/cshperspect.a012716.

[105] A. Karimian, Y. Ahmadi, and B. Yousefi, "Multiple functions of p21 in cell cycle, apoptosis and transcriptional regulation after DNA damage," *DNA Repair*, vol. 42, pp. 63–71, Jun. 2016, doi: 10.1016/j.dnarep.2016.04.008.

[106] G. H. Stein, L. F. Drullinger, A. Soulard, and V. Dulić, "Differential roles for cyclin-dependent kinase inhibitors p21 and p16 in the mechanisms of senescence and differentiation in human fibroblasts," *Mol Cell Biol*, vol. 19, no. 3, pp. 2109–2117, Mar. 1999, doi: 10.1128/MCB.19.3.2109.

[107] A. Krämer *et al.*, "Alterations of the cyclin D1/pRb/p16INK4A pathway in multiple myeloma," *Leukemia*, vol. 16, no. 9, Art. no. 9, Sep. 2002, doi: 10.1038/sj.leu.2402609.

[108] D. Álvarez *et al.*, "IPF lung fibroblasts have a senescent phenotype," *Am J Physiol Lung Cell Mol Physiol*, vol. 313, no. 6, pp. L1164–L1173, Dec. 2017, doi: 10.1152/ajplung.00220.2017.

[109] C. T. Cottage *et al.*, "Targeting p16-induced senescence prevents cigarette smoke-induced emphysema by promoting IGF1/Akt1 signaling in mice," *Commun Biol*, vol. 2, no. 1, Art. no. 1, Aug. 2019, doi: 10.1038/s42003-019-0532-1.

[110] R. Yosef *et al.*, "Directed elimination of senescent cells by inhibition of BCL-W and BCL-XL," *Nat Commun*, vol. 7, no. 1, Art. no. 1, Apr. 2016, doi: 10.1038/ncomms11190.

[111] C. Lawless, C. Wang, D. Jurk, A. Merz, T. von Zglinicki, and J. F. Passos, "Quantitative assessment of markers for cell senescence," *Experimental Gerontology*, vol. 45, no. 10, pp. 772–778, Oct. 2010, doi: 10.1016/j.exger.2010.01.018.

[112] M. Siganaki *et al.*, "Deregulation of apoptosis mediators' p53 and bcl2 in lung tissue of COPD patients," *Respiratory Research*, vol. 11, no. 1, p. 46, Apr. 2010, doi: 10.1186/1465-9921-11-46.

[113] Y. He *et al.*, "Therapeutic Effects of the Bcl-2 Inhibitor on Bleomycin-induced Pulmonary Fibrosis in Mice," *Frontiers in Molecular Biosciences*, vol. 8, 2021, Accessed: Mar. 04, 2022. [Online]. Available: https://www.frontiersin.org/article/10.3389/fmolb.2021.645846

[114] Y. E. Miller *et al.*, "Bronchial Epithelial Ki-67 Index Is Related to Histology, Smoking, and Gender, but Not Lung Cancer or Chronic Obstructive Pulmonary Disease," *Cancer Epidemiology, Biomarkers & Prevention*, vol. 16, no. 11, pp. 2425–2431, Nov. 2007, doi: 10.1158/1055-9965.EPI-07-0220.

[115] N. J. Lomas, K. L. Watts, K. M. Akram, N. R. Forsyth, and M. A. Spiteri, “Idiopathic pulmonary fibrosis: immunohistochemical analysis provides fresh insights into lung tissue remodelling with implications for novel prognostic markers,” *Int J Clin Exp Pathol*, vol. 5, no. 1, pp. 58–71, Jan. 2012.

[116] F. J. K. Gninzeko, C. K. Tho, M. S. Valentine, E. N. Wandling, and R. L. Heise, “Mechanical Ventilation induced DNA Damage and P21 in an Acute Aging Model of Lung Injury.” bioRxiv, p. 2022.03.08.483505, Mar. 08, 2022. doi: 10.1101/2022.03.08.483505.

[117] N. N. Mohamad Anuar, N. S. Nor Hisam, S. L. Liew, and A. Ugusman, “Clinical Review: Navitoclax as a Pro-Apoptotic and Anti-Fibrotic Agent,” *Frontiers in Pharmacology*, vol. 11, 2020, Accessed: Mar. 04, 2022. [Online]. Available: https://www.frontiersin.org/article/10.3389/fphar.2020.564108

[118] H. Yang *et al.*, “Navitoclax (ABT263) reduces inflammation and promotes chondrogenic phenotype by clearing senescent osteoarthritic chondrocytes in osteoarthritis,” *Aging*, vol. 12, no. 13, pp. 12750–12770, Jul. 2020, doi: 10.18632/aging.103177.

[119] H. Schutte *et al.*, “Bronchoalveolar and systemic cytokine profiles in patients with ARDS, severe pneumonia and cardiogenic pulmonary oedema,” *European Respiratory Journal*, vol. 9, no. 9, pp. 1858–1867, Sep. 1996.

[120] M. S. Zinter *et al.*, “Early Plasma Matrix Metalloproteinase Profiles. A Novel Pathway in Pediatric Acute Respiratory Distress Syndrome,” *Am J Respir Crit Care Med*, vol. 199, no. 2, pp. 181–189, Jan. 2019, doi: 10.1164/rccm.201804-0678OC.

[121] C. Agostini and C. Gurrieri, “Chemokine/Cytokine Cocktail in Idiopathic Pulmonary Fibrosis,” *Proc Am Thorac Soc*, vol. 3, no. 4, pp. 357–363, Jun. 2006, doi: 10.1513/pats.200601-010TK.

[122] J. T. Benjamin *et al.*, “Neutrophilic inflammation during lung development disrupts elastin assembly and predisposes adult mice to COPD,” *J Clin Invest*, vol. 131, no. 1, p. e139481, doi: 10.1172/JCI139481.

[123] L. J. Celada *et al.*, “PD-1 up-regulation on CD4+ T cells promotes pulmonary fibrosis through STAT3-mediated IL-17A and TGF-β1 production,” *Sci Transl Med*, vol. 10, no. 460, p. eaar8356, Sep. 2018, doi: 10.1126/scitranslmed.aar8356.

[124] A. Kale, A. Sharma, A. Stolzing, P.-Y. Desprez, and J. Campisi, "Role of immune cells in the removal of deleterious senescent cells," *Immunity & Ageing*, vol. 17, no. 1, p. 16, Jun. 2020, doi: 10.1186/s12979-020-00187-9.

[125] M. Easter, S. Bollenbecker, J. W. Barnes, and S. Krick, "Targeting Aging Pathways in Chronic Obstructive Pulmonary Disease," *International Journal of Molecular Sciences*, vol. 21, no. 18, Art. no. 18, Jan. 2020, doi: 10.3390/ijms21186924.

[126] J. R. Baker, L. E. Donnelly, and P. J. Barnes, "Senotherapy: A New Horizon for COPD Therapy," *Chest*, vol. 158, no. 2, pp. 562–570, Aug. 2020, doi: 10.1016/j.chest.2020.01.027.

[127] S. Palumbo *et al.*, "Dysregulated Nox4 ubiquitination contributes to redox imbalance and age-related severity of acute lung injury," *American Journal of Physiology-Lung Cellular and Molecular Physiology*, vol. 312, no. 3, pp. L297–L308, Jan. 2017, doi: 10.1152/ajplung.00305.2016.

[128] P. Radermacher, S. M. Maggiore, and A. Mercat, "Fifty Years of Research in ARDS. Gas Exchange in Acute Respiratory Distress Syndrome," *Am J Respir Crit Care Med*, vol. 196, no. 8, pp. 964–984, Oct. 2017, doi: 10.1164/rccm.201610-2156SO.

[129] A. A. Birukova, P. Fu, J. Xing, I. Cokic, and K. G. Birukov, "Lung endothelial barrier protection by iloprost in the two-hit models of VILI involves inhibition of Rho signaling," *Transl Res*, vol. 155, no. 1, p. 44, Jan. 2010, doi: 10.1016/j.trsl.2009.09.002.

[130] E. Fan, J. Villar, and A. S. Slutsky, "Novel approaches to minimize ventilator-induced lung injury," *BMC Med*, vol. 11, p. 85, Mar. 2013, doi: 10.1186/1741-7015-11-85.

[131] S. Dodig, I. Čepelak, and I. Pavić, "Hallmarks of senescence and aging," *Biochem Med (Zagreb)*, vol. 29, no. 3, p. 030501, Oct. 2019, doi: 10.11613/BM.2019.030501.

[132] G. Nelson, O. Kucheryavenko, J. Wordsworth, and T. von Zglinicki, "The senescent bystander effect is caused by ROS-activated NF-κB signalling," *Mechanisms of Ageing and Development*, vol. 170, pp. 30–36, Mar. 2018, doi: 10.1016/j.mad.2017.08.005.

[133] D. Upadhyay, E. Correa-Meyer, J. I. Sznajder, and D. W. Kamp, "FGF-10 prevents mechanical stretch-induced alveolar epithelial cell DNA damage via MAPK activation," *American Journal of Physiology-Lung Cellular and Molecular Physiology*, vol. 284, no. 2, pp. L350–L359, Feb. 2003, doi: 10.1152/ajplung.00161.2002.

[134] C. D. Wood, T. M. Thornton, G. Sabio, R. A. Davis, and M. Rincon, "Nuclear Localization of p38 MAPK in Response to DNA Damage," *Int J Biol Sci*, vol. 5, no. 5, pp. 428–437, Jun. 2009.

[135] C. Huidobro *et al.*, "Cellular and molecular features of senescence in acute lung injury," *Mech Ageing Dev*, vol. 193, p. 111410, Jan. 2021, doi: 10.1016/j.mad.2020.111410.

[136] J. Yang *et al.*, "The development and plasticity of alveolar type 1 cells," *Development*, vol. 143, no. 1, pp. 54–65, Jan. 2016, doi: 10.1242/dev.130005.

[137] M. Strunz *et al.*, "Alveolar regeneration through a Krt8+ transitional stem cell state that persists in human lung fibrosis," *Nat Commun*, vol. 11, no. 1, Art. no. 1, Jul. 2020, doi: 10.1038/s41467-020-17358-3.

[138] Y. Kobayashi *et al.*, "Persistence of a regeneration-associated, transitional alveolar epithelial cell state in pulmonary fibrosis," *Nat Cell Biol*, vol. 22, no. 8, pp. 934–946, Aug. 2020, doi: 10.1038/s41556-020-0542-8.

[139] A. Jubran *et al.*, "Long-Term Outcome after Prolonged Mechanical Ventilation. A Long-Term Acute-Care Hospital Study," *Am J Respir Crit Care Med*, vol. 199, no. 12, pp. 1508–1516, Jun. 2019, doi: 10.1164/rccm.201806-1131OC.

[140] H. Jamaati, M. Nazari, R. Darooei, T. Ghafari, and M. R. Raoufy, "Role of shear stress in ventilator-induced lung injury," *The Lancet Respiratory Medicine*, vol. 4, no. 8, pp. e41–e42, Aug. 2016, doi: 10.1016/S2213-2600(16)30159-X.

[141] J. H. T. Bates and B. J. Smith, "Ventilator-induced lung injury and lung mechanics," *Annals of Translational Medicine*, vol. 6, no. 19, Art. no. 19, Oct. 2018, doi: 10.21037/atm.2018.06.29.

[142] N. de Prost, J.-D. Ricard, G. Saumon, and D. Dreyfuss, “Ventilator-induced lung injury: historical perspectives and clinical implications,” *Annals of Intensive Care*, vol. 1, no. 1, p. 28, Jul. 2011, doi: 10.1186/2110-5820-1-28.

[143] J. A. Herbert *et al.*, “Conservative Fluid Management Prevents Age-Associated Ventilator Induced Mortality,” *Exp Gerontol*, vol. 81, pp. 101–109, Aug. 2016, doi: 10.1016/j.exger.2016.05.005.

[144] H. Schulte, C. Mühlfeld, and C. Brandenberger, “Age-Related Structural and Functional Changes in the Mouse Lung,” *Front Physiol*, vol. 10, p. 1466, Dec. 2019, doi: 10.3389/fphys.2019.01466.

[145] S. M. Ruwanpura *et al.*, “Interleukin-6 Promotes Pulmonary Emphysema Associated with Apoptosis in Mice,” *Am J Respir Cell Mol Biol*, vol. 45, no. 4, pp. 720–730, Oct. 2011, doi: 10.1165/rcmb.2010-0462OC.

[146] J. R. Beitler, A. Malhotra, and B. T. Thompson, “Ventilator-Induced Lung Injury,” *Clin Chest Med*, vol. 37, no. 4, pp. 633–646, Dec. 2016, doi: 10.1016/j.ccm.2016.07.004.

[147] S. Han and R. K. Mallampalli, “The acute respiratory distress syndrome: from mechanism to translation,” *J Immunol*, vol. 194, no. 3, pp. 855–860, Feb. 2015, doi: 10.4049/jimmunol.1402513.

[148] M. A. Matthay and G. A. Zimmerman, “Acute Lung Injury and the Acute Respiratory Distress Syndrome,” *Am J Respir Cell Mol Biol*, vol. 33, no. 4, pp. 319–327, Oct. 2005, doi: 10.1165/rcmb.F305.

[149] M. A. Matthay *et al.*, “Acute respiratory distress syndrome,” *Nat Rev Dis Primers*, vol. 5, no. 1, Art. no. 1, Mar. 2019, doi: 10.1038/s41572-019-0069-0.

[150] K. F. Udobi, E. Childs, and K. Toujier, “Acute Respiratory Distress Syndrome,” *AFP*, vol. 67, no. 2, pp. 315–322, Jan. 2003.

[151] A. J. Walkey, R. Summer, V. Ho, and P. Alkana, “Acute respiratory distress syndrome: epidemiology and management approaches,” *Clin Epidemiol*, vol. 4, pp. 159–169, Jul. 2012, doi: 10.2147/CLEP.S28800.

[152] C. M. Bobba *et al.*, “Nanoparticle delivery of microRNA-146a regulates mechanotransduction in lung macrophages and mitigates injury during mechanical ventilation,” *Nat Commun*, vol. 12, no. 1, Art. no. 1, Jan. 2021, doi: 10.1038/s41467-020-20449-w.

[153] C. Lu *et al.*, "Cell Apoptosis: Requirement of H2AX in DNA Ladder Formation but not for the Activation of Caspase-3," *Mol Cell*, vol. 23, no. 1, pp. 121–132, Jul. 2006, doi: 10.1016/j.molcel.2006.05.023.

[154] K. E. C. Blokland, S. D. Pouwels, M. Schuliga, D. A. Knight, and J. K. Burgess, "Regulation of cellular senescence by extracellular matrix during chronic fibrotic diseases," *Clin Sci (Lond)*, vol. 134, no. 20, pp. 2681–2706, Oct. 2020, doi: 10.1042/CS20190893.

[155] F. Olivieri *et al.*, "DNA damage response (DDR) and senescence: shuttled inflamma-miRNAs on the stage of inflamm-aging," *Oncotarget*, vol. 6, no. 34, pp. 35509–35521, Sep. 2015.

[156] J. Y. J. Wang, "Cell Death Response to DNA Damage," *Yale J Biol Med*, vol. 92, no. 4, pp. 771–779, Dec. 2019.

[157] Y. Zhu *et al.*, "The Achilles' heel of senescent cells: from transcriptome to senolytic drugs," *Aging Cell*, vol. 14, no. 4, pp. 644–658, Aug. 2015, doi: 10.1111/acel.12344.

[158] M. Y. Terzi, M. Izmirli, and B. Gogebakan, "The cell fate: senescence or quiescence," *Mol Biol Rep*, vol. 43, no. 11, pp. 1213–1220, Nov. 2016, doi: 10.1007/s11033-016-4065-0.

[159] B. Shamloo and S. Usluer, "p21 in Cancer Research," *Cancers (Basel)*, vol. 11, no. 8, p. 1178, Aug. 2019, doi: 10.3390/cancers11081178.

[160] M. Shtutman, B.-D. Chang, G. P. Schools, and E. V. Broude, "Cellular Model of p21-Induced Senescence," *Methods Mol Biol*, vol. 1534, pp. 31–39, 2017, doi: 10.1007/978-1-4939-6670-7_3.

[161] J. Xu, S. Lamouille, and R. Derynck, "TGF-β-induced epithelial to mesenchymal transition," *Cell Res*, vol. 19, no. 2, pp. 156–172, Feb. 2009, doi: 10.1038/cr.2009.5.

[162] J. F. Santibañez, M. Quintanilla, and C. Bernabeu, "TGF-β/TGF-β receptor system and its role in physiological and pathological conditions," *Clinical Science*, vol. 121, no. 6, pp. 233–251, May 2011, doi: 10.1042/CS20110086.

[163] P. C. H. Hsieh *et al.*, "Bone morphogenetic protein 4: Potential regulator of shear stress-induced graft neointimal atrophy," *J Vasc Surg*, vol. 43, no. 1, pp. 150–158, Jan. 2006, doi: 10.1016/j.jvs.2005.08.008.

[164] O. Eickelberg and R. E. Morty, “Transforming Growth Factor β/Bone Morphogenic Protein Signaling in Pulmonary Arterial Hypertension: Remodeling Revisited,” *Trends in Cardiovascular Medicine*, vol. 17, no. 8, pp. 263–269, Nov. 2007, doi: 10.1016/j.tcm.2007.09.003.

[165] S. Minagawa *et al.*, “Accelerated epithelial cell senescence in IPF and the inhibitory role of SIRT6 in TGF-β-induced senescence of human bronchial epithelial cells,” *Am J Physiol Lung Cell Mol Physiol*, vol. 300, no. 3, pp. L391–L401, Mar. 2011, doi: 10.1152/ajplung.00097.2010.

[166] K. Tominaga and H. I. Suzuki, “TGF-β Signaling in Cellular Senescence and Aging-Related Pathology,” *Int J Mol Sci*, vol. 20, no. 20, p. 5002, Oct. 2019, doi: 10.3390/ijms20205002.

[167] P.-J. Wipff, D. B. Rifkin, J.-J. Meister, and B. Hinz, “Myofibroblast contraction activates latent TGF-β1 from the extracellular matrix,” *J Cell Biol*, vol. 179, no. 6, pp. 1311–1323, Dec. 2007, doi: 10.1083/jcb.200704042.

[168] Y. TAN, Q. XU, Y. LI, X. MAO, and K. ZHANG, “Crosstalk between the p38 and TGF-β signaling pathways through TβRI, TβRII and Smad3 expression in plancental choriocarcinoma JEG-3 cells,” *Oncol Lett*, vol. 8, no. 3, pp. 1307–1311, Sep. 2014, doi: 10.3892/ol.2014.2255.

[169] V. Lafarga, A. Cuadrado, I. Lopez de Silanes, R. Bengoechea, O. Fernandez-Capetillo, and A. R. Nebreda, “p38 Mitogen-Activated Protein Kinase- and HuR-Dependent Stabilization of p21Cip1 mRNA Mediates the G1/S Checkpoint,” *Mol Cell Biol*, vol. 29, no. 16, pp. 4341–4351, Aug. 2009, doi: 10.1128/MCB.00210-09.

[170] A. Hernandez-Segura, J. Nehme, and M. Demaria, “Hallmarks of Cellular Senescence,” *Trends in Cell Biology*, vol. 28, no. 6, pp. 436–453, Jun. 2018, doi: 10.1016/j.tcb.2018.02.001.

[171] D. Papadopoulos, R. Magliozzi, D. D. Mitsikostas, V. G. Gorgoulis, and R. S. Nicholas, “Aging, Cellular Senescence, and Progressive Multiple Sclerosis,” *Frontiers in Cellular Neuroscience*, vol. 14, 2020, Accessed: Feb. 22, 2022. [Online]. Available: https://www.frontiersin.org/article/10.3389/fncel.2020.00178

[172] T. Kuilman, C. Michaloglou, W. J. Mooi, and D. S. Peeper, “The essence of senescence,” *Genes Dev*, vol. 24, no. 22, pp. 2463–2479, Nov. 2010, doi: 10.1101/gad.1971610.

[173] D. V. Faget, Q. Ren, and S. A. Stewart, “Unmasking senescence: context-dependent effects of SASP in cancer,” *Nat Rev Cancer*, vol. 19, no. 8, Art. no. 8, Aug. 2019, doi: 10.1038/s41568-019-0156-2.

[174] R. Brown *et al.*, “The Impact of Aging in Acute Respiratory Distress Syndrome: A Clinical and Mechanistic Overview,” *Front Med (Lausanne)*, vol. 7, p. 589553, Oct. 2020, doi: 10.3389/fmed.2020.589553.

[175] S.-C. Yang, Y.-F. Tsai, Y.-L. Pan, and T.-L. Hwang, “Understanding the role of neutrophils in acute respiratory distress syndrome,” *Biomed J*, vol. 44, no. 4, pp. 439–446, Aug. 2021, doi: 10.1016/j.bj.2020.09.001.

[176] C.-C. Chiang, M. Korinek, W.-J. Cheng, and T.-L. Hwang, “Targeting Neutrophils to Treat Acute Respiratory Distress Syndrome in Coronavirus Disease,” *Frontiers in Pharmacology*, vol. 11, 2020, Accessed: Feb. 22, 2022. [Online]. Available: https://www.frontiersin.org/article/10.3389/fphar.2020.572009

[177] S. Minucci, R. L. Heise, M. S. Valentine, F. J. K. Gninzeko, and A. M. Reynolds, “Mathematical modeling of ventilator-induced lung inflammation,” *Journal of Theoretical Biology*, vol. 526, p. 110738, 2021, doi: https://doi.org/10.1016/j.jtbi.2021.110738.

[178] G. F. Curley, J. G. Laffey, H. Zhang, and A. S. Slutsky, “Biotrauma and Ventilator-Induced Lung Injury: Clinical Implications,” *Chest*, vol. 150, no. 5, pp. 1109–1117, Nov. 2016, doi: 10.1016/j.chest.2016.07.019.

[179] J. L. Kirkland and T. Tchkonia, “Senolytic drugs: from discovery to translation,” *J Intern Med*, p. 10.1111/joim.13141, Aug. 2020, doi: 10.1111/joim.13141.

[180] G. Bugedo, J. Retamal, and A. Bruhn, “Does the use of high PEEP levels prevent ventilator-induced lung injury?,” *Rev Bras Ter Intensiva*, vol. 29, no. 2, pp. 231–237, 2017, doi: 10.5935/0103-507X.20170032.

[181] T. Rana *et al.*, “PAI-1 Regulation of TGF-β1-induced ATII Cell Senescence, SASP Secretion, and SASP-mediated Activation of Alveolar Macrophages,” *Am. J. Respir. Cell Mol. Biol.*, Sep. 2019, doi: 10.1165/rcmb.2019-0071OC.

[182] M. Cazzola, M. G. Matera, P. Rogliani, and L. Calzetta, “Senolytic drugs in respiratory medicine: is it an appropriate therapeutic approach?,” *Expert Opinion on Investigational Drugs*, vol. 27, no. 7, pp. 573–581, Jul. 2018, doi: 10.1080/13543784.2018.1492548.

[183] B. Zhu *et al.*, “The Nuclear Receptor Peroxisome Proliferator-activated Receptor-β/δ (PPARβ/δ) Promotes Oncogene-induced Cellular Senescence through Repression of Endoplasmic Reticulum Stress *,” *Journal of Biological Chemistry*, vol. 289, no. 29, pp. 20102–20119, Jul. 2014, doi: 10.1074/jbc.M114.551069.

[184] Z. Wang, D. Wei, and H. Xiao, “Methods of Cellular Senescence Induction Using Oxidative Stress,” in *Biological Aging: Methods and Protocols*, T. O. Tollefsbol, Ed. Totowa, NJ: Humana Press, 2013, pp. 135–144. doi: 10.1007/978-1-62703-556-9_11.

[185] T. Kiyoshima *et al.*, “Oxidative stress caused by a low concentration of hydrogen peroxide induces senescence-like changes in mouse gingival fibroblasts,” *International Journal of Molecular Medicine*, vol. 30, no. 5, pp. 1007–1012, Nov. 2012, doi: 10.3892/ijmm.2012.1102.

[186] P. Guha, E. Kaptan, P. Gade, D. V. Kalvakolanu, and H. Ahmed, “Tunicamycin induced endoplasmic reticulum stress promotes apoptosis of prostate cancer cells by activating mTORC1,” *Oncotarget*, vol. 8, no. 40, pp. 68191–68207, Jul. 2017, doi: 10.18632/oncotarget.19277.

[187] O. Pluquet, A. Pourtier, and C. Abbadie, “The unfolded protein response and cellular senescence. A Review in the Theme: Cellular Mechanisms of Endoplasmic Reticulum Stress Signaling in Health and Disease,” *American Journal of Physiology-Cell Physiology*, vol. 308, no. 6, pp. C415–C425, Mar. 2015, doi: 10.1152/ajpcell.00334.2014.

[188] J. Y. J. Wang, “DNA damage and apoptosis,” *Cell Death Differ*, vol. 8, no. 11, Art. no. 11, Nov. 2001, doi: 10.1038/sj.cdd.4400938.

[189] R. Kumari and P. Jat, "Mechanisms of Cellular Senescence: Cell Cycle Arrest and Senescence Associated Secretory Phenotype," *Frontiers in Cell and Developmental Biology*, vol. 9, 2021, Accessed: Feb. 23, 2022. [Online]. Available: https://www.frontiersin.org/article/10.3389/fcell.2021.645593

[190] C. Abbadie and O. Pluquet, "Unfolded Protein Response (UPR) Controls Major Senescence Hallmarks," *Trends in Biochemical Sciences*, vol. 45, no. 5, pp. 371–374, May 2020, doi: 10.1016/j.tibs.2020.02.005.

[191] B. G. Childs, M. Durik, D. J. Baker, and J. M. van Deursen, "Cellular senescence in aging and age-related disease: from mechanisms to therapy," *Nat Med*, vol. 21, no. 12, Art. no. 12, Dec. 2015, doi: 10.1038/nm.4000.

[192] J. L. Goldman *et al.*, "Pleiotropic effects of interleukin-6 in a 'two-hit' murine model of acute respiratory distress syndrome," *Pulmonary Circulation*, vol. 4, no. 2, pp. 280–288, 2014, doi: 10.1086/675991.

[193] S.-H. Yang *et al.*, "Membrane Translocation of IL-33 Receptor in Ventilator Induced Lung Injury," *PLOS ONE*, vol. 10, no. 3, p. e0121391, Mar. 2015, doi: 10.1371/journal.pone.0121391.

[194] H. D. Foda *et al.*, "Ventilator-Induced Lung Injury Upregulates and Activates Gelatinases and EMMPRIN," *Am J Respir Cell Mol Biol*, vol. 25, no. 6, pp. 717–724, Dec. 2001, doi: 10.1165/ajrcmb.25.6.4558f.

[195] M. Amigoni *et al.*, "Unilateral Acid Aspiration Augments the Effects of Ventilator Lung Injury in the Contralateral Lung," *Anesthesiology*, vol. 119, no. 3, pp. 642–651, Sep. 2013, doi: 10.1097/ALN.0b013e318297d487.

[196] S. Hoegl *et al.*, "Capturing the multifactorial nature of ARDS – 'Two-hit' approach to model murine acute lung injury," *Physiol Rep*, vol. 6, no. 6, Mar. 2018, doi: 10.14814/phy2.13648.

[197] W. Bernhard, "Lung surfactant: Function and composition in the context of development and respiratory physiology," *Annals of Anatomy - Anatomischer Anzeiger*, vol. 208, pp. 146–150, Nov. 2016, doi: 10.1016/j.aanat.2016.08.003.

[198] L. Marseglia *et al.*, “Role of oxidative stress in neonatal respiratory distress syndrome,” *Free Radical Biology and Medicine*, vol. 142, pp. 132–137, Oct. 2019, doi: 10.1016/j.freeradbiomed.2019.04.029.

[199] Y.-S. Chao and A. Grobelna, *Curosurf (poractant alfa) for the Treatment of Infants At Risk For or Experiencing Respiratory Distress Syndrome: A Review of Clinical Effectiveness, Cost-Effectiveness, and Guidelines*. Ottawa (ON): Canadian Agency for Drugs and Technologies in Health, 2018. Accessed: Feb. 28, 2022. [Online]. Available: http://www.ncbi.nlm.nih.gov/books/NBK538371/

[200] N. B. Ray *et al.*, “Dynamic regulation of cardiolipin by the lipid pump, ATP8b1, determines the severity of lung injury in experimental bacterial pneumonia,” *Nat Med*, vol. 16, no. 10, pp. 1120–1127, Oct. 2010, doi: 10.1038/nm.2213.

[201] M. A. Matthay *et al.*, “Acute respiratory distress syndrome,” *Nat Rev Dis Primers*, vol. 5, no. 1, p. 18, 2019, doi: 10.1038/s41572-019-0069-0.

[202] B. H. Katira, “Ventilator-Induced Lung Injury: Classic and Novel Concepts,” *Respiratory Care*, vol. 64, no. 6, pp. 629–637, Jun. 2019, doi: 10.4187/respcare.07055.

[203] J. Kim, R. L. Heise, A. M. Reynolds, and R. M. Pidaparti, “Quantification of Age-Related Lung Tissue Mechanics under Mechanical Ventilation,” *Medical Sciences*, vol. 5, no. 4, Art. no. 4, Dec. 2017, doi: 10.3390/medsci5040021.

[204] F. Cipulli, F. Vasques, E. Duscio, F. Romitti, M. Quintel, and L. Gattinoni, “Atelectrauma or volutrauma: the dilemma,” *J Thorac Dis*, vol. 10, no. 3, pp. 1258–1264, Mar. 2018, doi: 10.21037/jtd.2018.02.71.

[205] L. Chen, H.-F. Xia, Y. Shang, and S.-L. Yao, “Molecular Mechanisms of Ventilator-Induced Lung Injury,” *Chin Med J (Engl)*, vol. 131, no. 10, pp. 1225–1231, May 2018, doi: 10.4103/0366-6999.226840.

[206] J. Birch and J. Gil, “Senescence and the SASP: many therapeutic avenues,” *Genes Dev*, vol. 34, no. 23–24, pp. 1565–1576, Dec. 2020, doi: 10.1101/gad.343129.120.

[207] D. McHugh and J. Gil, “Senescence and aging: Causes, consequences, and therapeutic avenues,” *J Cell Biol*, vol. 217, no. 1, pp. 65–77, Jan. 2018, doi: 10.1083/jcb.201708092.

[208] E. J. Novais *et al.*, “Long-term treatment with senolytic drugs Dasatinib and Quercetin ameliorates age-dependent intervertebral disc degeneration in mice,” *Nat Commun*, vol. 12, no. 1, Art. no. 1, Sep. 2021, doi: 10.1038/s41467-021-25453-2.

[209] D. Matthaios, P. Hountis, P. Karakitsos, D. Bouros, and S. Kakolyris, “H2AX a Promising Biomarker for Lung Cancer: A Review,” *Cancer Investigation*, vol. 31, no. 9, pp. 582–599, Nov. 2013, doi: 10.3109/07357907.2013.849721.

[210] J.-T. Pai, M.-W. Hsu, Y.-L. Leu, K.-T. Chang, and M.-S. Weng, “Induction of G2/M Cell Cycle Arrest via p38/p21Waf1/Cip1-Dependent Signaling Pathway Activation by Bavachinin in Non-Small-Cell Lung Cancer Cells,” *Molecules*, vol. 26, no. 17, p. 5161, Aug. 2021, doi: 10.3390/molecules26175161.

[211] “https://imagej.nih.gov/ij/macros/tools/Zoom_in_Images_and_Stacks.txt.” Accessed: Apr. 25, 2022. [Online]. Available: https://imagej.nih.gov/ij/macros/tools/Zoom_in_Images_and_Stacks.txt